Economic Geology, v. 101, pp. 347–383

Igneous Geology of the Carlin Trend, Nevada: Development of the Eocene Plutonic Complex and Significance for Carlin-Type Gold Deposits

MICHAEL W. RESSEL*

Department of Geological Sciences, University of Nevada, Reno, Nevada 89557-0088

AND CHRISTOPHER D. HENRY†

Nevada Bureau of Mines and Geology, University of Nevada, Reno, Nevada 89557-0088

Abstract

The Carlin trend contains the largest concentration of Carlin-type gold deposits in the world. Two major controversies about these giant gold deposits have been their age, which is now firmly established as Eocene, and the source of heat, fluids, and metals, which remains debated. We present data that demonstrate an intense period of Eocene magmatism coincided in time and space with deposit formation and was arguably the primary heat source. Geologic studies over the last 40 years have emphasized the stratigraphy and structure of Paleozoic sedimentary rocks, which are the major ore hosts. However, four igneous episodes affected the Carlin trend, in the Jurassic, Cretaceous, Eocene, and Miocene. A Jurassic diorite-granodiorite laccolith and related dikes were emplaced at about 158 Ma in the northern Carlin trend. A Cretaceous granite intruded the north-central part of the trend at 112 Ma. Abundant Eocene dikes intruded along most of the trend and were accompanied by lavas in a large volcanic field along the southwest edge of the trend between ~40 and 36 Ma. Miocene rhyolite lavas erupted just west of and across the southern part of the trend at ~15 Ma.

Exposed Eocene rocks consist predominantly of silicic to intermediate dikes, lavas, and epizonal intrusions, which we interpret to be sourced from a large Eocene plutonic complex underlying the Carlin trend. Eocene dikes are present in most deposits, are generally altered, but, with a few exceptions, were poor ore hosts. Distinct Eocene igneous suites, which are restricted to specific areas of the trend, are from north to south: (1) 40.3 to 39.0 Ma rhyolite to dacite dikes in the northern Carlin trend, centered approximately on the Betze-Post deposit and the richest part of the trend; (2) 37.6 Ma porphyritic rhyolite dikes including those that host ore at the Beast deposit; (3) 38.6 Ma intermediate to silicic intrusions of Welches Canyon; (4) 38.1 to 37.4 Ma andesite to dacite lavas and shallow intrusions of the Emigrant Pass volcanic field; (5) 36.2 Ma rhyolite dikes in the Emigrant Pass field that are indistinguishable from the 37.6 Ma suite except for age and location; and (6) ~37.5 Ma rhyolite to dacite intrusions and lavas of the southern Carlin trend (Rain subdistrict). Additionally, a few basaltic andesite dikes were emplaced at 37.8 Ma near Dee in the northernmost part of the trend and at 38.2 Ma near Rain.

The petrography, distribution, and age of the Eocene igneous suites and aeromagnetic data indicate that each suite is underlain by a major, silicic pluton. The longer lived suites require either multiple plutons or long-lived magma chambers. All Eocene dikes cannot have come from any single magma chamber, for example, from a chamber beneath the Welches Canyon intrusions as proposed by some. In this case, some igneous suites would have been emplaced only 12 to 15 km north of the northern edge of the source pluton, would not have been emplaced above or symmetrically around the source pluton, and would be distinct in age from the proposed source pluton. These requirements are not consistent with the distribution and age of the igneous suites.

The combined data for the Eocene igneous rocks require a plutonic complex about 50 km long (north-south), essentially coincident with the northern and central Carlin trend, and between 12 and 23 km across, underlying an area of ~1,000 km^2. This complex was emplaced over ~4 million years that coincided with the formation of the Carlin-type deposits of the Carlin trend. Although many factors contributed to the formation of the deposits and the Carlin trend, magmatic heat was abundant in the right place and at the right time to generate the deposits. The Carlin trend may be the largest concentration of Carlin-type deposits because the Eocene igneous episode there was the largest and longest lived of the Great Basin.

Introduction

THE 60-KM-LONG Carlin trend is the most important of several major gold-producing areas of north-central Nevada and contains the greatest concentration of Carlin-type gold deposits in the world. Gold production, reserves, and resources from the sedimentary rock-hosted or Carlin-type deposits of the Carlin trend are estimated to exceed 3,800 metric tons (t), or more than 60 percent of past production and reserves from all such deposits in the Great Basin (Hofstra and Cline, 2000; Cline et al., 2005). The deposits of the trend are hosted mainly in Paleozoic sedimentary rocks, particularly Devonian and Silurian carbonate rocks. Other host rocks include calc-silicate hornfels derived from Devonian and Silurian carbonate rocks, Silurian and Ordovician chert and argillite, and Jurassic and Eocene intrusive rocks. Eocene dikes are the youngest ore-bearing rocks of the trend (Ressel et al., 2000a, b).

The Carlin trend and Carlin-type deposits have been intensely studied for about 40 years (Hausen and Kerr, 1968; Radtke et al., 1980; Bakken, 1990; Kuehn and Rose, 1992;

† Corresponding author: e-mail, chenry@unr.edu

*Present address: Newmont Mining Corporation, 337 W. Commercial Street, Elko, Nevada 89801.

0361-0128/06/3579/347-37 $6.00

Arehart et al., 1993; Hofstra and Cline, 2000; Cline et al., 2005). Two major controversies have surrounded the origin of these deposits. The first was the age of formation, which was variously interpreted as Mesozoic (~117 Ma; Arehart et al., 1993), Eocene (~40 Ma; Seedorff, 1991; McKee et al., 1995; Thorman et al., 1995; Emsbo et al., 1996; Henry and Boden, 1998b; Henry and Ressel, 2000a; Ressel et al., 2000a), or Miocene (~15 Ma; Radtke et al., 1980). Abundant data in the last 10 years unequivocally demonstrate an Eocene age (Emsbo et al., 1996; Leonardson and Rahn, 1996; Phinisey et al., 1996; Groff et al., 1997; Hall et al., 1997, 2000; Hofstra et al., 1999; Hofstra and Cline, 2000; Johnston, 2000; Ressel et al., 2000a, b; Tretbar et al., 2000; Arehart et al., 2003; Chakurian et al., 2003; Cline et al., 2005).

The second controversy, which remains unresolved and is a subject of this paper, is the source of heat, fluids, and metals for the deposits. Models for the generation of Carlin-type deposits in the Great Basin include (1) an entirely amagmatic origin (Ilchik and Barton, 1997; Seedorff, 1991; Hofstra and Cline, 2000; Seedorff and Barton, 2004) involving deep circulation of meteoric water under high geothermal gradients driven by extension and large-scale (10^2–10^3 km^3) leaching of rocks in the middle and upper crust; (2) a mixing of deep, gold-bearing metamorphic fluids with meteoric fluids (Seedorf, 1991; Arehart, 1996; Hofstra and Cline, 2000; Tosdal et al., 2003a, Cline et al., 2005), possibly along crustal-scale faults; (3) a partly magmatic origin in which Eocene magmatism was the heat source but not necessarily the source of metals (Henry and Boden, 1998b; Henry and Ressel, 2000a; Ressel et al., 2000a, b); (4) a strictly magmatic origin (Sillitoe and Bonham, 1990; Johnston, 2003; Johnston and Ressel, 2004) for ore components and heat; and (5) a leaching of gold from Paleozoic sedimentary exhalative Pb-Zn-Ag-Au deposits in carbonate host rocks (Emsbo et al., 1999, 2003).

Stable isotope and other geochemical compositions of hydrothermal fluids indicate the dominance of meteoric fluids in some Carlin-type deposits and magmatic or deep metamorphic fluids in others (Hofstra and Cline, 2000; Cline et al., 2003, 2005). Hydrogen and oxygen isotope compositions of ore-related kaolinite from the Deep Star deposit of the northern Carlin trend indicate that a gold-bearing, magmatic or deep metamorphic fluid mixed with meteoric water (Heitt et al., 2003). Although sulfur isotope compositions indicate sedimentary sources for most sulfur (Hofstra and Cline, 2000), compositions of ore-related pyrite in part of the giant Betze-Post (Goldstrike) deposit are typical of a magmatic source (Kesler et al., 2003).

Some of the controversy about the origin of the deposits arises because early studies focused on the Paleozoic host rocks (Evans and Mullens, 1976; Radtke et al., 1980; Radtke, 1985, Bakken, 1990; Kuehn and Rose, 1992), and the highly altered and weathered igneous rocks in the upper parts of deposits were difficult to recognize. This gave the impression that igneous rocks were insignificant or even absent. In fact, intrusive rocks, particularly Eocene and Jurassic dikes, are ubiquitous features of deposits of the Carlin trend, and four significant episodes of magmatism have affected the rocks of the trend. These are (1) Jurassic diorite, rhyolite, and lamprophyre intrusions; (2) Cretaceous granite intrusion; (3) Eocene silicic to intermediate intrusions and volcanism; and (4) Miocene rhyolitic volcanism. A fifth episode of Paleozoic basaltic volcanism was limited to the allochthon of the Roberts Mountains thrust and is excluded from this discussion because the basalts are not rooted in the Carlin trend and generally distant from ore deposits. Intrusive rocks played important roles in nearly all deposits by localizing ore due to their contrasting physical and hydrologic properties with sedimentary hosts and their association with high-angle faults. The intrusive rocks provide key age constraints on magmatism, mineralization, and the structural history of the district and information on the depths at which the deposits formed.

This paper builds on our previous work on the Beast and Meikle-Griffin deposits of the northern Carlin trend (Ressel et al., 2000a, b) and a regional overview of Eocene magmatism (Henry and Ressel, 2000a). Here, we characterize and contrast Jurassic, Cretaceous, Eocene, and Miocene igneous rocks by providing comprehensive data about their age, emplacement style, extent, volume, mineralogy, and composition. Of particular importance are Jurassic and Eocene intrusions, which are spatially associated with all of the more than 40 gold deposits of the Carlin trend (Teal and Jackson, 1997). Dikes of these suites intruded structures that also controlled ore fluids. No Cretaceous or Miocene intrusions are recognized in any deposit. Although we discuss all igneous rocks, we emphasize the Eocene magmatic pulse because of its close spatial and temporal association with gold deposition.

Regional Geologic Setting

The Carlin trend is located in the northern Great Basin, which is part of the Basin and Range province of western North America (Fig. 1). The trend lies near the Proterozoic rifted margin of the North American craton (DePaolo and Farmer, 1984; Wooden et al., 1998; Tosdal et al., 2000). The plate margin underwent multiple episodes of contraction beginning in the Late Devonian-Early Mississippian and continuing into the early Mesozoic. During the earliest episode, deep-water marine rocks deposited west of the plate edge were thrust over autochthonous or parautochthonous shelf- and slope-facies marine rocks along the regional Roberts Mountains thrust (e.g., Roberts, 1964). Subsequent contraction in the Paleozoic produced a series of accretionary wedges that stacked sequentially westward, although thrusting continued far inland as well.

Mesozoic, particularly Cretaceous, granitic rocks are abundant in western Nevada, part of the great chain of Cordilleran batholiths of western North America that are broadly contemporaneous with subduction. Plutons diminish in abundance eastward and crop out only in scattered ranges in northeastern Nevada (Barton, 1996). Additional plutons may underlie Cenozoic cover. The largest Jurassic igneous center in eastern Nevada is in the Cortez Mountains (Fig. 1), where both intrusions and associated volcanic rocks are present. Other Jurassic plutons include those of the northern Fish Creek Mountains (Emmons and Eng, 1995), Ruby Mountains (Howard et al., 1979), Buffalo Mountain (Erickson et al., 1978), and the Goldstrike intrusion in the Carlin trend (Arehart et al., 1993). U-Pb and $^{40}Ar/^{39}Ar$ ages focus narrowly around 158 to 159 Ma (Mortensen et al., 2000; Table 1). The oldest biotite K-Ar ages, which are presumed to be most reliable given the likelihood of Ar loss, are indistinguishable

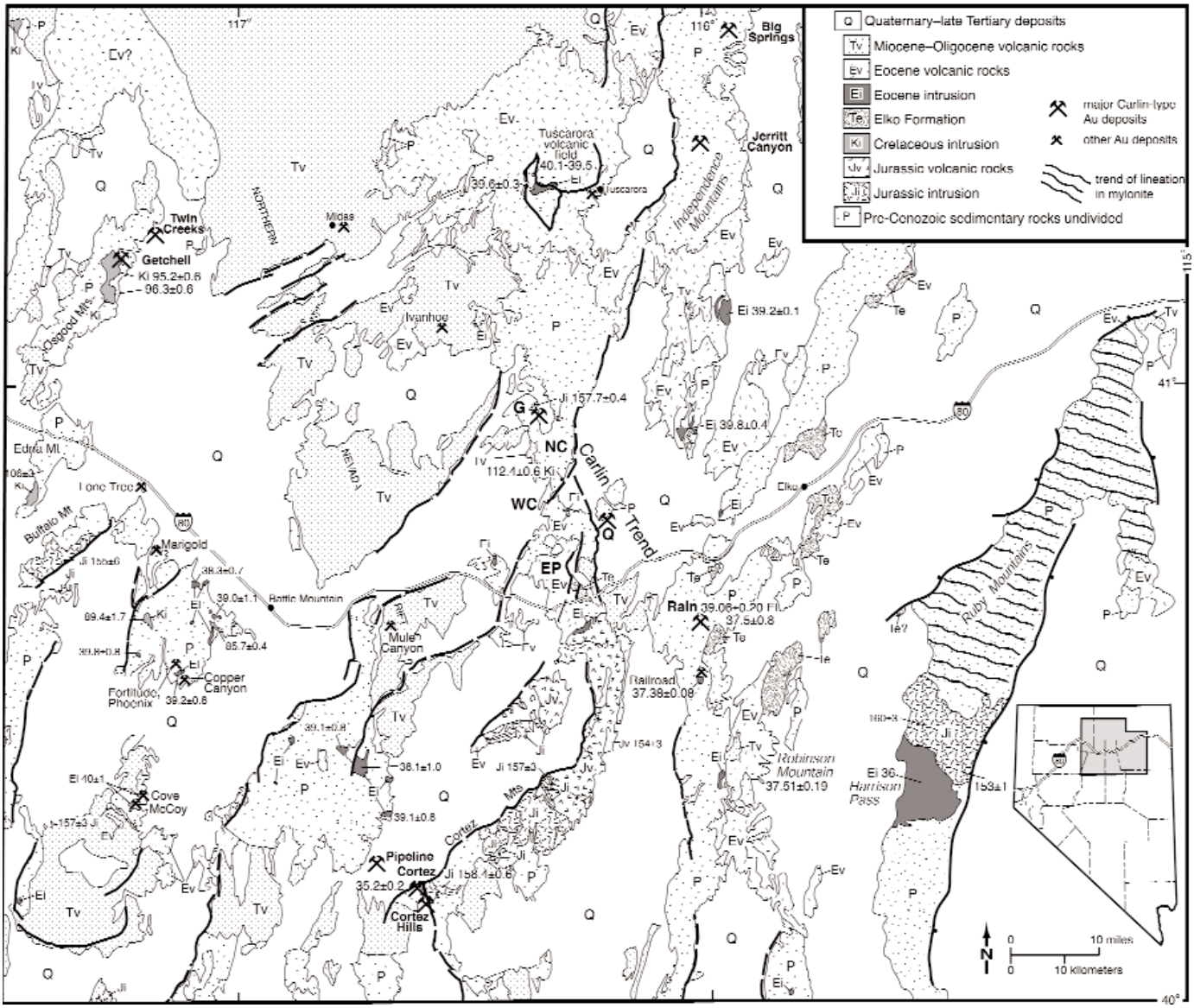

FIG. 1. Geologic map of northeastern Nevada (modified from Stewart and Carlson, 1976, 1978), showing the Carlin trend, major Carlin-type and other gold deposits, and ages of major Jurassic, Cretaceous, and Eocene intrusions and volcanic rocks. U-Pb and $^{40}Ar/^{39}Ar$ ages are in larger type; K-Ar ages, most of which are on biotite, are in smaller type. Jurassic intrusions in this and adjacent areas have ages that cluster tightly at ~158 Ma. Cretaceous intrusions have a wider range of ages between 112 and 86 Ma. Sources: Armstrong (1970), Erickson et al. (1978), Kistler et al. (1981), Emmons and Eng (1995), Mortensen et al. (2000), Theodore (2000), Castor et al. (2003), Sloan et al. (2003), this study. EP = Emigrant Pass volcanic field, G = Goldstrike mine, NC = northern Carlin trend, Q = Gold Quarry mine, WC = Welches Canyon.

within their large uncertainties from the U-Pb and $^{40}Ar/^{39}Ar$ ages. Cretaceous intrusions are less common than Jurassic intrusions in northeast Nevada (Fig. 1) but have a much wider age range from ~86 to 112 Ma. The largest Cretaceous pluton is in the Osgood Mountains (Groff et al., 1997), and other plutons are present in the Edna Mountains (Erickson et al., 1978), at Battle Mountain (Theodore et al., 1973; Theodore, 2000), and in the Carlin trend (Evans, 1980; Mortensen et al., 2000). Deeply emplaced Cretaceous granites are common in the Ruby Mountains but are not shown in Figure 1 because they are sills that are complexly interleaved with Paleozoic rocks (Snoke et al., 1997; Howard, 2000).

Magmatism resumed in the Eocene in the northern Great Basin with widespread eruption of high K, calc-alkaline volcanic rocks and emplacement of shallow intrusions. This activity was part of much more extensive Eocene magmatism that swept southward as east-west belts from southern British Columbia beginning at about 54 Ma and reaching Nevada at about 43 Ma (Christiansen and Yeats, 1992; Henry and Ressel, 2000a). Eocene magmatism was contemporaneous with subduction along the west coast of North America and broadly with the onset of crustal extension. However, this activity was far inboard of the plate margin, and the east-west belts were perpendicular to the plate margin, unlike typical

TABLE 1. $^{40}Ar/^{39}Ar$ and U-Pb Age Data for Igneous Rocks of the Carlin Trend

Sample no.[1]	Ref.	Rock type, location	W. long	N. lat	Mineral	Age Method	n (%^{39}Ar[3])	Age[4] (Ma)	±1σ	isochron	±1σ	40/36	±1σ	MSWD	total gas	±1σ
Jurassic rocks																
Goldstrike and related intrusions																
96-M-207	6	Goldstrike diorite			Titanite	U-Pb, range, three $^{206}Pb/^{238}U$ ages		*159.1*	4.4							
96-M-209	6	Monzonite sill			Zircon	U-Pb, lower intercept		*157.7*	0.4							
EX-24C	6	Rhyolite dike, Meikle			Zircon	U-Pb, mean, two $^{207}Pb/^{206}Pb$ ages		*159.3*	4.2							
GSS-1	2	Goldstrike diorite	116°21.8'	40°58.3'	Biotite	Step heating wtd mean	96	*159.9*	1.7	NA					158.6	
GSS-1	2	Goldstrike diorite	116°21.8'	40°58.3'	Hornblende	Step heating wtd mean	72	*160.8*	2.1	NA					162.4	
GSS-2	2	Goldstrike diorite	116°21.8'	40°58.3'	Biotite	Step heating wtd mean	94	*160.2*	1.7	NA					157.7	
97-Zia-7[1]	1	Microdiorite, Zia claims	116°21.4'	40°56.5'	Matrix	Step heating disturbed		~159		NM					139.8	0.80
98-Zia-9[1]	1	Rhyolite, Zia claims	116°23.2'	40°56.7'	Biotite	Step heating plateau	86.9	*157.4*	0.3	*157.6*	0.2	286	3	5.5		
Lan-34L[1]	1	Rhyolite dike, Lantern mine	116°21.7'	40°55.35'	Sericite/ albite	Step heating disturbed		111		NM						
Lamprophyre dikes																
186804	3	Phlogopite lamprophyre	116°19.25'	40°47.4'	Hornblende	Step heating plateau	47.3	*158.9*	0.2	NA						
I-5	4	Phlogopite lamprophyre	116°22.0'	40°57.2'	Phlogopite	Step heating plateau	93.0	*163.9*	1.1	165.7	10.3	160	7			
B5-95-11	7	Hornblende lamprophyre	116°21.75'	40°57.7'	Hornblende	Step heating disturbed	31.0	167.4	2.4	NM					210.0	3.3
Intrusions of the Dee mine area																
94B50/49/ DD58	8	Phlogopite lamprophyre	116°25.6'	41°02.35'	Biotite	Step heating disturbed		>148.7		NA						
DC-95-2-2146[2]	1	Altered Jurassic dike	116°25.6'	41°02.25'	Biotite	Step heating disturbed		157.2		152	4	376	480	257	148	1
BRS-4C-1190[2]	1	Altered dike	116°25.55'	41°02.5'	Sericite	Step heating disturbed		143		145	10	208	425	3	140	1
BRS-4C-1410[2]	1	Altered basaltic dike	116°25.55'	41°02.5'	Wr (illite)	Step heating disturbed		106		NM						
Cretaceous rocks																
RS-1 (H97-23)	6	Richmond granite	116°18.5'	40°51.06'	Zircon	U-Pb, mean two $^{206}Pb/^{238}U$ ages		*112.4*	0.6							
Eocene rocks																
Northern Carlin trend																
Plagioclase-biotite±quartz rhyolite																
BP-2[1]	1	Goldstrike pit	116° 21.9'	40° 58.6'	Biotite	Step heating plateau	98.5	*39.32*	0.11	*39.26*	0.05	308	1	11	*39.34*	0.20
BP-2[1]	1	Goldstrike pit	116° 21.9'	40° 58.6'	Plagioclase	Step heating disturbed	55.1	38.35	0.19	38.71	0.08	313	1	22	43.98	7.70
BP-2[1]	1	Goldstrike pit	116° 21.9'	40° 58.6'	Matrix	Step heating no plateau		excess Ar		NM						
DSU-192-906[2]	1	Deep Star	116°21.7'	40°57.5'	Biotite	Step heating disturbed	65.8	39.84	0.26	*40.03*	0.38	300	50	160	*39.90*	0.20
H00-50[2]	1	Genesis pit	116°21.7'	40°57.2'	Biotite	Step heating disturbed	58.2	39.3	0.2	38.81	0.29	683	240	0.045	39.69	0.20
I-13	4	Genesis pit	116°22.1'	40°56.8'	Biotite	Step heating plateau	100	*40.3*	0.2	40.2	2.0	310	21			
Plagioclase-biotite-hornblende dacite																
96-M-208	6	Post-Betze pit			Zircon	U-Pb, lower intercept		*37.8*	2.1							
G11-12-1	6	Dacite dike, Griffin			Zircon	U-Pb, range $^{206}Pb/^{238}U$ ages	*38.1*	0.8								
G11-005-4-492[1]	1	Griffin deposit	116°22.4'	40°59.8'	Biotite	Step heating plateau	76.9	*39.46*	0.08	*39.58*	0.05	270	2	3.5	*39.54*	0.11
H00-46[2]	1	Post-Betze pit	116°21.9'	40°58.7'	Hornblende	Step heating plateau	69.5	*38.95*	0.22	*39.03*	0.23	300	13	11.6	39.66	0.22
H00-49[2]	1	Post-Betze pit	116°22.0'	40°58.75'	Biotite	Step heating wtd mean	66.5	*40.13*	0.21	39.8	1.2	384	190	13	40.12	0.21
POD-1	2	Post-Betze pit	116°22.0'	40°58.7'	Biotite	Step heating wtd mean	95	*39.5*	0.4	NA					39.3	

TABLE 1. *(Cont.)*

Sample no.[1]	Ref.	Rock type, location	W. long	N. lat	Mineral	Age Method		*n* (%^{39}Ar[3])	Age[4] (Ma)	±1σ	isochron	±1σ	40/36	±1σ	MSWD	total gas	±1σ
Aphyric rhyolite																	
DSU-150-106[2]	1	Deep Star, core	116°21.7'	40°57.8'	Matrix	Step heating	wtd mean	59.6	*39.15*	0.26	*39.07*	0.33	228.0	8.0	2.5	36.75	0.22
DS-13[1]	1	Deep Star	116°21.7'	40°57.8'	Matrix	Step heating	disturbed				*38.98*	0.05	282	1	43		
DS-150-105[1]	1, 9	Deep Star, core	116°21.7'	40°57.8'	Matrix	Step heating	disturbed		~38		38.27	0.05	176	2	49	36.94	0.70
Basaltic andesite																	
98 Dee-8[2]	1	Dike, Dee mine	116°25.6'	41°02.0'	Matrix	Step heating	plateau	61.4	*37.80*	0.21	*37.73*	0.17	295.3	3.8		40.13	0.21
Plagioclase-biotite-hornblende-quartz±sanidine rhyolite																	
BST 114[1]	1	Beast pit	116°21.3'	40°56.4'	Sanidine	Single crystal	wtd mean	14	*37.58*	0.06							
BST 114[1]	1	Beast pit	"	"	Sanidine	Step heating	plateau	72.6	*37.61*	0.06						37.63	0.17
BST-30[1]	1	Beast pit	116°21.3'	40°56.5'	Biotite	Step heating	plateau	60.5	*37.55*	0.07	37.76	0.05	300	2	9.4	37.66	0.20
Rich-10[1]	1	Richmond Mtn	116°18.2'	40°51.8'	Sanidine	Single crystal	wtd mean	15	*37.58*	0.05							
H97-22b[1]	1	Welches Canyon	116°18.4'	40°48.0'	Sanidine	Single crystal	wtd mean	14	*37.43*	0.06							
Welches Canyon - Richmond Mountain area																	
H97-21[1]	1	Plagioclase-biotite-hornblende dacite	116°19.2'	40°47.4'	Hornblende	Step heating	plateau	88.3	*38.59*	0.17	*38.84*	0.11	300	3	5	38.45	0.70
WC-31[1]	1	Granodiorite	116°17.9'	40°47.7'	Plagioclase	Step heating	plateau	61.7	*38.59*	0.12	*38.74*	0.08	308	2	29	39.18	0.15
WC-106[2]	1	Plag-biot-hbl-qtz dacite	116°19.55'	40°50.6'	Biotite	Step heating	disturbed				43.1	2.1	278	100	543	*39.49*	0.23
Emigrant Pass Volcanic Field																	
Porphyritic (plagioclase-biotite-hornblende-quartz±sanidine) rhyolite dikes																	
H98-102[1]	1	Porphyritic dacite	116°17.1'	40°44.7'	Plagioclase	Single crystal	wtd mean	33	*36.45*	0.09							
H98-87[1]	1	Porphyritic rhyolite	116°19.1'	40°43.0'	Sanidine	Single crystal	wtd mean	14	*36.21*	0.04							
H98-61[1]	1	Porphyritic rhyolite	116°19.8'	40°40.8'	Sanidine	Single crystal	wtd mean	15	*36.12*	0.04							
Bob Creek lava (hornblende basaltic andesite)																	
H98-21C[1]	1	Rhyolite inclusion	116°21.0'	40°40.7'	Sanidine	Single crystal	wtd mean	15	*37.06*	0.04							
H98-20[1]	1	Porphyritic andesite	116°20.7'	40°40.8'	Hornblende	Step heating	plateau	90.6	*37.43*	0.10	*37.59*	0.10	286	5	4.7	37.44	0.49
Mack Creek lavas (plagioclase-hornblende dacite-andesite)																	
H98-78[1]	1	Porphyritic dacite	116°21.8'	40°42.7'	Hornblende	Step heating	plateau	50.3	*37.56*	0.18	*37.88*	0.09	269	3	6.3	33.79	0.25
H98-78[1]	1	Porphyritic dacite	116°21.8'	40°42.7'	Plagioclase	Single crystal	wtd mean	34	*37.31*	0.12							
H98-95C[1]	1	Porphyritic dacite	116°19.6'	40°44.9'	Sanidine	Single crystal	wtd mean	15	*37.83*	0.05							
H98-95C[1]	1	Porphyritic dacite	116°19.6'	40°44.9'	Hornblende	Step heating	plateau	76.6	*37.84*	0.10	*37.90*	0.06	290	2	2.6	37.04	0.70
Mack Creek intrusions (plagioclase-hornblende dacite-andesite), Bobs Flat Quadrangle																	
H98-1[1]	1	Porphyritic dacite	116°24.8'	40°41.6'	Hornblende	Step heating	plateau	95.1	*37.64*	0.18	*37.73*	0.15	291	5	3.4	37.65	0.46
EM-N2[2]	1	Porphyritic dacite	116°27.2'	40°42.7'	Hornblende	Step heating	plateau	62.8	*38.11*	0.21	*37.93*	0.31	302	20	23	38.50	0.21
Primeaux lavas (plagioclase-hornblende-pyroxene andesite-dacite)																	
H98-27[1]	1	Coarse hornblende andesite	116°16.5'	40°39.0'	Hornblende	Step heating	plateau	92.4	*37.85*	0.13	*38.16*	0.08	255	4	2	36.26	0.23
H98-109[1]	1	Hornblende andesite intrusion	116°17.5'	40°43.5'	Hornblende	Step heating	plateau	93.1	*38.06*	0.12	*38.13*	0.09	280	5	2.2	37.14	1.10
Rain-Railroad Area (southern Carlin trend)																	
RCR-9-676	5	Monzonite porphyry dike, Emigrant Springs			Zircon	U-Pb SHRIMP		11	*37.5*	0.8							
RCR-62-2151[2]	1	Basaltic andesite dike	116°2.4'	40°38.4'	Matrix	Step heating	wtd mean	56.3	*38.21*	0.20	*37.8*	1.2	378	73	220	39.42	0.20
RCR-61-2092[2]	1	Porphyritic diorite dike	116°2.4'	40°38.4'	Biotite	Step heating	wtd mean	97.5	*39.06*	0.20	*39.13*	0.18	294	13	27	38.60	0.20
NEP-44[1]	1	Biotite quartz-feldspar intrusion	116°0.5'	40°30.5'	Sanidine	Single crystal	wtd mean	14	*37.38*	0.08							

TABLE 1. (*Cont.*)

Sample no.[1]	Ref.	Rock type, location	W. long	N. lat	Mineral	Age Method	*n* (%^{39}Ar[3])	Age[4] (Ma)	±1σ	isochron	±1σ	40/36	±1σ	MSWD	total gas	±1σ
99-DJ-31[2]	1	Rhyolite intrusion	115°53.3'	40°23.5'	Sanidine	Single crystal wtd mean	9	*37.51*	0.19							
99-DJ-40[2]	1	Rhyolite ash-flow tuff	115°53.9'	40°27.8'	Sanidine	Single crystal wtd mean	9	*37.70*	0.19							
Miocene rocks																
99-468[2]	1	Rhyolite lava, Marys Mountain	116°16.1'	40°42.7'	Sanidine	Single crystal wtd mean	12	*15.32*	0.04							

[1] Data from this study, sample analyzed at the New Mexico Geochronological Research Laboratory (methodology in McIntosh et al., 2003)
[2] Data from this study, sample analyzed at the Nevada Isotope Geochronology Laboratory (Justet and Spell, 2001; Leavitt et al., 2004); sources of data: 1 = this study; 2 = Arehart et al. (1993); 3 = Emsbo et al. 1996; 4 = Farmer (Newmont Gold Company unpub. report, 1996); 5 = S. Garwin *in* Longo et al. (2002); 6 = Mortensen et al. (2000); 7 = Orobona (1996); 8 = Theodore et al. (1998); 9 = Heitt et al. (2003)
[3] *n* = number of single grains analyzed; %^{39}Ar = percent ^{39}Ar used in plateau
[4] Ages in italics are best estimates of emplacement age
Notes: NA = not available; NM = isochron calculation did not give a meaningful age
^{40}Ar/^{39}Ar ages for all samples, including those from other studies, were calculated or recalculated with a monitor age of 28.02 Ma for Fish Canyon sanidine (Renne et al., 1998;) samples I-5 and I-13 were analyzed at the Massachusetts Institute of Technology and give the oldest apparent Eocene and Jurassic ages, respectively; either these ages are distinctly older than ages determined elsewhere or we have not correctly allowed for a different monitor age; decay constants and isotopic abundances after Steiger and Jäger (1977); $\lambda_\beta = 4.963 \times 10^{-10}$ yr^{-1}; $\lambda_{\varepsilon+\varepsilon'} = 0.581 \times 10^{-10}$ yr^{-1}; ^{40}K/K = 1.167×10^{-4}

continental volcanic arcs. Humphreys (1995) interpreted an origin of magmatism related to foundering of a formerly shallowly dipping, subducted Farallon slab. He proposed that the slab detached along east-west lines near the United-Canada and United States-Mexico borders and sank in the middle. The detached ends pulled towards this sinking middle, and asthenosphere welled up in their wake. Magmas were generated by pressure-release melting of the asthenosphere, and this magmatism propagated southward across the northwestern United States.

Whatever their tectonic setting, Eocene igneous rocks are abundant throughout northeastern Nevada (Fig. 1; Brooks et al., 1995a, b; Henry and Boden, 1998; Henry and Ressel, 2000a, b; Castor et al., 2003). Most centers in northeastern Nevada are dominated by andesite to dacite lavas, with lesser rhyolite lava and ash-flow tuff, and subvolcanic intrusions. The largest, most diverse volcanic center is the Tuscarora volcanic field, which was active between 40.1 and 39.5 Ma (Henry and Boden, 1998a; Castor et al., 2003). Other major Eocene intrusive and volcanic areas of northeastern Nevada include the Emigrant Pass volcanic field adjacent to the Carlin trend (Henry and Faulds, 1999), the Robinson Mountain volcanic field south of the Carlin trend (Smith and Ketner, 1978), the numerous Au-Cu–related porphyries at Battle Mountain (Theodore, 2000), hypabyssal intrusions and related volcanic rocks in the southern Independence Mountains (Ketner, 1998; Henry and Ressel, 2000b), and volcanic and intrusive rocks of the Jerritt Canyon gold district in the Independence Mountains (Phinisey et al., 1996; Hofstra et al., 1999).

Middle Miocene volcanism was focused in the northern Nevada rift (Fig. 1), a 500-km-long, north-northwest–striking magnetic anomaly that lies west of the Carlin trend. The rift is characterized by numerous rhyolitic and basaltic eruptive centers, most of which were active between 16 and 14 Ma (Zoback et al., 1994; John et al., 2000; Wallace, 2003a). Miocene rocks of the rift host numerous epithermal Au-Ag deposits (John and Wallace, 2000; John, 2001; John et al., 2003; Wallace, 2003b). Miocene rhyolite lavas and tuffaceous sedimentary rocks are widespread in northern Nevada, including within and adjacent to the Carlin trend.

Episodic Cenozoic extension in northeastern Nevada was, in part, contemporaneous with Eocene and Miocene magmatism (John et al., 2000; Henry et al., 2001). Earliest extension probably generated the Elko basin and other Eocene basins at about 46 Ma (Henry et al., 2001; Haynes et al., 2002, 2003) and therefore predates Eocene magmatism. Near the Carlin trend, the extensional history and geometry are best known in the Emigrant Pass volcanic field (Fig. 2; Henry and Faulds, 1999; Henry et al., 2001), where episodes of extension are recognized (1) in the Eocene to generate the Elko basin (~46 Ma: Haynes et al., 2002), (2) following deposition of Elko basin deposits and preceding 38 to 36 Ma volcanism, (3) between 25 and 15 Ma, and (4) at about 15 Ma, contemporaneous with development of the northern Nevada rift (John et al., 2000). The greatest amount of extension probably occurred in the episode between 25 and 15 Ma, which may correlate with the time of most rapid cooling and inferred uplift of the Ruby Mountains core complex at 23 Ma (McGrew and Snee, 1994). Eocene and late Oligocene (25 Ma) volcanic rocks are tilted

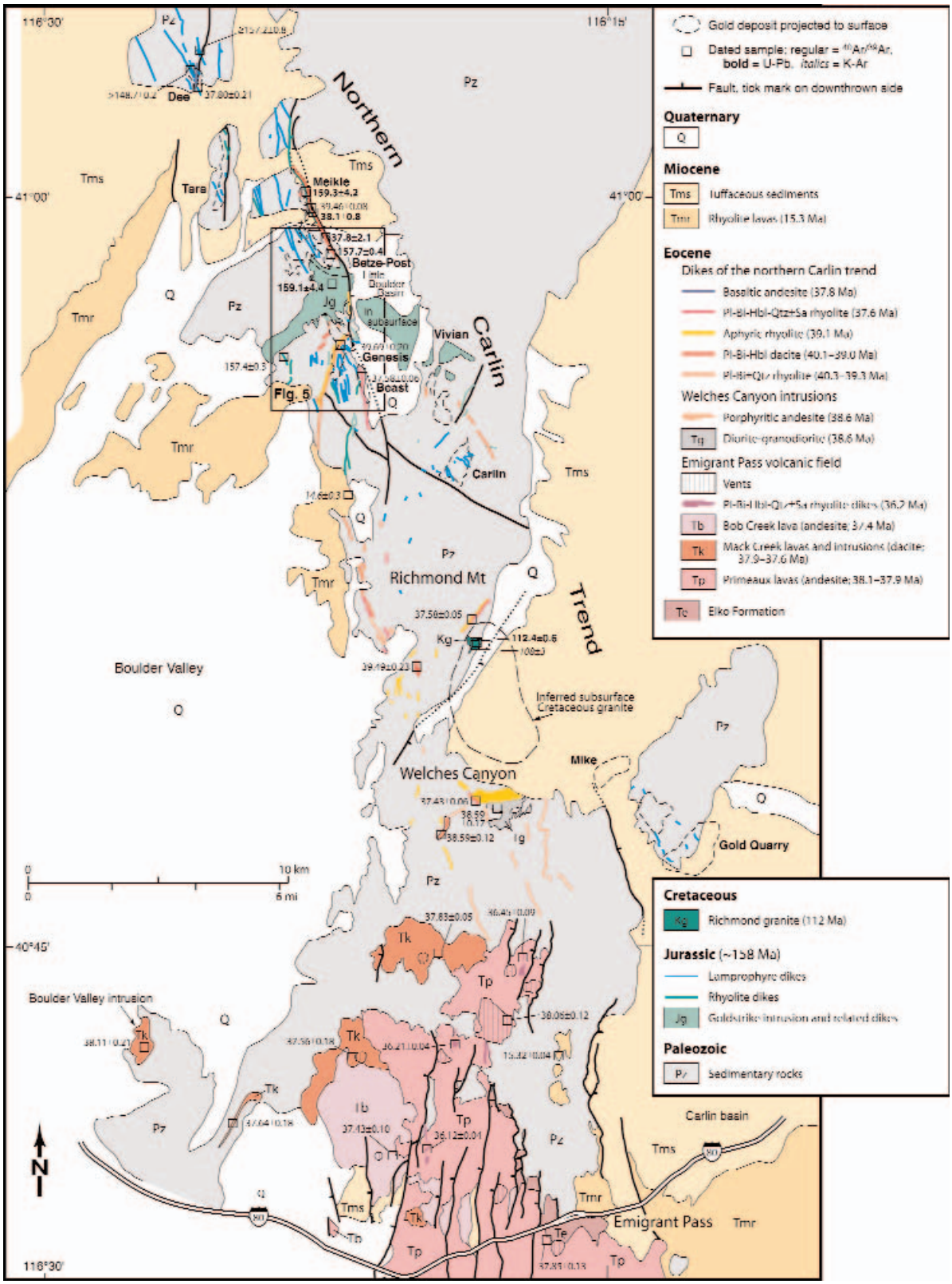

FIG. 2. Geologic map of the northern and central Carlin trend, emphasizing Jurassic, Cretaceous, Eocene, and Miocene igneous rocks. Jurassic and Eocene dikes and shallow intrusions are abundant throughout this area. Eocene magmatism occurred between ~40 and 36 Ma and was contemporaneous with formation of Carlin-type deposits. The box shows the area of the more detailed map of Figure 5. Geology from Evans (1974a, b), Stewart and Carlson (1976), Henry and Faulds (1999), Moore (2002), Norby (2002), Peters (2003), and this study. Ages and age groups are from this study (Table 1) and Evans (1974a, b). Bi = biotite, Hbl = hornblende, Pl = plagioclase, Qtz = quartz, Sa = sanidine.

as much as 30° to the east by numerous north- to north-northeast–striking normal faults in the Emigrant Pass field (Figs. 1–2). However, these faults and tilts die out northward into the northern Carlin trend. Paleozoic to Cenozoic structural and stratigraphic features are negligibly tilted in the trend, indicating only minor total extension there.

General Geochronology

We present 33 new and 22 published $^{40}Ar/^{39}Ar$ dates as well as seven published U-Pb dates of igneous rocks of the Carlin trend (Table 1). The Appendix provides analytical methods and general interpretation of the $^{40}Ar/^{39}Ar$ ages.

Modern $^{40}Ar/^{39}Ar$ and U-Pb dating demonstrates that magmatism in the Carlin trend occurred in four distinct pulses at ~158, 112, 40 to 36, and ~15 Ma (Figs. 3–4, Table 1; Mortensen et al., 2000; Ressel et al., 2000a, b). Early K-Ar dates of Mesozoic igneous rocks in the Carlin trend scatter widely (Fig. 3) and appear to indicate protracted magmatism. This scatter resulted from reheating of older intrusions, mostly the Jurassic Goldstrike intrusion, by younger igneous activity, and hydrothermal alteration, which produced intergrowths of secondary minerals such as chlorite. Reheating induced partial Ar loss from biotite, the most commonly dated phase. K-Ar dates on the Goldstrike intrusion range from 149 Ma (Hausen et al., 1983), only slightly younger than the true age of 158 Ma (Mortensen et al., 2000), to as young as 78 Ma (Morton et al., 1977). In contrast, most early K-Ar dates of Eocene and Miocene volcanic rocks closely match the more recent work, probably because reheating by younger igneous activity was negligible.

Jurassic Intrusions (~158 Ma)

Goldstrike laccolith and sills

Jurassic intrusions consist of the mainly quartz diorite Goldstrike laccolith and related sills and mostly northwest-striking lamprophyre and rhyolite dikes (Figs. 2, 5–7; Tables 2–3). These intrusions appear to have been emplaced during a short interval at ~158 Ma (Table 1). Outcrop, drill, and mine data demonstrate that the tabular, gently southwest-dipping Goldstrike body was emplaced along and below the Roberts Mountains thrust and other low-angle structures. The Goldstrike intrusion extends at least 2.5 km from its southwestern limit, where it is more than 600 m thick, to the Post fault, where it is ~300 to 350 m thick (Fig. 2; Leonardson and Rahn, 1996; Bettles, 2002). The buried Little Boulder Basin intrusion is a probable continuation east of the Post fault; here, the top of the intrusion is in upper plate rocks (i.e., above the Roberts Mountains thrust). A series of quartz diorite sills (Vivian sills) crop out still farther southeast in the main fault block of the Tuscarora Mountains (Fig. 2), where they intrude allochthonous rocks well above the Roberts Mountains thrust (Mohling, 2002). Intrusions in all three areas are of similar rock that most likely formed a single contiguous body that cut up section to the east (Dunbar, 2001; Chakurian et al., 2003). If so, this intrusion underlies ~7 km^2; with an average thickness of 400 m, total volume is about 3 km^3. The Goldstrike laccolith was most likely fed from a deeper magma chamber, the depth and size of which are unknown.

The Goldstrike body is dominantly quartz diorite (Fig. 7) but is crudely zoned, from mostly granodiorite along the southern or upper margin to a main mass of diorite and quartz diorite, with irregular segregations of gabbro most abundant along the northern or lower margin. Numerous porphyritic diorite to monzonite sills and other apophyses are present, especially along the northeast margin of the Goldstrike body in the Betze-Post deposit (Bettles, 2002).

The composite Goldstrike intrusion has a relatively weak magnetic anomaly and an extensive diopside hornfels and marble halo (Hildenbrand and Kucks, 1988; Bettles, 2002). The weak anomaly probably reflects the tabular form of the relatively magnetite-rich rocks and is strongest near its western, thickest end, which probably marks a feeder. The metamorphic halo is widest, ≥1 km, above the southern or upper margin near the Genesis mine (Fig. 2).

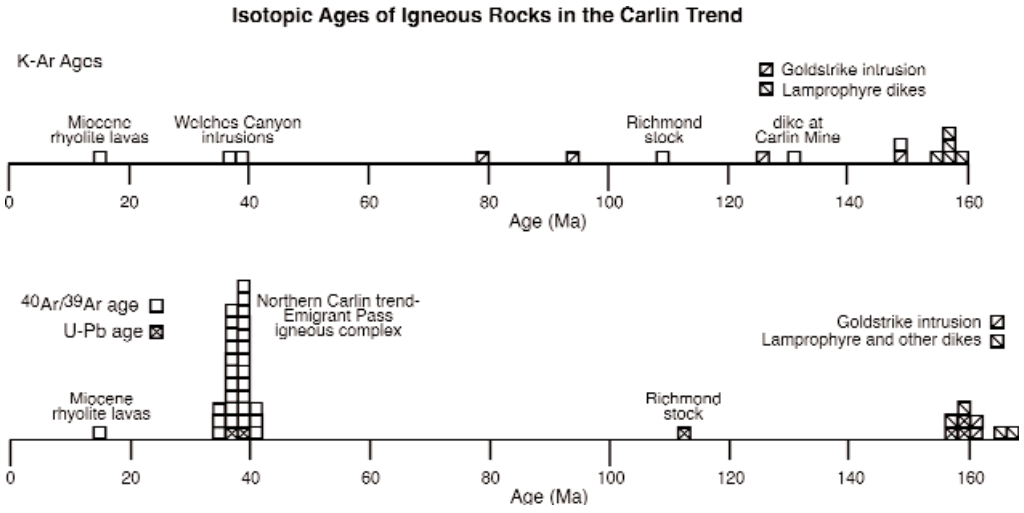

FIG. 3. Histograms of isotopic ages of igneous rocks of the Carlin trend. Early K-Ar dating suggested a wide range of activity in the Mesozoic. More precise $^{40}Ar/^{39}Ar$ and U-Pb dating demonstrate that igneous activity was concentrated in four distinct episodes at ~158, 112, 40 to 36, and 15 Ma. Data from Table 1 and Evans (1980), Hausen et al. (1983), and Mortensen et al. (2000).

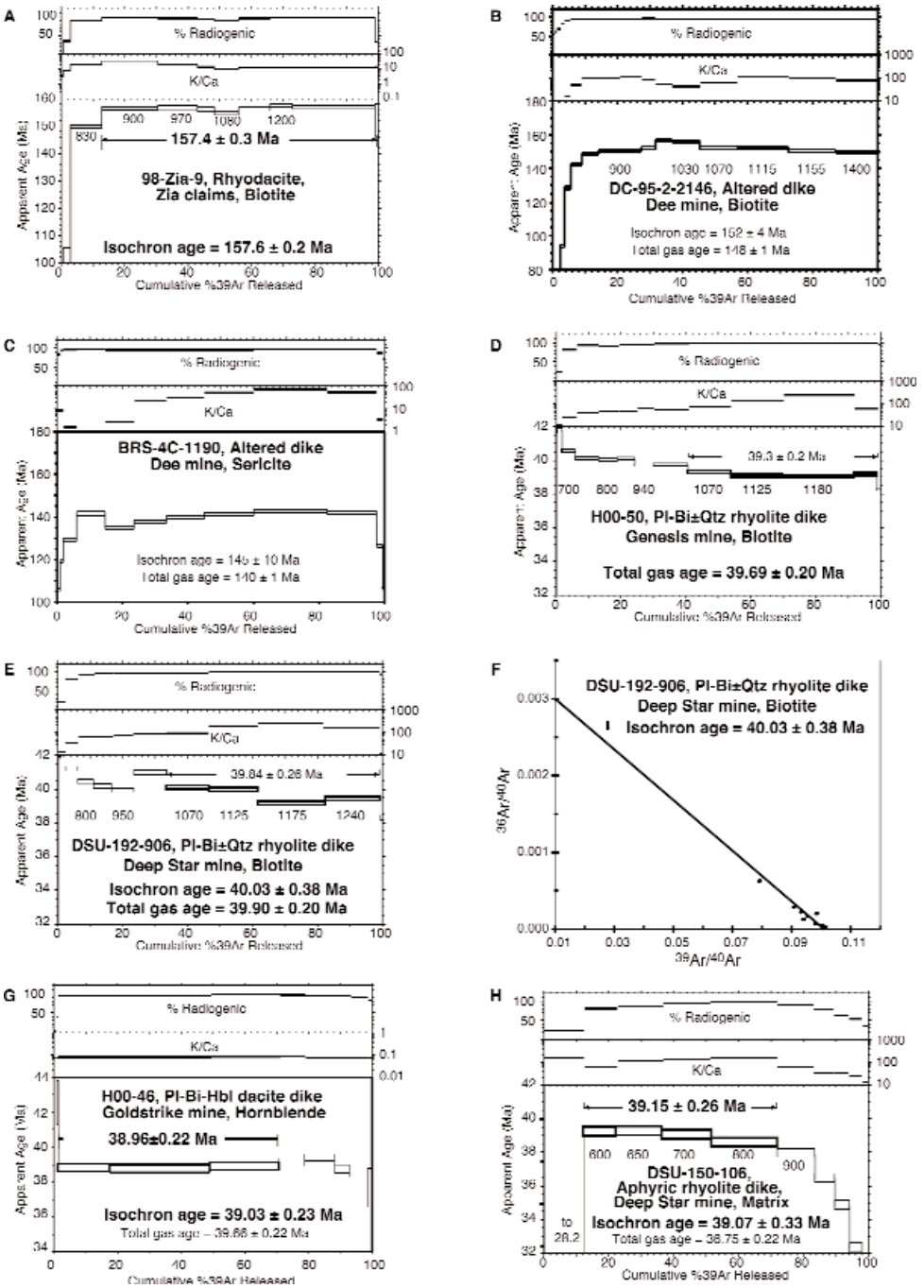

FIG. 4. Representative $^{40}Ar/^{39}Ar$ age spectra, isochrons, and single crystal analyses. Additional spectra are presented in Ressel et al. (2000a, b). Bi = biotite, Hbl = hornblende, Pl = plagioclase, Qtz = quartz, Sa = sanidine. A. 98-Zia-9, biotite from a rhyodacite dike, Zia claims. The mostly flat spectrum gives a plateau age of 157.4 ± 0.3 Ma. Low apparent ages from low-temperature steps suggest minor reheating and Ar loss. B. DC-95-2-2146, biotite from an altered dike, Dee mine. The best age estimate from this slightly disturbed spectrum is about 157 Ma, corresponding to the two oldest steps. Low ages at low temperature probably reflect Ar loss from reheating. C. BRS-4C-1190, sericite from an altered dike, Dee mine. The relatively disturbed spectrum indicates a probable alteration age greater than 143 Ma, the age of the highest temperature steps, and significant Ar loss. D. H00-50, biotite from a rhyolite dike, Genesis mine. The dropping spectrum suggests ^{39}Ar loss from recoil, probably related to minor chloritization of the biotite. The total gas age of ~39.7 Ma is probably the best estimate of emplacement. E. DSU-192-906, biotite from a rhyolite dike, Deep Star mine. The irregular spectrum probably indicates ^{39}Ar loss from recoil, probably related to minor chloritization. The best age estimate is 40.0 Ma from the isochron (Fig. 5F), which is consistent with a total gas age of 39.9 Ma. F. DSU-192-906, biotite from a rhyolite dike, Deep Star mine. The isochron indicates an age of ~40.0 Ma. G. H00-46, hornblende from a dacite dike, Goldstrike mine. The flat spectrum gives a plateau age of 38.95 ± 0.22 Ma, which is consistent with the isochron age of 39.03 ± 0.23 Ma. H. DSU-150-106, whole-rock sample of aphyric rhyolite, Deep Star mine. The disturbed spectrum probably reflects poor Ar retention and ^{39}Ar recoil from the fine matrix of potassium feldspar and quartz.

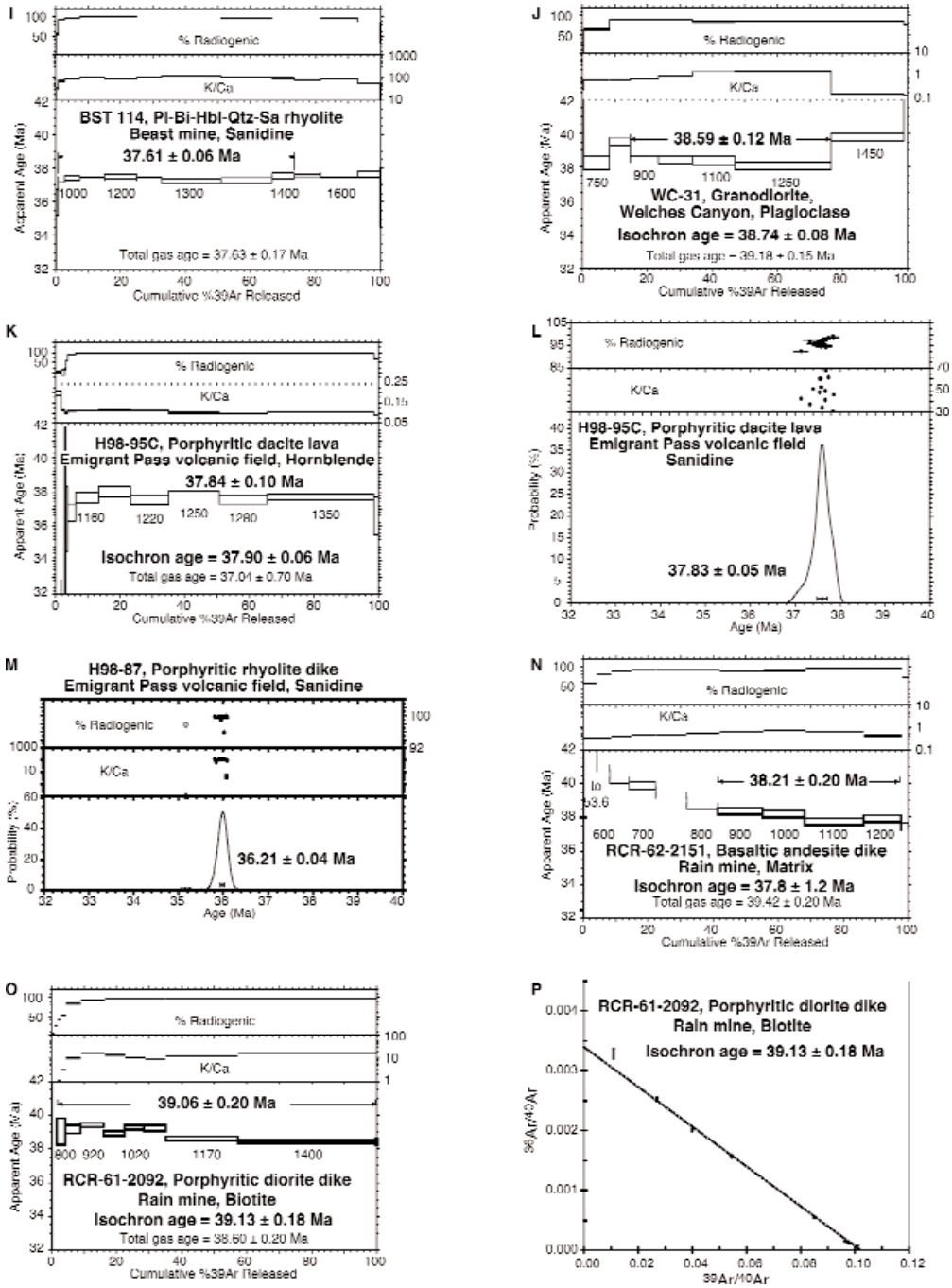

FIG. 4. *(Cont.)* Although somewhat arbitrary, the best age estimate appears to be 39.15 ± 0.26 Ma, a weighted mean of the four steps in bold. This is supported by an indistinguishable isochron age of 39.07 ± 0.33 Ma. I. BST 114, sanidine from a rhyolite dike, Beast mine. The well behaved, flat spectrum gives an age of 37.61 ± 0.11 Ma, which is consistent with ages of 37.58 ± 0.06 Ma from a single crystal analysis of the same sample and 37.55 ± 0.07 Ma from step heating of biotite (Ressel et al., 2000a). J. WC-31, plagioclase from a granodiorite, Welches Canyon. The slightly disturbed spectrum gives a plateau age of 38.59 ± 0.17 Ma, which is consistent with the isochron age of 38.74 ± 0.08 Ma. Isochron data suggest minor excess Ar. K. H98-95C, hornblende from a dacite lava, Emigrant Pass volcanic field. The plateau age of 37.84 ± 0.10 Ma agrees well with a single crystal sanidine age of 37.83 ± 0.05 Ma from the same sample (Fig. 5L). L. H98-95C, sanidine from a dacite lava, Emigrant Pass volcanic field. Analyses of 15 single grains of sanidine give a weighted mean age of 37.83 ± 0.05 Ma. M.. H98-87, sanidine from a rhyolite dike, Emigrant Pass volcanic field. Analyses of 14 single grains of sanidine give a weighted mean age of 36.21 ± 0.04 Ma. One age of ~35.2 Ma on a plagioclase grain, indicated by low K/Ca, was discarded. N. RCR-62-2151, matrix of a basaltic andesite dike, Rain mine. The slightly disturbed, dropping spectrum probably indicates ^{39}Ar loss from the fine-grained matrix. The best age estimates are ~38.2 Ma, a weighted mean of four steps from the relatively flat part of the spectrum, and ~37.8 Ma from the isochron. O. RCR-61-2092, biotite from a diorite dike, Rain mine. The slightly irregular spectrum gives a weighted mean age of 39.06 ± 0.20 Ma, in good agreement with the isochron age of 39.13 ± 0.18 Ma (P). P. RCR-61-2092, biotite from a diorite dike, Rain mine. The isochron indicates an age of 39.1 Ma.

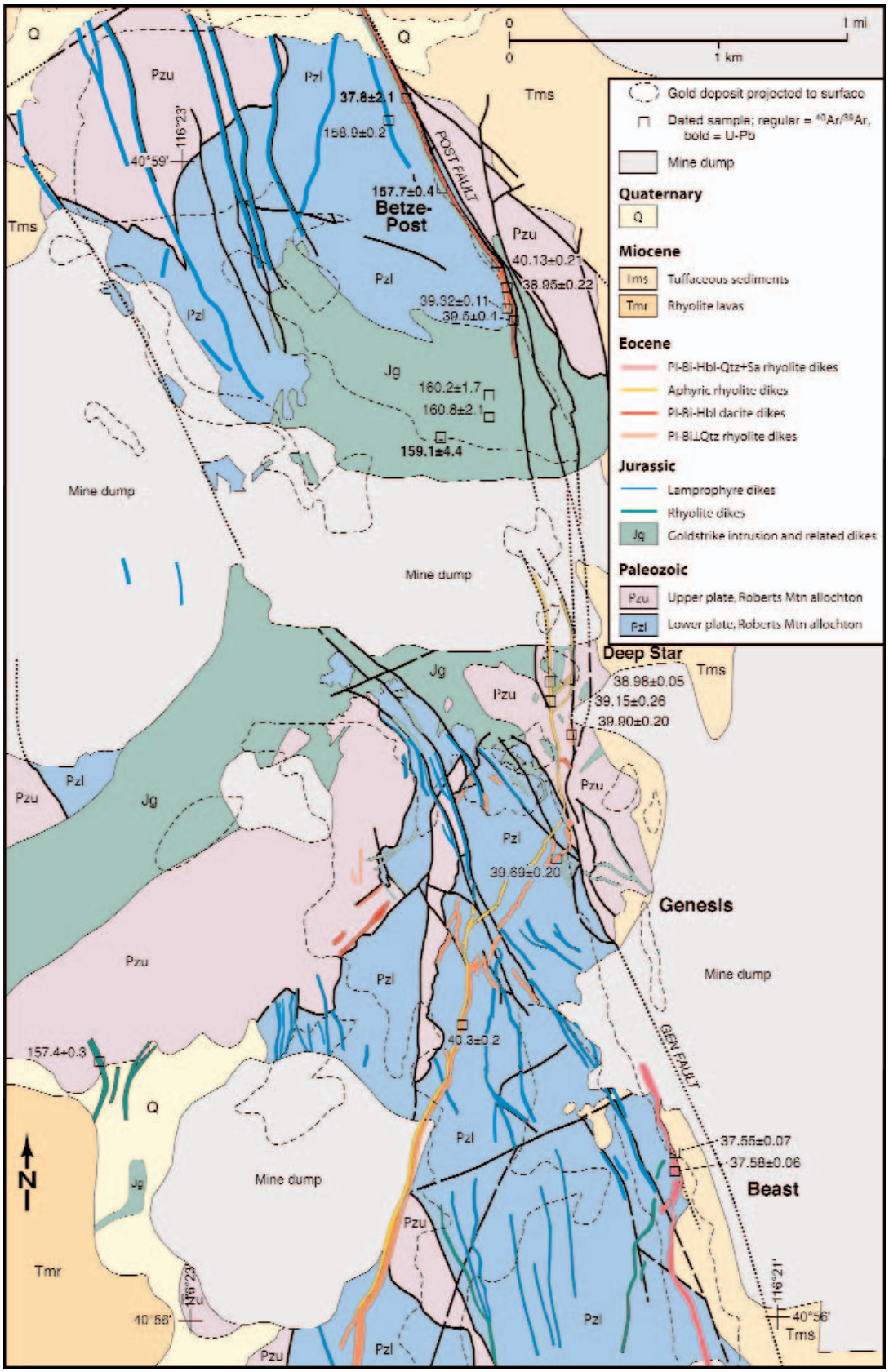

FIG. 5. Geologic map of part of the northern Carlin trend extending from the Betze-Post to the Beast mines (from Evans, 1974b; Moore, 2002; this study). Ages and age groups are from this study (Table 1). Bi = biotite, Hbl = hornblende, Pl = plagioclase, Qtz = quartz, Sa = sanidine.

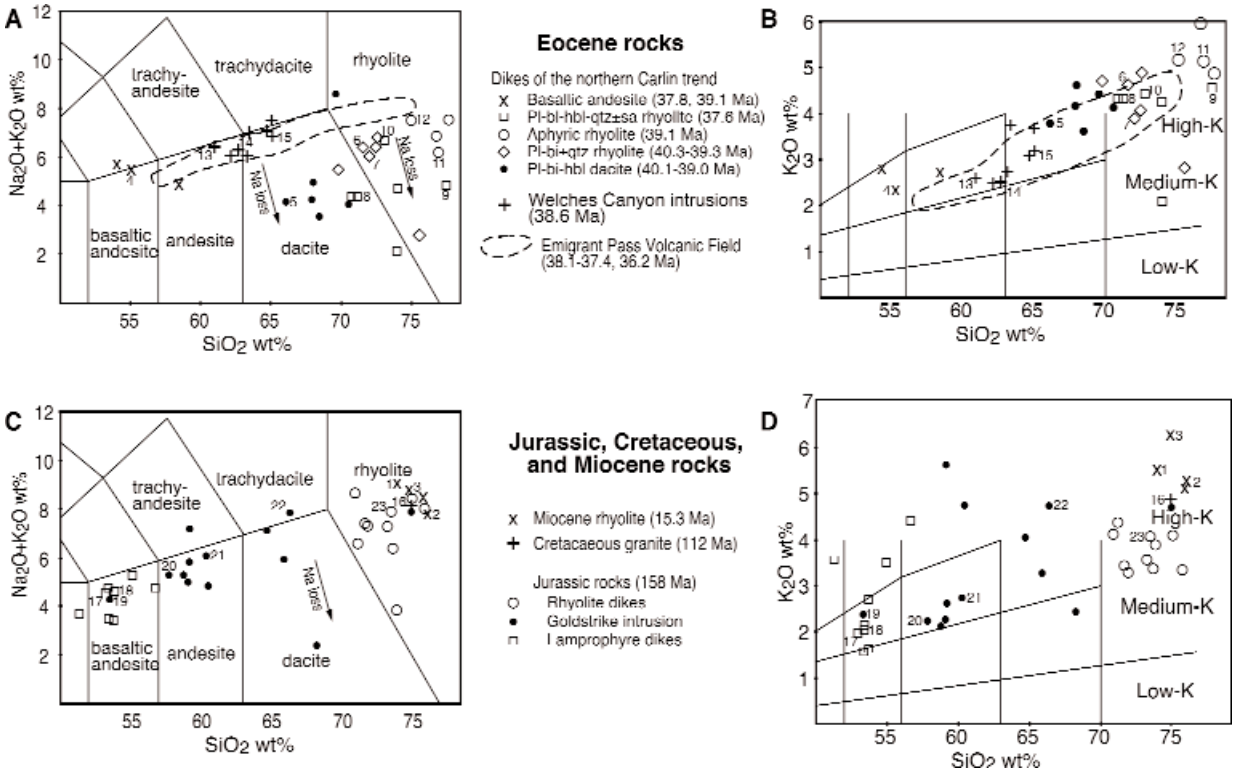

FIG. 6. Total alkalis ($Na_2O + K_2O$) vs. SiO_2 and K_2O vs. SiO_2 diagrams, illustrating the range of compositions of the four igneous suites of the Carlin trend. A. Total alkalis vs. SiO_2 for Eocene rocks. B. K_2O vs. SiO_2 for Eocene rocks. C. Total alkalis vs. SiO_2 for Jurassic, Cretaceous, and Miocene rocks. D. K_2O vs. SiO2 for Jurassic, Cretaceous, and Miocene rocks. Low total alkalis in Eocene and Jurassic rocks reflect Na loss due to alteration. The field of compositions of rocks from the Emigrant Pass is probably the best indication of prealteration compositions of Eocene dikes of the northern Carlin trend. Miocene rhyolite and Cretaceous granite have undergone little alteration because they postdate Carlin-type mineralization and are away from areas of mineralization, respectively. Age groups are from this study (Table 1). Rock classifications from Peccerillo and Taylor (1976) and LeBas et al. (1986). Data: Table 3 and M.W. Ressel and C.D. Henry, unpub. Bi = biotite, Hbl = hornblende, Pl = plagioclase, Qtz = quartz, Sa = sanidine.

Lamprophyre dikes

Porphyritic mafic dikes are abundant in the Carlin trend as a northwest-trending, 3- to 4-km-wide swarm extending nearly 25 km from south of the Carlin mine to north of the Dee mine. These dikes are concentrated near the Goldstrike intrusion. Individual dikes are 0.1 to 2 m wide, generally high angle, and as much as 1 km long. The rocks are highly porphyritic, lack feldspar phenocrysts, and contain at least one hydrous mafic phenocryst, either magnesian amphibole or

FIG. 7. Photographs of representative igneous rocks. Large divisions on the scale are 1 cm; fine divisions are 1 mm. A. Equigranular intermediate rocks of the Goldstrike laccolith (158 Ma). The upper sample is plagioclase-hornblende-biotite-quartz granodiorite from the southern, upper part of the laccolith at the North Star mine. The lower sample is plagioclase-hornblende-clinopyroxene-biotite diorite from the central part of the laccolith at the Goldstrike mine. B. Phlogopite-phyric lamprophyre (158 Ma) from a dike at the Goldstrike mine. The large dark minerals are clinopyroxene and hornblende(?) altered to a mixture of chlorite and carbonate minerals. The groundmass consists of potassium feldspar, phlogopite, and lesser quartz. C. Quartz-sericite–altered, finely porphyritic rhyolite (158 Ma) from a dike at the Meikle mine. The white minerals are plagioclase phenocrysts altered to sericite. Other phenocrysts not resolvable in the image are biotite altered to sericite and rare quartz. D. Coarse-grained granite (112 Ma) from the Richmond stock, which contains large phenocrysts of perthite (pe) and quartz (gray), with smaller grains of plagioclase (white) and sparse biotite (black). E. Finely porphyritic (plagioclase-biotite ± quartz) rhyolite (40.3–39.3 Ma) with brown glassy matrix from a dike at the Goldstrike mine. F. Weakly clay altered, porphyritic (plagioclase-biotite-hornblende) dacite (40.1–39.0 Ma) from a dike at the Goldstrike mine. Conspicuous hornblende phenocrysts (hbl) are altered to montmorillonite and calcite, whereas biotite (bi) is unaltered. G. Aphyric rhyolite (39.1 Ma) from a dike at the Deep Star mine. The sample on the left consists of flow-banded, hydrated red glass that characterizes margins of dikes; the sample on the right is from the devitrified core of a dike, which consists mainly of spherulitic potassium feldspar and quartz intergrowths. H. Argillically altered porphyritic (plagioclase-biotite-hornblende-quartz-sanidine) rhyolite (37.6 Ma) from a thick dike at the Beast mine. The large sanidine (sa) phenocryst is altered to kaolinite and barite; biotite (bi) phenocrysts are fresh; qtz = quartz phenocryst. I. Basaltic andesite (37.8 Ma) from the Dee mine. Phenocrysts consist of plagioclase (pl), clinopyroxene (px), and altered olivine (ol) in a holocrystalline matrix. J. Flow-banded rhyolite (~15 Ma) from a lava flow west of the Carlin mine. Sparse phenocrysts consist of sanidine, quartz, and fayalitic olivine.

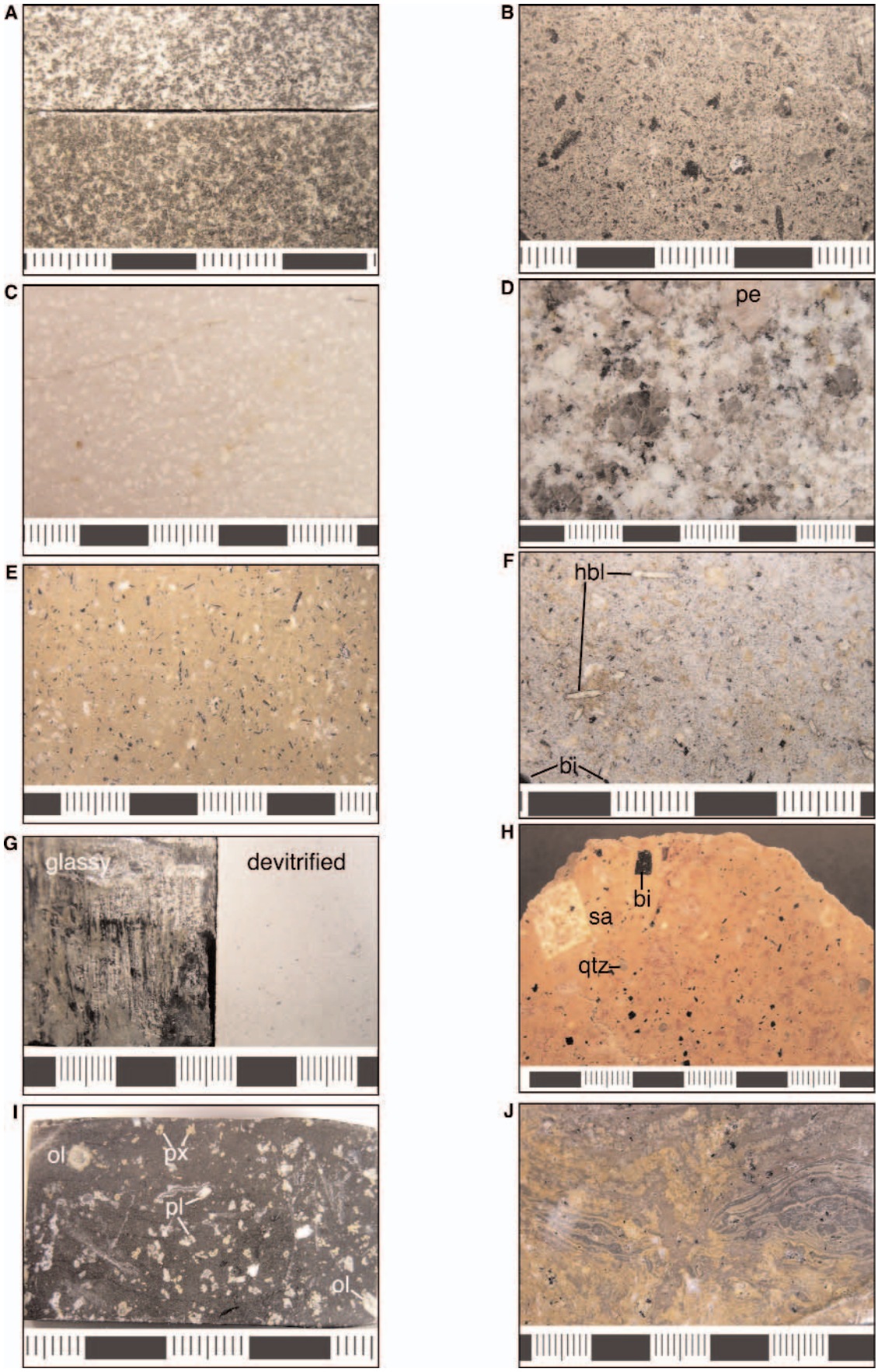
A
B
C
D
pe
E
F
hbl
bi
G
glassy
devitrified
H
bi
sa
qtz
I
ol
px
pl
ol
J

TABLE 2. Characteristics of Jurassic, Cretaceous, and Miocene Igneous Rocks of the Carlin Trend.

Unit	Rock type	Texture	Phenocrysts or phaneritic mineralogy	Age (Ma)	Distinguishing features	Extent
Miocene						
Sparsely porphyritic sa-qtz-ol-px rhyolite lava and associated porous, glassy tuff	High silica rhyolite	Porphyritic, aphanitic, flow-banded, locally glassy	Qtz: 0–2%, 1–4 mm sa: 2–3%, 1–3 mm Ol (fayalite): ≤1%, 2–4 mm Px (orthopyroxene): ≤1, 2–4 mm	14.6 (K-Ar)	Sparsely porphyritic, ol-phyric lava and nonwelded fall/surge tuff; commonly glassy, flow-banded, locally lithophysal	Widespread in morthern Carlin trend along eastern flank of Boulder Valley
Sparsely porphyritic sa-qtz±bi±px rhyolite lava and associated tuff	Rhyolite to high silica rhyolite	Sparsely porphyritic, aphanitic, flow-banded, locally glassy	Qtz: <0–2%, <3 mm Sa:1–2%, <3 mm Bi: <1%, <2 mm Px: <15, <2 mm	15.3	Sparsely porphyritic, commonly flow-banded lava and fall/surge tuff	Widespread in southern Carlin trend, west, east, and south of Gold Quarry mine
Cretaceous						
Coarse-grained granite	Granite	Coarsely phaneritic, with Kf phenocrysts	Pl: 45–55%, 0.4–1 cm Qtz: 20–30%, 0.2–0.8 cm Kf: 20–30%, 0.4–2 cm Bi: <7%, 0.03–0.6 cm	112	Coarse-grained, with large Kf phenocrysts; locally dikes and small pods of aplite-pegmatite	Small stock at Richmond Mountain, 0.4 km^2 outcrop; possibly ~20 km^2 subsurface
Jurassic						
Goldstrike dioritic laccolith and satellite intrusions	Diorite, lesser gabbro near base, granodiorite, tonalite common at top	Main phase: equigranular, medium grained phaneritic; locally pl-hbl porphyritic and fine grained	Pl: 45–65%, 4–10mm Kf: 0–15%, 4–10 mm Hbl: 10–20%, 5–10 mm Bi: 0–10%, 2–8 mm Px: 0–10%, 2–10 mm Qtz: 1–15%, 2–10 mm	~158	Medium-grained, compositionally zoned, equigranular granitoid; intermediate compositions predominate	Laccoliths and other sill-like intrusions at Goldstrike, Little Boulder Basin, and Vivian areas; ~7 km^2 total
Qtz-bi-hbl diorite dikes and sills	Porphyritic quartz diorite	Moderately to coarsely porphyritic	Bi: 0–25%, 1–8 mm Hbl: 0–20%, 1–8 mm Qtz: <2%, with reaction rims	~158	Strongly porphyritic bi- or hbl-phyric dikes with distinctive quartz xenocrysts(?)	1–10 m wide, NW-striking dikes/sills centered on Goldstrike and satellite intrusions
Lamprophyre dikes	Lamprophyre	Finely to coarsely porphyritic, aphanitic	Phl: 0–40%, 1–8 mm Hbl: 0–40%, 1–8 mm Qtz: <2%, 1–4 mm, with reaction rims Ol: <1%, 2–4 mm Px: <1%, 2–4 mm	~158	Sparsely porphyritic; lack of pl phenocrysts; commonly glassy	NW-striking dike swarm centered on Goldstrike and satellite intrusions
Finely porphyritic rhyolite dikes	Rhyolite	Finely porphyritic, aphanitic	Pl: 5–8%, 1–3 mm Bi: 1–3%, 1–3 mm Qtz: 0–1%, 1–3 mm	~158	Finely porphyritic, aphanitic; distinctive sodic alteration assemblage	1–15 m wide dikes within ±5 km radius of Goldstrike intrusion

Abbreviations: bi = biotite, hbl = hornblende, Kf = potassium feldspar, ol = olivine, phl = phlogopite, pl = plagioclase, px = pyroxene, qtz = quartz, sa = sanidine

phlogopite (Fig. 7), and therefore are defined as lamprophyres; this definition has no genetic implication. Phlogopitic lamprophyres contain alkali feldspar in their groundmass whereas amphibole-bearing lamprophyres contain plagioclase in the groundmass. Aligned phlogopite commonly imparts a distinct foliation.

Porphyritic (plagioclase-biotite ± quartz) rhyolite dikes

Abundant, finely porphyritic rhyolite dikes form a northwest-striking swarm centered on and within ~5 km of the Goldstrike intrusion. Individual dikes are as much as 15 m wide and as much as 2 km long.

Geochronology

U-Pb and $^{40}Ar/^{39}Ar$ dates on Jurassic intrusions suggest emplacement during a narrow time span around 158 Ma (Table 1; Figs. 2–5). The best U-Pb date is a lower intercept age of 157.7 ± 0.4 from five zircon fractions from a monzonite sill related to the Goldstrike intrusion in the Betze-Post mine (Mortensen et al., 2000). Less precise U-Pb dates on the Goldstrike diorite

and a rhyolite dike are 159.1 ± 4.4 and 159.3 ± 4.2 Ma. Most $^{40}Ar/^{39}Ar$ ages range from 157.4 ± 0.3 to 160.8 ± 2.1 Ma and overlap with the U-Pb ages within analytical uncertainty. Relative ages among the Jurassic rocks are sparse, but porphyritic rhyolite cuts diorite and lamprophyre dikes at Meikle, Beast, and nearby deposits (Bettles, 2002). Among K-Ar ages, those of lamprophyres most closely match the modern U-Pb and $^{40}Ar/^{39}Ar$ ages, which indicate they cooled rapidly following emplacement and have not been significantly reheated (Fig. 3).

Chemical composition

A thorough petrogenetic study of Carlin trend igneous rocks is beyond the scope of this report and will be difficult because of the alteration. Almost all igneous rocks of the northern Carlin trend are altered to some degree. Argillization leading to some alkali loss is particularly common (Drews-Armitage et al., 1996; Leonardson and Rahn, 1996; Ressel et al., 2000a, b). Nevertheless, total alkali/SiO_2 and K_2O/SiO_2 variations allow rock classification (LeBas et al., 1986) and comparison of the different suites (Fig. 6). However, we also use rare earth elements (REE), which are relatively immobile during hydrothermal alteration (Fig. 8).

Jurassic rocks contain from ~51 to 77 percent SiO_2 (Fig. 6, Table 3). SiO_2 concentrations fall into three groups that match the three rock types. The least altered samples of lamprophyre contain 51 to 55 percent SiO_2, samples of the Goldstrike diorite mostly contain 57 to 59 percent SiO_2 with the related but volumetrically less significant granodiorites containing about 66 percent SiO_2, and rhyolite dikes contain 71 to 77 percent SiO_2. As with most Mesozoic and younger igneous rocks in the interior of the Great Basin, Jurassic rocks are moderately alkalic (Fig. 6).

All Jurassic rocks have steep, concave-upward REE patterns (Fig. 8). Despite being the most mafic Jurassic rock type, lamprophyres have the highest concentrations, especially of LREE, and the greatest variation in concentrations despite negligible variation in, or relationship to, SiO_2. REE concentrations of Goldstrike rocks largely overlap with those of the lamprophyres and generally increase with increasing SiO_2, which makes a simple genetic tie between the two unlikely. Rhyolites have the lowest REE concentrations, which generally decrease with SiO_2.

Cretaceous "Richmond" Granite and Aplite-Pegmatite (112 Ma)

The only Cretaceous rock in the Carlin trend is a coarse-grained granite that intruded and thermally metamorphosed Paleozoic quartzite and limestone on the south flank of Richmond Mountain (Fig. 2). The rock is true granite, with 75 percent SiO_2 (Fig. 6; Table 3) and characterized by phenocrysts of perthite up to 2 cm across (Fig. 7). Aplite is common as a border phase and as dikes cutting the main body; pegmatite pods are also common. Concordant $^{206}Pb/^{238}U$ ages of two zircon fractions demonstrate intrusion at 112.4 ± 0.6 Ma (Table 1, Fig. 2; Mortensen et al., 2000). A biotite K-Ar age of 108 ± 3 Ma (Evans, 1974b) suggests relatively rapid cooling after emplacement at no more than moderate depth and negligible reheating.

Outcrop area is small, ~0.4 km^2, but aeromagnetic data, the coarseness of the intrusion, a broad zone of thermally metamorphosed rock around it, and K-Ar ages of hornfels minerals at the Mike composite Cu-Au deposit indicate that the Richmond granite may underlie an area of as much as 20 km^2 (Fig. 2). A positive aeromagnetic anomaly extends southeastward from the granite to within 1.8 km of the deposit, but distinguishing the magnetic anomaly of the Richmond granite from that associated with the Eocene Welches Canyon intrusions is uncertain (Norby and Orobona, 2002). K-Ar ages of replacement K-feldspar of 107 ± 2 and 111 ± 2 Ma from, respectively, an altered lamprophyre dike and Paleozoic siltstone in the Mike deposit (Branham and Arkell, 1995; Norby and Orobona, 2002) indicate that hornfels developed contemporaneously with the Richmond intrusion. Implication of these data for the extent of the Richmond intrusion is complicated because Paleozoic rocks surrounding the Eocene Welches Canyon intrusions are also thermally altered (Evans, 1974b). Also, Evans (1974b) mapped several dikes around the Richmond intrusion as Cretaceous, but our $^{40}Ar/^{39}Ar$ dates and petrographic comparison demonstrate that all of these are Eocene in age.

Eocene Igneous Rocks of the Carlin Trend (40–36 Ma)

The most abundant igneous rocks in and around the Carlin trend are Eocene dikes, small stocks, and lavas (Figs. 2, 5; Tables 1, 4). Eocene rocks include (1) abundant, mostly rhyolite dikes in the northern Carlin trend from the Carlin deposit north to the Dee deposit, (2) small andesite to rhyolite stocks and dikes in Welches Canyon, (3) abundant andesite to dacite lavas and rhyolite dikes of the Emigrant Pass volcanic field, and (4) basaltic andesite to rhyolite dikes in the southern Carlin trend near the Rain mine. Isotopic ages indicate nearly continuous magmatism that generally migrated southward between 40 and 36 Ma (Table 1, Fig. 2).

Eocene dikes of the northern Carlin trend (40.3–37.6 Ma)

Eocene dikes range from high SiO_2 rhyolite to dacite, with minor basaltic andesite at the Dee deposit. These dikes intrude several major ore-controlling structures, including the Post fault zone and the Dee fault (Teal and Jackson, 1997; Dobak et al., 2002; this study). Commonly, the north-northwest–striking, steeply dipping dikes and faults are the immediate hanging wall to ore, but Eocene dikes locally host ore at the Meikle-Griffin, Betze-Post, and Beast deposits (Ressel et al., 2000a, b).

Five types of dikes are recognized based on phenocryst assemblage and age (Tables 1, 4): (1) finely porphyritic (plagioclase-biotite ± quartz) rhyolite (~40.3–39.3 Ma); (2) porphyritic (plagioclase-biotite-hornblende) dacite (~40.1–39.0 Ma); (3) aphyric, high silica rhyolite (~39.1 Ma); (4) olivine-phyric basaltic andesite (~37.8 Ma); and (5) coarsely porphyritic (plagioclase-biotite-hornblende-quartz ± sanidine) rhyolite (~37.6 Ma).

Porphyritic (plagioclase-biotite ± quartz) rhyolite (40.3–39.3 Ma): Finely porphyritic rhyolite dikes are exposed over a nearly 9-km strike length from Betze-Post to south of Genesis (Figs. 2, 5, 7). Most dikes are concentrated along the north-northwest–striking and major ore-controlling Post fault zone (Teal and Jackson, 1997), but one, nearly 6 km-long dike diverges from the fault zone at Genesis to a south-southwest strike. The dikes are 1 to 8 m wide. Concentration of the

TABLE 3. Representative Chemical Analyses of Least Altered Miocene, Eocene, Cretaceous,

Age	Miocene			Eocene			
	Rhyolite lavas and tuffs			Dikes of the northern Carlin trend			
Rock type[1]	Rhyolite	Rhyolite	Rhyolite	Basaltic andesite	Pl-bi-hbl dacite	Pl-bi-qtz rhyolite	
Sample no.	LAN-65	H98-112	H98-14	CD96 10C-1455	PNC 213-1787	GEN-2	BP-2
No. in Figure 6	1	2	3	4	5	6	7
Sample type	Outcrop	Outcrop	Outcrop	Core	Core	Pit	Pit
Latitude	40°54.42'	40°39.8'	40°39.8'	40°59.5'	40°58.0'	40°56.85'	40°58.6'
Longitude	116°22.15'	116°21.4'	116°15.6'	116°24.9'	116°22.0'	116°22.05'	116°21.9'
Occurrence	Lava	Tuff	Lava	Dike	Dike	Dike	Dike
Alteration	Hydrated glass	Hydrated glass	Hydrated glass		Moderate clay	Mild clay	Hydrated glass
Analyses[2]	U, N	W, C	W	U, C	U, A	U, A	U, A
SiO_2	74.27	76.03	74.94	55.24	66.06	71.59	72.01
TiO_2	0.26	0.30	0.28	1.28	0.39	0.32	0.29
Al_2O_3	12.45	12.05	13.35	16.83	16.34	15.82	15.81
FeO^3	2.95	2.34	1.41	6.71	2.97	2.11	2.17
MnO	0.06	0.06	0.03	0.07	0.11	0.07	0.06
MgO	0.11	0.52	0.05	4.85	1.61	1.42	0.74
CaO	0.86	0.92	1.07	9.12	8.13	2.12	2.73
Na_2O	3.51	2.53	2.49	3.01	0.39	1.82	2.18
K_2O	5.50	5.22	6.27	2.39	3.79	4.60	3.88
P_2O_5	0.02	0.04	0.11	0.50	0.21	0.13	0.13
LOI	0.05			1.98	4.76	3.99	3.08
Total[4]	99.53	96.59	98.80		99.06	100.17	100.44
Sc	1	1	6				
V	8	8	13	185	40	8	<5
Cr		<1	1		29	13	24
Co	3	7.8		27	4.1	2.9	2.4
Ni	5	0.7	9	87	<10	<10	<10
Cu	7.0	36.5	4	26	<10	<10	<10
Zn	145	108	53	525	56	43	50
Ga	20	24	16	19	19	19	18
As	3.6	4.4		209	51	<5	39
Rb	180	158	279	62	139	154	99
Sr	13	61	127	641	107	145	592
Y	84.0	86	42	21	19.0	18	18.0
Zr	577	528	213	173	186	158	146
Nb	44	46.5	29.3	15	16	19	19
Mo	15.0	4.64		1.7	2.1	1.7	2.0
Sb	0.2	0.62		11	7.8	0.5	44.0
Ba	140	1006	826	1076	931	1085	1395
La	120	71.3	47	42	44.0	43	44.0
Ce	200	146.5	103	83	75.0	81	83.0
Pr		17.5		9.6	9.0	8.7	8.8
Nd	99	67.8		35	31.0	30	30.0
Sm	15.0	14		6.4	5.4	5.1	4.9
Eu	1.3	1.4		1.7	1.2	1.14	1.1
Gd		14		5.3	4.0	3.8	3.9
Tb	2.3	2.2		0.7	0.6	0.6	0.6
Dy		13.3		3.6	3.0	2.8	2.9
Ho		2.9		0.6	0.5	0.5	0.5
Er		8.5		1.8	1.7	1.6	1.6
Tm		1.2		0.25	0.25	0.24	0.23
Yb	9.5	7.9		1.6	1.5	1.5	1.5
Lu	1.43	1.2		0.23	0.22	0.23	0.25
Hf	19.0	16.7		4.6	4.8	4.6	4.3
Ta		3.25		0.9	1.2	1.65	1.7
W	6.0			1	1.3	1.6	1.3
Tl		1.16		0.6	6.0	0.9	2.0
Pb	32.0	25	24	26	21.0	18	30.0
Bi		0.77		0.4	1.9	0.6	1.7
Th	19.0	18	19	9.3	10.0	12	12.0
U	5.8	5.7		1.9	3.6	4	5.2

and Jurassic Igneous Rocks In and Adjacent to the Carlin Trend, Northeastern Nevada

					Welches Canyon intrusions		
Pl-bi-hbl-qtz±sa rhyolite			Aphyric rhyolite		Diorite	Pl-bi-hbl andesite–dacite	
BST-130	RICH-10	H97-22A	DSU-143-30	DS-1	WC-31	H97-21	WC-3
8	9	10	11	12	13	14	15
Pit	Outcrop	Outcrop	Core	Underground	Outcrop	Outcrop	Outcrop
40°56.37'	40°51.8'	40°47.9'	40°57.7'	40°57.7'	40°47.73'	40°47.4'	40°47.75'
116°21.40'	116°18.2'	116°18.4'	116°21.7'	116°21.7'	116°17.92'	116°19.1'	116°18.08'
Dike	Dike	Dike	Dike	Dike	Intrusion	Dike	Dike
Mild clay	Mild clay	Fresh	Devitrified	Hydrated glass	Fresh	Fresh	Fresh
U, N	U, N	W, C	U, N	U, N	U	W, C	U, A
71.21	77.33	72.59	76.98	75.09	61.28	62.64	64.96
0.31	0.21	0.30	0.07	0.05	0.83	0.74	0.59
15.19	14.72	14.66	14.09	14.64	17.34	17.14	17.48
2.05	1.58	1.88	0.88	0.86	5.79	5.34	3.71
1.37	0.06	0.04	0.09	0.09	0.13	0.13	0.08
3.10	0.55	0.84	0.68	0.06	2.33	2.41	1.13
2.25	0.52	2.99	0.99	1.57	5.47	5.08	4.27
0.10	0.46	2.20	1.07	2.39	3.88	3.66	4.35
4.32	4.45	4.38	5.12	5.18	2.62	2.54	3.20
0.11	0.11	0.13	0.04	0.05	0.32	0.33	0.22
7.13	3.40		4.97	8.14	0.48		0.23
100.09	99.33	97.33	99.38		98.93	98.09	98.83
5	2	6	2	2		14	
46	20	22	2	8		93	47
		2				1	63
	2	11.1	<1			18.7	7.5
9	5	1.1	2	2		1.6	35
5	<2	3.9	2	1		9.9	35
52	25	45	28	44		105	40
	23	18	29	13		20.5	20
12.8		1.3	17.0	32.0		<0.2	<5
149	289	139	150	299		61	93
58	55	328	91	862		725	673
10.0	16	14	20.0	50.0		18	23.0
	69	133	72	72		158	199
	13	17.2		29		13.3	15
<2	4	0.62	3.0	6.0		0.91	2.6
7.6	3.9	0.91	1.8	6.5		0.08	0.4
1100	723	1406	640	1300	1180	1261	1070
27.6	25	36.9	12.0	12.0		39.1	48.0
51.0	36	67.8	23.0	23.0		73.5	90.0
		7.4				8.8	10.1
18.0	21	26.6	9.0	9.0		34.5	37.0
3.5	3	4.8	2.5	2.5		6.8	6.4
1.0	0.8	0.8	0.6	0.5		1.6	1.6
		4.1				5.8	5.0
<0.5	0.6	0.4	<0.5	<0.5		0.6	0.7
		2.2				3.3	3.7
		0.3				0.6	0.7
		1.2				1.9	2.2
		0.1				0.2	0.33
1.1	2.1	1.1	1.8	2.2		1.7	1.9
0.17	0.2	0.1	0.30	0.26		0.2	0.30
	1	2.1	2.0	2.0		1.9	5.6
1.0	0	1.34	2.3	2.4		1.12	1.2
3.0							1.0
		0.7				0.14	0.4
30.0	27	30	28.0	21.0		19	16.0
		0.27				<0.01	0.3
13.8	11	13	4.9	4.9		9	13.0
5.7	10	5.4	6.3	6.4		2.1	3.6

TABLE 3

Age	Emigrant Pass volcanic field								
Rock type[1]	Bob Creek lava Hbl andesite	Primeaux lavas Pl-px±hbl andesite–dacite			Mack Creek lavas Pl-bi-hbl andesite–dacite			Late porphyritic Pl-bi-hbl-qtz±sa rhyolite	
Sample no.	H98-20	H98-27	H98-68	H98-101	H98-97	H98-1	H98-96	H98-56	H98-102
No. in Figure 6	Emigrant Pass analyses shown as field of data, not as individual samples, on Fig. 6								
Sample type	Outcrop	Outcrop	Outcrop	Outcrop	Outcrop	Outcrop	Outcrop	Outcrop	Outcrop
Latitude	40°40.8'	40°39.0'	40°41.6'	40°45.1'	40°44.5'	40°41.6'	40°44.7'	40°42.2'	40°44.7'
Longitude	116°20.7'	116°16.5'	116°20.0'	116°17.1'	116°20.0'	116°24.8'	116°20.7'	116°18.1'	116°17.1'
Occurrence	Lava	Lava	Lava	Lava	Lava	Intrusion	Lava	Dike	Dike
Alteration	Fresh	Fresh	Fresh	Fresh	Fresh	Fresh	Fresh	Fresh	Fresh
Analyses[2]	W, C	W, C	W, C	W, C	W, C	W, C	W, C	W, C	W, C
SiO_2	57.89	60.30	63.61	65.88	59.76	65.11	67.10	68.53	71.45
TiO_2	1.20	0.94	0.78	0.64	0.98	0.73	0.62	0.46	0.41
Al_2O_3	16.10	17.26	16.67	16.75	16.83	15.98	15.20	16.07	14.53
FeO[3]	7.79	6.15	5.03	4.14	6.86	4.55	3.73	2.70	2.09
MnO	0.13	0.11	0.12	0.09	0.10	0.11	0.09	0.04	0.05
MgO	3.37	2.65	2.08	1.05	2.84	2.29	1.87	1.18	1.15
CaO	7.72	6.01	4.88	3.99	6.46	4.68	3.99	2.96	3.23
Na_2O	2.98	4.12	3.75	3.92	3.36	2.97	3.20	3.77	3.51
K_2O	2.37	2.15	2.80	3.28	2.52	3.32	4.00	4.09	3.40
P_2O_5	0.43	0.32	0.28	0.25	0.31	0.27	0.20	0.21	0.16
LOI									
Total[4]	99.16	99.32	98.63	99.77	98.77	97.68	98.80	99.22	99.60
Sc	24	19	13	12	17	8	12	4	3
V	202	148	106	67	156	97	89	49	52
Cr	94	7	4	2	41	19	20	6	10
Co	26.2	20.7	21.1	13.3	21.7	19.9	23.9	15.5	23.1
Ni	30.4	3.9	3.3	2	24.5	6.8	10.3	9.2	5.6
Cu	9.7	6.2	7.9	5.3	19.2	23	12.5	6.3	4.8
Zn	83	85	82	67	92	89	68	88	48
Ga	20.6	21	21.8	21.8	23.3	20.2	20.4	21.6	18.95
As	3.7	2.9	0.6	2.2	1	7.2	4.5	2.9	3.3
Rb	38	56	71	94	64	86	113	111	133
Sr	839	892	699	668	740	565	528	536	516
Y	25	19	21	21	22	20	18	14	11
Zr	174	203	196	191	149	181	152	143	115
Nb	13.5	12.4	14.7	20.6	13.9	14.8	17.0	14.8	12.8
Mo	0.43	1.49	0.96	1.1	1.15	1.32	2.76	1.27	0.7
Sb	0.48	0.55	0.11	0.13	0.2	1.12	0.46	0.55	0.49
Ba	981	1217	1326	1134	1122	1424	1084	1713	1007
La	37.8	43.3	44.5	42.3	31	40.1	30.6	31.4	25.7
Ce	75.3	78.6	82.8	77.9	58	74.2	57.1	58.8	46.4
Pr	8.6	9.2	9.4	9	7.5	8.5	6.5	6.5	5.5
Nd	36.4	35.4	34.5	34	31.4	31.8	25.9	25.3	19.9
Sm	6.5	6	6.2	5.8	5.9	5.7	4.4	4.1	3.4
Eu	1.7	1.6	1.6	1.4	1.6	1.5	1.1	1	0.8
Gd	6.1	5.5	5.6	5.3	5.5	5.2	4.1	3.8	3.1
Tb	0.8	0.7	0.7	0.7	0.7	0.7	0.5	0.4	0.3
Dy	4.7	3.6	3.7	3.5	3.9	3.4	2.8	2.3	1.8
Ho	0.9	0.7	0.7	0.6	0.8	0.6	0.5	0.4	0.3
Er	2.6	1.9	2.1	2	2.1	1.9	1.6	1.2	1
Tm	0.3	0.2	0.2	0.2	0.3	0.2	0.2	0.1	0.1
Yb	2.1	1.6	1.8	1.7	1.8	1.7	1.5	1	0.9
Lu	0.3	0.2	0.3	0.2	0.2	0.2	0.2	0.1	0.1
Hf	4.7	5.6	2.8	5.1	3.4	2.2	4	3.1	2.2
Ta	0.85	0.93	1.44	1.47	0.86	1.86	2.11	1.56	1.91
W									
Tl	0.12	0.28	0.38	0.39	0.2	0.46	0.71	0.58	0.57
Pb	6	12	16	17	16	18	24	22	20
Bi	0.02	0.03	0.01	0.08	0.02	0.05	0.2	0.12	0.09
Th	7	10	12	11	7	12	12	9	7
U	1.5	2	2.2	3.8	2.2	3.7	6.7	4.6	3.1

[1] Bi = biotite, hbl = hornblende, phl = phlogopite, pl = plagioclase, px = pyroxene, qtz = quartz, sa = sanidine

[2] Analytical methods: A = ICP/MS at Actlabs, C = ICP/MS and ICP/AES at ALS Chemex, N = INAA at XRAL Laboratories (SGS Canada), U = XRF at

[3] Total Fe reported as FeO

[4] Total before normalization to 100% anhydrous

(Cont.)

	Cretaceous Richmond intrusion	Jurassic Lamprophyre dikes		Goldstrike and related intrusions				Rhyolite dike
dikes –dacite	Granite	Phl lamprophyre	Hbl lamprophyre	Diorite	Diorite	Diorite	Granodiorite	Pl-bi±qtz rhyolite
H98-61	RICH-1	GEN-3	DS-40	TURF-11	NS-1	98-ZIA-7	GEN-2-1534	98-Zia-9
	16	17	18	19	20	21	22	23
Outcrop	Outcrop	pit	underground	Outcrop	pit	Outcrop	core	Outcrop
40°40.8'	40°51'05"	40°57'00"	40°51.67'	40°56.97'	40°57.42'	40°56.47'	40°57.5'	40°56.18'
116°19.8'	116°18'25"	116°21'40"	116°21.75'	116°18.95'	116°21.47'	116°21.40'	116°22.0'	116°23.22'
Dike	intrusion	Dike	Dike	Intrusion	Intrusion	Intrusion	Dike	Dike
Fresh	Fresh	Chlorite/carbonate	Mild epidote	Slight propylitic	Fresh	Fresh	Fresh	Fresh
W, C	U, A	U, A	U, N	U, N	U, A	U, N	U, N	U, N
74.78	75.04	52.69	53.85	53.47	58.01	60.43	66.44	73.57
0.23	0.17	1.04	1.08	1.05	0.94	0.99	0.80	0.21
13.49	13.73	12.27	13.85	13.17	15.95	18.02	15.38	15.23
1.47	1.32	7.93	7.69	8.76	6.26	5.94	3.88	1.02
0.03	0.03	0.09	0.13	0.12	0.11	0.11	0.05	0.03
0.28	0.41	11.42	9.98	11.12	6.40	2.47	2.04	0.36
1.61	1.16	9.29	8.25	7.71	6.77	5.70	3.42	1.67
3.54	3.21	2.69	2.76	1.92	3.07	3.32	3.08	3.76
4.46	4.86	2.03	2.04	2.36	2.22	2.74	4.72	4.06
0.10	0.08	0.54	0.38	0.32	0.27	0.29	0.19	0.09
	0.62	8.28		0.10	0.70	0.04	2.15	0.72
99.52	100.69	99.40	98.96	96.73	98.51	99.05		97.56
4			21	19		11	9	4
9	7	185	181	146	164	127	82	24
1								
18.2	1.6	43	35	24	21	10	9.0	1.0
1.1	37	211	327	88	31	2	30	26
2.9	280	144	36	16	<10	9	24	11
44	14	58	66	81	67	68	44	157
18.1	16	16	12	17	19	20	18	12
1.6	<5	9.0	4.6	2.5	<5	1.7	8.1	3.9
154	285	68	54	59	72	93	167	99
316	202	1398	1200	771	1012	844	501	507
19	16.0	27.0	21.0	23	28.0	32.0	31.0	30.0
175	112	182	234	203	191	270	340	151
18.3	29	9	14	22	15	25	26	25
1.93	1.0	0.8	4.0	<1	1.4	8.0	4.0	8.0
0.33	0.2	1.6	0.4	0.4	0.5	0.1	1.8	0.8
1146	482	1390	1242	960	826	938	666	2062
42.2	34.0	133.0	76.0	52	56.0	60.0	94.0	58.0
75.1	62.0	265.0	150.0	100	113.0	89.0	140.0	93.0
8.3	6.0	28.3			13.3			
29.1	19.0	107.0	55.0	30	50.0	39.0	49.0	36.0
4.9	2.9	18.0	9.2	6.4	8.9	6.4	7.7	4.9
1	0.5	4.3	3.1	2	2.2	1.9	1.8	1.6
4.4	2.1	12.0			6.7			
0.6	0.3	1.3	<0.5	0.8	0.9	0.8	<0.5	<0.5
2.8	1.8	5.2			4.9			
0.5	0.4	0.8			0.9			
1.6	1.3	2.4			2.7			
0.2	0.28	0.26			0.37			
1.4	2.0	1.6	1.8	2.4	2.3	2.5	2.1	2.3
0.2	0.40	0.24	0.30	0.38	0.35	0.47	0.45	0.34
3.5	3.7	5.0	6.0	7	5.4	7.0	13.0	6.0
2.46	3.4	0.7	1.4	1	1.1	1.5	2.2	1.8
	23	0.9	<1	<1	1.0	<1	<1	<1
0.87	1.6	0.3			0.3			
21	15.0	8.0	19.0	12	16.0	18.0	18.0	44.0
0.01	45.0	1.1			0.5			
16	41	32	13	12	12	11	29	13
4.7	14.0	5.2	3.0	3.5	2.3	3.6	8.7	4.3

University of Nevada, Reno, W = XRF at Washington State University; all analyses normalized to 100% anhydrous

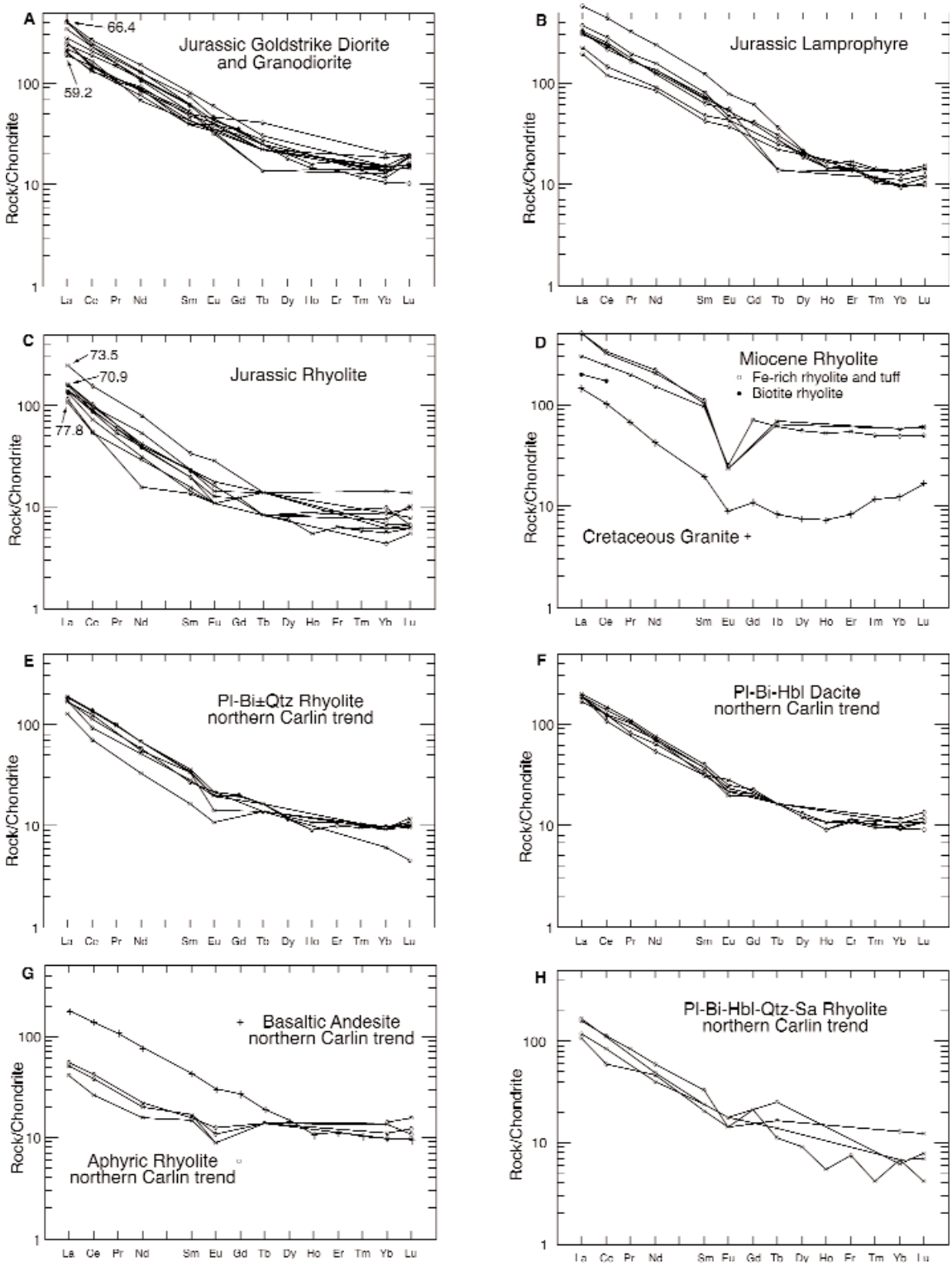

FIG. 8. Chondrite-normalized rare earth element patterns for rocks of the Carlin trend (normalization values from Anders and Grevesse, 1989). Bi = biotite, Hbl = hornblende, Pl = plagioclase, Qtz = quartz, Sa = sanidine. A.-C. Jurassic rocks. LREE concentrations generally increase with increasing SiO_2 in the Goldstrike diorite and related rocks. Number labels at La are wt percent SiO_2 for the most and least silicic samples. Lamprophyres have the highest REE concentrations of any Jurassic rocks. LREE generally decrease with increasing SiO_2 in rhyolite (labels at La), with one anomalous sample. D. Miocene rhyolite and Cretaceous granite. Biotite rhyolite was analyzed by XRF only, and only La and Ce were determined. E.-M. Eocene rocks. Irregular HREE patterns are due to the low concentrations of odd atomic number elements (Tb, Ho, Tm, and Lu), which were near detection limits. A trend through the even-numbered elements (Gd, Dy, Er, and Yb) is probably more representative of the patterns.

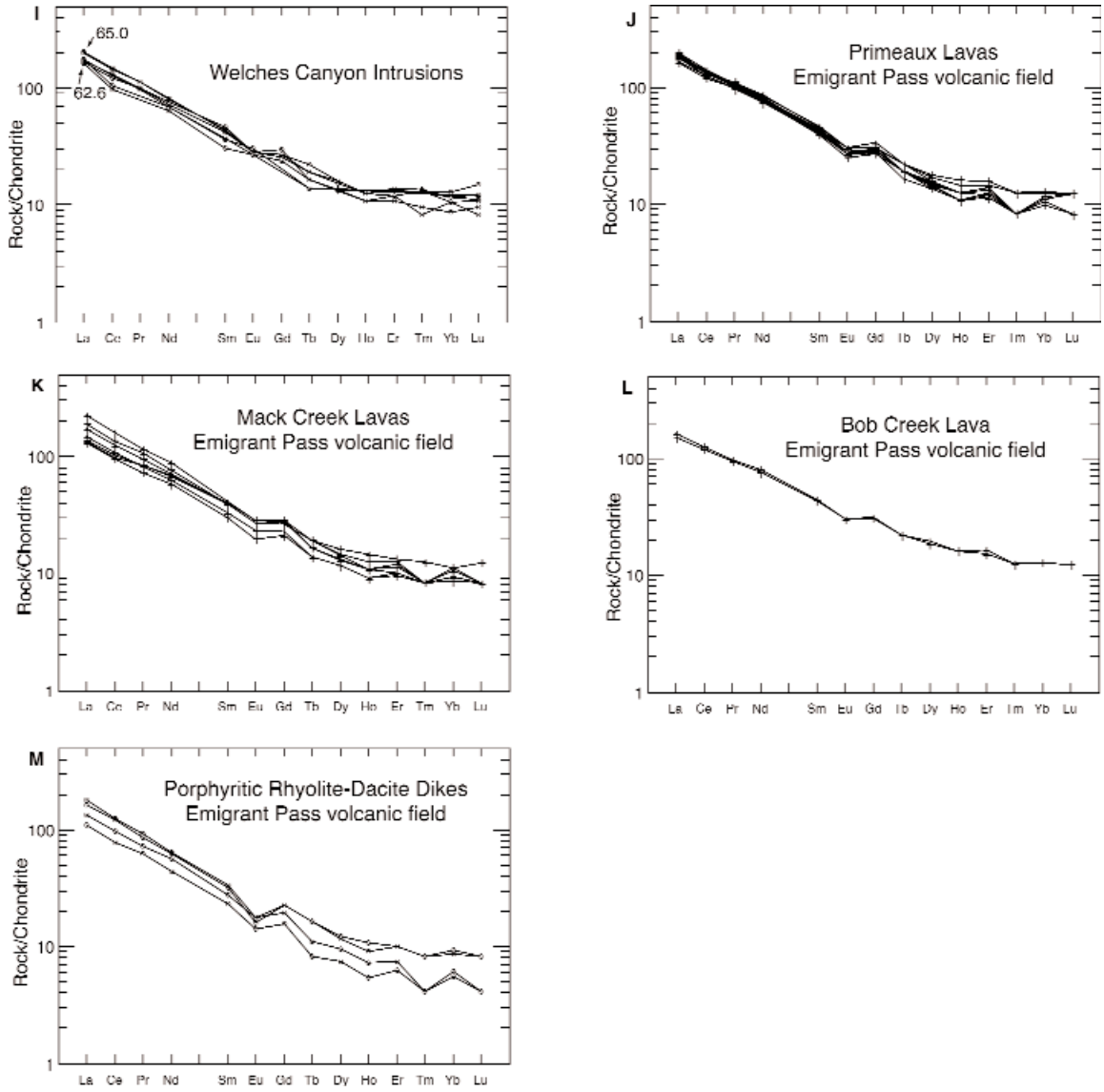

FIG. 8. *(Cont.)*

dikes along the Post fault zone and merging of the long dike with the fault zone suggest that intrusion and fault movement were coeval. Composite dikes in which porphyritic rhyolite adjoins porphyritic dacite or aphyric rhyolite are common.

Porphyritic rhyolite dikes are among the oldest Eocene dikes of the Carlin trend. $^{40}Ar/^{39}Ar$ ages of biotite from four samples range from 40.3 ± 0.2 Ma at Genesis to 39.32 ± 0.11 Ma at Betze-Post (Table 1). The oldest and youngest samples also have the flattest and, what we consider, the most reliable age spectra and are supported by similar isochron ages. Two other samples have disturbed, decreasing spectra, the true age of which, other than ~39-40 Ma, are difficult to interpret (Fig. 4). Weighted mean, isochron, and total gas ages agree relatively well at about 39.9 Ma for sample DSU-190-906. The three age calculations do not agree as well for sample H00-50. Its total gas age of 39.7 ± 0.2 Ma is slightly younger than the 40.3 ± 0.2 Ma age on what appears to be the same dike. Emplacement of similar rhyolite dikes may have continued for ~1 m.y.

Porphyritic (plagioclase-biotite-hornblende) dacite (40.1–39.0 Ma): Porphyritic dacite dikes are abundant in a 5-km-long belt between Meikle and Betze-Post where they parallel and intrude the Post fault zone. Dacite dikes are present mostly north of the porphyritic rhyolite dikes, but the two types occur together, commonly as composite dikes, in the Betze-Post deposit. The presence of large euhedral hornblende phenocrysts is a distinguishing feature. In all but one exposure, hornblende is altered to rims of biotite and cores of calcite and smectite but is recognizable by its shape (Fig. 7).

$^{40}Ar/^{39}Ar$ biotite ages range from 39.46 ± 0.08 Ma in the Griffin deposit to 40.13 ± 0.21 Ma in Betze-Post. Hornblende from the one location where it was unaltered gives a younger plateau age of 38.95 ± 0.22 Ma, which is supported by an isochron age of 39.03 ± 0.23 Ma. Relatively imprecise U-Pb

TABLE 4. Characteristics of Eocene Igneous Rocks of the Carlin Trend, Northeastern Nevada

Unit	Rock type	Texture	Phenocrysts	Age	Distinguishing features	Extent; volume
Northern Carlin trend						
Porphyritic (pl-bi-hbl-qtz ± sa) rhyolite dikes	Low silica rhyolite to high silica dacite	Coarsely porphyritic, aphanitic	Pl: 5–15%, 1–6 mm Qtz: 1–2%, 1–4 mm Sa: 0–2%, 1–15 mm Bi: 1–3%, 1–4 mm Hbl: 1–4, 1–2 mm	37.6 Ma	Ore host at Beast; identical to late porphyritic dikes of Emigrant Pass;	3-km-long dike at Beast mine; several dikes to south
Basaltic andesite dikes	Basalt to basaltic andesite	Sparsely porphyritic, aphanitic	Pl: <0–1%, <5 mm Px:1–2%, <3 mm Ol: 3%, <3 mm	37.8 Ma	Dense mafic dikes; altered, weakly mineralized at Dee	Several dikes near Dee and Goldstrike deposits
Aphyric rhyolite dikes	High silica rhyolite	Aphyric	Sparse microlites of feldspar, Fe-rich pyroxene, and zircon	~39.1 Ma	Commonly glassy; locally altered ± mineralized	Several dikes; total 8 km long
Porphyritic (pl-bi-hbl) dacite dikes	Dacite	Finely to coarsely porphyritic, aphanitic	Pl: 15%, 1–6 mm Bi: 2%, 1–5 mm Hbl: 3–5%, 2–10 mm Qtz: 0–1%, <3 mm	40.1–39.0 Ma	Hbl ghosts altered to bi rims and smectite-calcite cores; host ore at Griffin and Meikle; altered at Betze-Post	≥5-k-m-long swarm from Betze-Post to Meikle
Finely porphyritc (pl-bi ± qtz) rhyolite dikes	Rhyolite	Finely porphyritic, aphanitic	Pl: 5–7%; 1–2 mm Bi: 2–4%; 1–3 mm Qtz: 0–1%; 1–2 mm	40.3–39.3 Ma	Sparsely porphyritic; commonly glassy	Abundant dikes along Post fault system
Welches Canyon						
Aphyric rhyolite dome and dikes	Rhyolite	Aphyric		Post 38.6 Ma, pre 37.4 Ma	Flow-banded, partly glassy but clay-altered	Small volcanic dome and abundant dikes
Porphyritic andesite to dacite	Andesite to dacite	Strongly porphyritic, aphanitic	Pl: 5–15%, 1–6 mm Qtz: 1–2%, 1–4 mm Sa: 0–4%, 1–15 mm Bi: 1–3%, 1–4 mm Hbl: 1–4, 1–2 mm	38.6 Ma	Aphanitic, locally glassy, mostly coarsely porphyritic	Abundant N and NE dikes
Microdiorite (Tg)	Diorite	Fine-grained, equigranular, phaneritic	Pl: 55–60% Px: 15–20% Altered hbl: 10% Qtz: 10%	38.6 Ma	Fine-grained, equigranular, intermediate intrusion; propylitized	1-km² stock; south side of Welches Canyon
Emigrant Pass volcanic field						
Porphyritic (pl-bi-hbl-qtz ± sa) rhyolite-dacite dikes	Rhyolite to high silica dacite	Coarsely porphyritic	Pl: 5–15%, 1–6 mm Qtz: 1–2%, 1–4 mm Sa: 0–2%, 1–15 mm Bi: 1–3%, 1–4 mm Hbl: 1–4, 1–2 mm	36.2 Ma	Coarsely porphyritic	~10-km-long belt
Bob Creek lava (Tb)	Andesite (57% SiO_2)	Porphyritic	Hbl: 12%, 1–8 mm Px: 3–5%; 1 mm Pl: trace; ≤1cm	37.4 Ma	Hbl>>pl	30 km²; 3 km³
Mack Creek lavas and intrusions (Tk)	Dacite	Coarsely porphyritic	Pl: 15–30%, 1–5 mm Hbl: 6–10%, 1–7 mm Bi: 3%, ≤3 mm Qtz: 0–3%, 1–3 mm Px: 1–3%, 1 mm	37.9–37.6 Ma	Abundantly to moderately and coarsely porphyritic domes	~12 km²; ~5 km³
Primeaux lavas (Tp)	Andesite	Finely, abundantly porphyritic	Pl: 16–30%, ≤2 mm Hbl: 4–10%, 1–8 mm Px: 1–4%, ≤1 mm Bi: 0–2%, ≤3 mm	38.1–37.9 Ma	Finely porphyritic andesite, but coarse hbl	75 km²; ~30 km³
Rain-Railroad						
Diorite and basaltic andesite dikes	Andesite to basaltic andesite	Porphyritic, aphanitic	Pl: 5–10%; 1–3 mm Px: 1–3%; 1 mm Pl: <1 %; 2 mm Altered hbl: <2%; 2 mm	39.1, 38.2 Ma	Mafic porphyritic dikes; mostly highly altered along Rain fault	Several dikes; several km long at and NW of Rain
Porphyritic (pl-bi-hbl-qtz ± sa) rhyolite stock and dikes	Rhyolite to dacite	Coarsely porphyritic	Pl: 5–15%, 1–6 mm Qtz: 1–2%, 1–4 mm Sa: 0–2%, 1–15 mm Bi: 1–3%, 1–4 mm Hbl: 1–4, 1–2 mm	37.5–37.4Ma	Nearly identical to coarsely porphyritic rhyolite dikes of Carlin trend	1-km² porphyry stock at Railroad and radial dikes; also dikes at Emigrant Springs

Abbreviations: bi = biotite, hbl = hornblende, ol = olivine, pl = plagioclase, px = pyroxene, qtz = quartz, sa = sanidine

zircon ages of 37.8 ± 2.1 Ma from Betze-Post and 38.1 ± 0.8 Ma from Griffin (Mortensen et al., 2000) overlap with the hornblende age. Emplacement of these dikes probably spanned from ~40.1 to 39.0 Ma.

Aphyric rhyolite (39.1 Ma): Aphyric, glassy to devitrified, high SiO_2 rhyolite dikes are widely distributed in the Deep Star and Genesis mines, the western and southern flanks of Richmond Mountain, and in Welches Canyon. A larger (~1 km^2), probably extrusive body of aphyric rhyolite is present in Welches Canyon. A swarm of aphyric rhyolite dikes intrudes along the Post and parallel faults in the Deep Star mine. From crosscutting relationships, Dunbar (2001) and Heitt et al. (2003) suggested that two stages of aphyric rhyolite were emplaced closely in time and bracket the age of high-grade (>30 g/t) gold mineralization at Deep Star.

The dikes are distinguished by their lack of phenocrysts, prominent flow bands, green to red-brown glassy margins, and white felsitic cores (Fig. 7). Dikes range in width from 0.5 to 12 m. Thin dikes are entirely glassy. Cores of thick dikes are devitrified to a spherulitic and granophryic mix of sanidine and quartz.

The very fine grained, devitrified matrix and lack of phenocrysts have made a precise age of the aphyric rhyolites difficult to obtain (Ressel et al., 2000a; Heitt et al., 2003). Poor retention of radiogenic ^{40}Ar and redistribution of ^{39}Ar by recoil, the kinetic energy imparted on a ^{39}Ar atom by emission of a proton during irradiation, are problems for very fine grained samples such as devitrified rhyolite. The best estimates of the emplacement age are 39.15 ± 0.26 Ma (sample DSU-150-106, Table 1, Fig. 4), which provided the flattest spectra of the three analyzed samples and is supported by an indistinguishable isochron age (39.07 ± 0.33 Ma) and an isochron age of 38.98 ± 0.05 on sample DS-13. Petrographically similar, aphyric rhyolites around Richmond Mountain and in Welches Canyon are included in this group in Figure 2 but are undated and need not be the same age as the dated dikes in the Carlin trend.

Basaltic andesite (37.8 Ma): The only mafic Eocene intrusions in the northern Carlin trend are basaltic andesites at the Dee mine and covered by Miocene rocks about 2 km west of the Betze-Post mine. The dikes at Dee intruded along the north-striking, west-dipping Dee fault, the major ore-controlling structure (Dobak et al., 2002). A relatively fresh, podlike intrusion in the immediate footwall of the Dee fault contains sparse phenocrysts of calcic plagioclase, olivine, and clinopyroxene (Fig. 7). Matrix from a sample of this body yielded good plateau and isochron ages of 37.80 ± 0.21 and 37.73 ± 0.17 Ma (Table 1, Fig. 2), indicating that mineralization at Dee postdated ~37.8 Ma.

Porphyritic (plagioclase-biotite-hornblende-quartz ± sanidine) rhyolite and dacite (37.6 Ma): Dikes of coarsely porphyritic, low SiO_2 rhyolite and high SiO_2 dacite form a discontinuous, 16-km-long belt from the Beast deposit, where they host ore, southward to Welches Canyon (Figs. 2, 5–6: Ressel et al., 2000a). Coarse phenocrysts (e.g., biotite up to 1 cm and sanidine to 2 cm; Fig. 7) are particularly distinctive. Petrographically similar dikes are found in almost all Eocene igneous centers in Nevada (Ressel et al., 2000a; Castor et al., 2003).

In the northern Carlin trend, these dikes were emplaced along and parallel to the north-northwest–striking Gen, Beast, and other faults that make up the Post fault zone in that area. The dike at the Beast mine is one of the largest, at least 3 km long and as much as 55 m wide, and contained about half the ore mined there (Ressel et al., 2000a). Coarsely porphyritic dikes have nearly indistinguishable $^{40}Ar/^{39}Ar$ ages of 37.58 ± 0.06 Ma at the Beast mine, 37.58 ± 0.05 Ma at Richmond Mountain, and 37.43 ± 0.06 Ma in Welches Canyon (Table 1; Figs. 2, 5). The dike at Richmond Mountain was one of those mapped as Cretaceous by Evans (1974b).

Geochemistry: Almost all dikes of the Carlin trend are rhyolite or dacite with 66 to 77 percent SiO_2; the few basaltic andesites have ~55 percent (Fig. 6; Tables 3–4). All dikes are moderately alkalic, similar to Jurassic rocks. This is well illustrated by the K_2O/SiO_2 plot, but Na_2O loss due to alteration of plagioclase has distorted total alkali/SiO_2 trends. The relatively unaltered rocks of the Emigrant Pass volcanic field are probably the best indicators of prealteration alkali contents of the dikes.

Major oxide and REE concentrations of the different suites of dikes support our field, petrographic, and age subdivisions (Figs. 6, 8). With the exception of the plagioclase-biotite ± quartz and plagioclase-biotite-hornblende-quartz ± sanidine rhyolites, the different dikes have distinct SiO_2 contents, which are consistent with their petrographic characteristics. Apparent variations in SiO_2 may partly relate to alteration. For example, analyzed SiO_2 contents in six dacites range from 66 to 70.5 percent, but REE concentrations are almost indistinguishable, with steep slopes and small Eu anomalies (Fig. 8). The dacites and basaltic andesites have the highest REE concentrations, although the difference is mostly in LREE. Progressively more silicic rocks have progressively lower LREE concentrations and generally larger Eu anomalies. The plagioclase-biotite ± quartz and plagioclase-biotite-hornblende-quartz ± sanidine rhyolites again overlap. Eocene rocks have distinctly lower REE, especially LREE, concentrations than do Jurassic Goldstrike intrusions or lamprophyres.

Igneous rocks of Welches Canyon

Eocene intrusions of Welches Canyon are distinguished as a separate group because they include the northernmost occurrence of larger, stocklike intrusions (Fig. 2) and range from rhyolite through andesite, a wider compositional range than dikes of the northern Carlin trend (Fig. 6, Table 3). Eocene rocks fall into three categories: aphyric rhyolite, porphyritic andesite-dacite, and fine-grained diorite-granodiorite. Aphyric rhyolites in Welches Canyon are similar to the dikes in the northern Carlin trend but are discussed separately because they are 10 km south of the northern cluster, include one much larger intrusion or volcanic dome, and are probably a different age.

Aphyric rhyolite (~38 Ma): Aphyric rhyolite dikes are common in a 10-km belt from north of the Cretaceous Richmond granite to south of the larger body in Welches Canyon (Fig. 2). Most dikes are single bodies a few meters wide, but the northernmost dike is part of a composite body together with the 37.6 Ma porphyritic rhyolite. The large (~1 km^2) body in Welches Canyon has steep flanks, contains a carapace breccia on its eastern flank, and has widespread curvilinear joints or "ramp" structures. These features suggest it may be a volcanic

dome. If so, it is the northernmost Eocene volcanic rock near the Carlin trend and thus could mark the closest recognized Eocene paleosurface. If it is intrusive, it must have underlain the surface by no more than ~200 m, based on the elevation of the Eocene paleosurface marked by Emigrant Pass volcanic rocks just to the south. This body must be younger than 38.6 Ma, the age of the fine-grained diorite it cuts, and older than 37.4 Ma, the age of a porphyritic rhyolite dike that cuts it.

Fine-grained diorite-granodiorite (38.6 Ma): A small intrusion consisting of fine-grained diorite and lesser granodiorite underlies an area of about 0.9 km² in Welches Canyon adjacent to the body of aphyric rhyolite (Fig. 2). Plagioclase from granodiorite yielded an $^{40}Ar/^{39}Ar$ age of 38.59 ± 0.12 Ma (Table 1). Most of the diorite has undergone a higher degree of hydrothermal alteration than the adjacent rhyolite, which suggests that the diorite is older.

Porphyritic (plagioclase-biotite-hornblende) andesite-dacite (38.6 Ma): One thick (200 m) and numerous thinner dikes of porphyritic andesite and dacite cut upper plate Paleozoic rocks around Welches Canyon. The dikes are similar mineralogically to fine-grained diorite, but are strongly porphyritic and locally glassy. Hornblende from the largest porphyritic andesite dike in Welches Canyon yielded an $^{40}Ar/^{39}Ar$ age of 38.59 ± 0.17 Ma, which is identical to the age of the diorite-granodiorite. Both rocks are slightly older than the oldest units of the Emigrant Pass field (~38.1 Ma) just 4 km to the south and fall within the 39.1 to 37.6 Ma hiatus in magmatism of the northern Carlin trend.

Geochemistry: Most Welches Canyon intrusions have between 61 and 65 percent SiO_2 and are distinctly less silicic than dikes of the Carlin trend (Fig. 6). The aphyric rhyolite in Welches Canyon is probably compositionally similar to the aphyric rhyolites of the Carlin trend but was not analyzed. Most Welches Canyon intrusions are less altered than are the Carlin dikes, which is apparent on the total alkali/SiO_2 plot. REE concentrations of Welches Canyon rocks vary only slightly but appear to increase with increasing SiO_2 and are similar to those of the Carlin trend dacites, which they resemble in composition and mineralogy (Fig. 8).

Emigrant Pass volcanic field (38.1–37.4, 36.2 Ma)

In contrast to the dikes and small intrusions of the northern Carlin trend and Welches Canyon, lavas, their eruptive vents, and a few shallow intrusions and dikes dominate the Emigrant Pass field (Fig. 2). Also, in contrast to the Carlin trend dikes, rocks of the Emigrant Pass field are dominantly andesite to dacite, with lesser rhyolite (Fig. 6). The rocks are divided into four sequences on the basis of stratigraphy, age, petrography, and composition (Tables 1, 3–4; Henry and Faulds, 1999). From oldest to youngest, these are the Primeaux andesite lavas (38.1–37.9 Ma), Mack Creek dacite lavas (37.9–37.6 Ma), Bob Creek andesite lava (37.4 Ma), and late porphyritic rhyolite and dacite dikes (36.2 Ma). The Primeaux and Mack Creek lavas, which constitute the greatest volume, are composite units made up of numerous individual lava flows.

The Primeaux lavas are mostly finely and abundantly porphyritic andesite with lesser dacite (60–65% SiO_2, with most ≤63%). The lavas continue ~6 km south of the area shown in Figure 2. They average 300 to 400 m in thickness in the mapped area and have an estimated volume of at least 30 km³. Thick, massive bodies with concentric vertical flow foliations and concentric flow bands in surrounding lavas indicate the locations of at least six vents that fed the lavas. Hornblende $^{40}Ar/^{39}Ar$ plateau and isochron ages on the oldest and youngest parts based on field relationships are 38.1 to 37.9 Ma (Table 1).

The Mack Creek lavas, the younger of the two major sequences, are abundantly and more coarsely porphyritic dacite with lesser andesite (60–67% SiO_2, one sample <63% SiO_2). The more silicic magmas generated relatively localized, thick lava domes, which are restricted to the western parts of the volcanic field. Vents are recognized within the outcrop of two of the domes, and the thick, northeast-striking dike in the western part probably fed lava nearby to the east. The Boulder Valley intrusion (Fig. 2) also may have fed now eroded lavas. The total volume of preserved eruptive rocks is ~5 km³. $^{40}Ar/^{39}Ar$ dates on two lava domes and the two western intrusions range from ~38.1 to 37.6 Ma (Table 1).

The 37.4 Ma Bob Creek lava is a single, extensive andesite lava characterized by ~10 to12 vol percent hornblende phenocrysts and almost no plagioclase phenocrysts. At ~57 percent SiO_2, the Bob Creek lava is the most mafic igneous rock in the Emigrant Pass field. It erupted from a vent in the western part of the volcanic field, extended over an area of approximately 30 km², and is as much as 120 m thick.

The late, porphyritic rhyolite to dacite dikes form two discontinuous, north-northeast–striking belts through the central and northeastern part of the volcanic field. The western belt consists mostly of coarsely porphyritic rhyolite, whereas the eastern belt is mostly dacite. The western belt dikes are petrographically and compositionally indistinguishable from the 37.6 Ma rhyolite dikes of the northern Carlin trend but, at ~36.2 Ma, are distinctly younger.

Our $^{40}Ar/^{39}Ar$ dating indicates that the Primeaux, Mack Creek, and Bob Creek lavas and associated intrusions were emplaced nearly continuously over a period of about 700,000 yr. The distribution of identified vents and shallow intrusions suggests an underlying pluton of at least 20 × 12 km.

The two pulses in the Emigrant Pass volcanic field are compositionally distinct, with SiO_2 concentrations ranging from 57 to 67 percent in the older Primeaux, Mack Creek, and Bob Creek lavas and from 69 to 75 percent in the late, porphyritic rhyolite-dacite dikes (Fig. 6, Tables 3–4). Emigrant Pass rocks are unaltered, which is demonstrated by the narrow trends in the total alkali/SiO_2 and K_2O/SiO_2 plots (Fig. 6). Despite the wide range of SiO_2 concentrations, rocks of the Emigrant Pass field vary little in REE concentrations (Fig. 8). For example, SiO_2 in the Primeaux lavas varies by almost 6 wt percent but La varies only 38 to 46 ppm and does not correlate with SiO_2. The late, porphyritic rhyolite-dacite dikes, which are similar in field and petrographic characteristics to the plagioclase-biotie-hornblende-quartz ± sanidine rhyolite dikes of the Carlin trend, are also indistinguishable in major oxides and REE (Table 3, Fig. 8).

Intrusions of the Rain-Railroad area (39.1, 38.2, 37.5 Ma)

The Rain subdistrict, including the Rain mine and Emigrant deposit, constitutes the southern Carlin trend, which is

~24 km from the Gold Quarry mine, the southernmost mine of the central Carlin trend (Figs. 1, 9). The Rain and Emigrant deposits are in breccias in and near the unconformable contact between Mississippian and Devonian sedimentary rocks. Breccias and orebodies were controlled by, and spread along, the west-northwest–striking Rain fault for about 8 km, especially near intersections with northeast-striking faults (Williams et al., 2000; Mathewson, 2001; Longo et al., 2002). The Emigrant deposit is along the north-striking Emigrant fault. The Railroad mining district, which lies about 10 km south of Rain and Emigrant (Fig. 9) and is not part of the Carlin trend, produced Cu, Pb, and Ag from mantos and veins in Paleozoic rocks adjacent to the Eocene Bullion stock (Ketner and Smith, 1963). Jasperoid-hosted gold deposits are more distant from the stock (Gillerman, 1982; Rayias, 1999).

Eocene igneous rocks of the Rain-Railroad area have been mapped in detail in the Railroad district (Ketner and Smith, 1963; Smith and Ketner, 1978) and in less detail around the

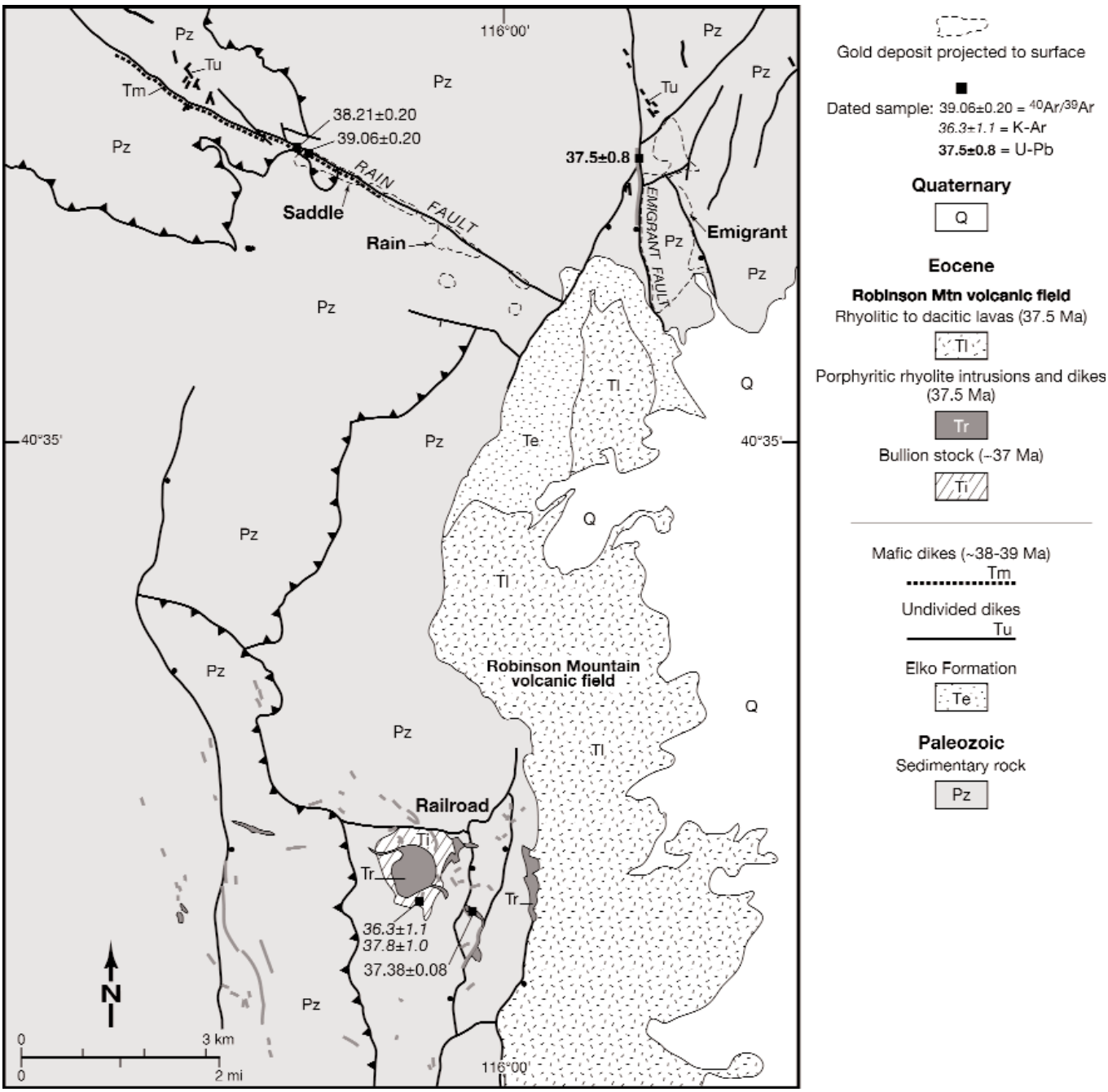

FIG. 9. Simplified geologic map of the Rain mine, Emigrant deposit, and Railroad mining district of the southern Carlin trend, modified from Ketner and Smith (1963), Smith and Ketner (1978), Mathewson (2001), Longo et al. (2002), and unpublished geologic maps by Newmont Mining Corporation. K-Ar dates in the Railroad district are from Smith and Ketner (1976), and the U-Pb date in the Emigrant area is from S. Garwin (*in* Longo et al., 2001).

Rain and Emigrant deposits (Longo et al., 2002). We identify two major packages on the basis of petrography and age (Figs. 1, 9). These are basaltic andesite to porphyritic diorite dikes that intruded along the Rain fault and the large Robinson Mountain volcanic field. The latter consists of a granitic stock in the Railroad district, porphyritic rhyolite to dacite dikes and small stocks around the Railroad district and Emigrant deposit, and porphyritic rhyolite to dacite lavas and tuffs, probably extrusive equivalents of the dikes (Figs. 1, 9). Many dikes around Rain are too altered to be characterized with any confidence and are shown as undivided in Figure 9.

Mafic dikes along the Rain fault are variably altered and locally host ore (Shallow, 1999; Longo et al., 2002). Less altered dikes are identifiable as basaltic andesite and porphyritic diorite, with altered to partly preserved phenocrysts of olivine, pyroxene and/or hornblende, and biotite. The least altered rocks are weakly propylitized but more typically are altered to clay and iron oxides at and near the surface and to clay and iron sulfides at depth. These dikes were initially interpreted as Jurassic lamprophyres because of their mafic phenocrysts (Longo et al., 2002), but our dating indicates that they are Eocene.

Two less altered dikes intersected in core from the Saddle deposit along the Rain fault were dated (Table 1; Figs. 4, 9). Biotite from a porphyritic diorite that contains fresh biotite and partly altered pyroxene and hornblende phenocrysts gives a slightly disturbed spectrum with a weighted mean age of 39.06 ± 0.20 Ma. This is supported by an isochron age of 39.13 ± 0.18 Ma, so reasonably indicates the time of emplacement.

The second dike, a porphyritic basaltic andesite, contains altered pyroxene and olivine phenocrysts in a groundmass of relatively fresh plagioclase. The dike has been propylitically altered with abundant carbonate and about 0.5 vol percent pyrite. A separate of the matrix, with altered phenocrysts, pyrite, and carbonate removed, yielded a disturbed, dropping $^{40}Ar/^{39}Ar$ age spectrum with ages ranging from ~41 to 37.8 Ma that probably indicates recoil. A weighted mean of the flattest, low-temperature part of the spectrum gives an apparent age of 38.21 ± 0.20 Ma (Table 1); an isochron of all steps gives an age of 37.8 ± 1.2 Ma. These data most likely indicate emplacement but possibly alteration at ~38 Ma.

The granitic Bullion stock of the Railroad district and Robinson Mountain field is cut by an inner stock and numerous dikes of porphyritic rhyolite to dacite, which extend as much as 4 km from the stock. The porphyritic dikes contain large phenocrysts of plagioclase, biotite, hornblende, quartz, ±sanidine and are petrographically similar to the coarsely porphyritic rhyolites of the northern Carlin trend and Emigrant Pass field. K-Ar ages of 36.3 ± 1.1 and 37.8 ± 1.0 Ma on rhyolite (Smith and Ketner, 1976) are confirmed by our sanidine date of 37.38 ± 0.08 Ma (Table 1); another hypabyssal intrusion or lava dome farther south in the Robinson field has an age of 37.51 ± 0.19 Ma (Fig. 1, Table 1). Porphyritic rhyolite dikes, termed monzonite porphyry in Longo et al. (2001), are also present in the Emigrant deposit. Longo et al. (2002) reported a zircon U/Pb SHRIMP age on one dike of 37.5 ± 0.8 Ma, which is indistinguishable from our dates (Fig. 9, Table 1). The area between Railroad and Emigrant has not been mapped in detail, and additional dikes may be present.

Numerous lavas and some ash-flow tuffs of coarsely porphyritic rhyolite to dacite, petrographically similar to the dikes at Railroad and Emigrant, make a thick pile that extends from Emigrant to more than 30 km south of the Railroad district (Figs. 1, 9). One of the tuffs gives a $^{40}Ar/^{39}Ar$ age of 37.70 ± 0.19 Ma (Table 1). This age and the petrographic similarity are consistent with the volcanic rocks being extrusive equivalents of the intrusions.

Mineralization at Rain postdates ~38.0 Ma, the age of the younger of the two dikes. That dike contains pyrite, and As and Sb have been added to both dikes. From similar data, Longo et al. (2002) concluded that mineralization at the Emigrant deposit postdates the 37.5 Ma porphyritic rhyolite.

Miocene Rhyolite (15 Ma)

Middle Miocene, sparsely porphyritic, rhyolite lavas are present along the west edge of the northern Carlin trend and between the Emigrant Pass volcanic field and the Rain subdistrict (Fig. 2). The lavas disappear beneath middle Miocene tuffaceous sedimentary rocks and Quaternary deposits in both areas, westward into Boulder Valley from the northern Carlin trend and eastward beneath the Carlin basin in the south. The northern sequence of flows thickens from only a few meters in the east, nearest the trend, to hundreds of meters to the west under Boulder Valley. The southern flows thicken eastward beneath the Carlin basin and southeastward to the southeastern corner (Fig. 2). Rhyolitic, pyroclastic-fall deposits are common in the lower parts of the Miocene stratigraphic sequence throughout the Carlin trend. Some tuffs are related to the rhyolite lavas, although Fleck et al. (1998) suggested that others erupted from sources in southwestern Idaho.

No sources are recognized for these lavas within the Carlin trend. The source of the northern flows could be buried beneath Boulder Valley. The source of the southern flows is probably beneath their thickest pile in the southeast. One of the southern flows east of the Emigrant Pass volcanic field gives a $^{40}Ar/^{39}Ar$ age on sanidine of 15.32 ± 0.08 Ma (Table 1). The northern flows have a K-Ar sanidine date of 14.6 ± 0.3 Ma (Evans, 1974b).

Both northern and southern rhyolite lavas contain 74 to 76 wt percent SiO_2, but they are petrographically and compositionally distinct (Fig. 6, Table 3). The northern lavas have sparse phenocrysts of olivine and Fe-rich pyroxene accompanying sanidine and quartz. They also have high Fe, Zr, Nb, and REE. Concentrations of the LREE are as high as in the Jurassic lamprophyres, but the Miocene rocks have higher HREE and large Eu anomalies (Fig. 8). A pyroclastic-fall deposit within Miocene sedimentary rocks at the southwestern edge of the Emigrant Pass volcanic field has the same chemical signature and probably is related to the lavas. Southern lavas are more typical rhyolites with phenocrysts of biotite accompanying sanidine and quartz and having lower concentrations of Fe, Zr, Nb, and REE. Both compositional types are present near Ivanhoe, but only the Fe-rich rhyolites are present in the northern Nevada rift near Midas (Wallace, 1993, 2003a; John et al., 2000). Miocene mafic to intermediate lavas, although abundant in the northern Nevada rift just 20 km to the west (John et al., 2000, 2003; John, 2001), are absent within the Carlin trend.

Aeromagnetic Data

Airborne magnetic data used in this study were acquired in 18 surveys flown between 1983 and 1999 for Newmont Mining Corporation, using inhouse and commercial helicopter-based cesium vapor magnetometers. In general, flight lines were east-west and spaced between 100 and 400 m, and survey altitudes ranged from 45 to 100 m. Corrections to total field data were made for diurnal and other variations in the Earth's field at the time of the survey. The data were then merged and the total field reprocessed. For this study, upward continuation of the composite magnetic data was used to better define anomalies at deeper levels. The method involves a two-fold transformation; first, raw surface data are modeled to the approximate depth of an anomaly, then projected to the surface (i.e., upward continuation; Dobrin and Savit, 1988). The effect of upward continuation is to amplify deeper sourced anomalies that otherwise would be potentially masked by higher level anomalies. Figures 10 and 11 show magnetic data upward continuation to 2,000 m for the northern and central Carlin trend and Rain area-southern Carlin trend, respectively. The significance of these data is discussed below.

Discussion

Temporal association of mineralization and Eocene magmatism in the Carlin trend

It is well established that Carlin-type deposits in the Great Basin formed in the Eocene, and dating in the Carlin trend substantiates that conclusion (Fig. 12). Arehart et al. (2003) determined an Rb-Sr age of 39.8 ± 0.6 Ma on galkhaite, a late ore-stage sulfosalt mineral from the Rodeo deposit north of Betze-Post. Coarse $2M_1$ illite replacing biotite phenocrysts in plagioclase-biotite-hornblende dacite at the Griffin (Meikle) deposit gave a complex $^{40}Ar/^{39}Ar$ spectrum; the best interpretation of its age is 39.6 ± 0.9 Ma from an isochron that used 84 percent of the released gas (Ressel et al., 2000b). Heitt et al. (2003) interpreted mineralization at Deep Star to be bracketed at ~39.1 Ma by two closely spaced stages of intrusion of aphyric rhyolite. Mineralization postdates 40.1 to 39.0 Ma dikes at Betze-Post, a 39.5 Ma dike at Griffin (Meikle), a 37.8 Ma dike at Dee, and a 37.6 Ma dike at Beast. These data suggest multiple episodes of mineralization that were contemporaneous with the multiple episodes of Eocene intrusion in the northern Carlin trend (Fig. 12). Episodes of mineralization include at least an older, ~39 to 40 Ma episode in the northern Betze-Post area, contemporaneous with the dikes there, and a younger episode after 37.6 Ma at Beast, no older than the dike there. Also, because mineralized Eocene dikes are present in almost all deposits, probably no mineralization occurred before ~40 Ma. An obvious question is what was special about the late Eocene and particularly about Eocene magmatism. Below we suggest that a series of large, partly deep-seated plutons underlie the Carlin trend and were primary heat sources to drive the large hydrothermal systems of the trend.

Number, size, and depth of emplacement of interpreted Eocene plutons

Henry and Ressel (2000a) noted that the abundant, Eocene, porphyritic, silicic dikes require the presence of an underlying plutonic complex. The large, positive aeromagnetic anomaly centered on the Emigrant Pass volcanic field (Hildenbrand and Kucks, 1988) is one major indicator of that plutonic complex (Grauch, 1996; Ressel et al., 2000a, 2001), and aeromagnetic data presented here strengthen that conclusion (Fig. 10). Silicic magmas represented by the dikes require large magma chambers to develop, either by differentiation of mantle-derived, basaltic magmas, by crustal melting or, more commonly, by a combination of differentiation and crustal melting-assimilation (Barker, 1981; Hildreth, 1981; Barnes et al., 2001). Therefore, we interpret the exposed dikes to be minor apophyses from an underlying plutonic complex. Suites of dikes determined from the age and petrographic data are areally restricted (Fig. 2). All Eocene dikes cannot have come from a single chamber or only from the complex indicated by the aeromagnetic anomaly centered on the Emigrant Pass volcanic field and Welches Canyon (see below). For example, the dikes in the Betze-Post area did not emanate from Welches Canyon. This would have required that individual suites of dikes only be emplaced 12 to 15 km north of the northern edge of the source pluton and not above it or symmetrically around it, and that they be a different age than the source pluton.

The age and distribution of Eocene dikes and volcanic rocks require a minimum of five or six plutons that mostly young toward the south (Figs. 10, 13). The oldest one or two plutons are inferred from the distribution of the three oldest suites of dikes of the northern Carlin trend: 40.3 to 39.3 Ma plagioclase-biotite ± quartz rhyolites, 40.1 to 39.0 Ma plagioclase-biotite-hornblende dacites, and the ~39.1 Ma aphyric rhyolites. The nearly continuous span of ages allows for either multiple magma chambers or a single, long-lived (≥1 m.y.) chamber. Either would have been centered beneath the Betze-Post deposit and the richest part of the Carlin trend (Figs. 10, 13). We suggest two plutons because the aphyric rhyolites are distinctly different from the porphyritic rocks. The composite plutons would have a diameter of about 10 km if the dikes rose vertically from them. Because even large crustal magma chambers cool rapidly, a long-lived system would require periodic replenishment by basaltic magma to remain molten (Cathles et al., 1997). A better understanding of the geochemical-isotopic characteristics and petrogenesis of the three suites of dikes would help evaluate these alternatives.

The aeromagnetic data are consistent with two or three plutons beneath the northern Carlin trend (Fig. 10). Positive anomaly A underlies the Jurassic Goldstrike intrusion and is discussed below. Anomaly B (the barbell-shaped body in Fig. 10) is itself composite and lies along the margin and just north of the pluton inferred from dike distributions only. The close proximity of the dike-inferred body to the aeromagnetic anomaly suggests that the latter marks a pluton or plutons that fed the dikes. The composite nature of anomaly B is consistent with the possibility of a composite or long-lived source. The low magnitude of the anomaly suggests that the pluton or plutons are relatively deep (Fig. 13).

The 37.6 Ma plagioclase-biotite-hornblende-quartz ± sanidine rhyolites require a third major source (Fig. 10). These dikes extend over a distance of about 18 km along the northern Carlin trend and are the most extensive of any of the silicic dikes of the trend. Their distribution is comparable to the

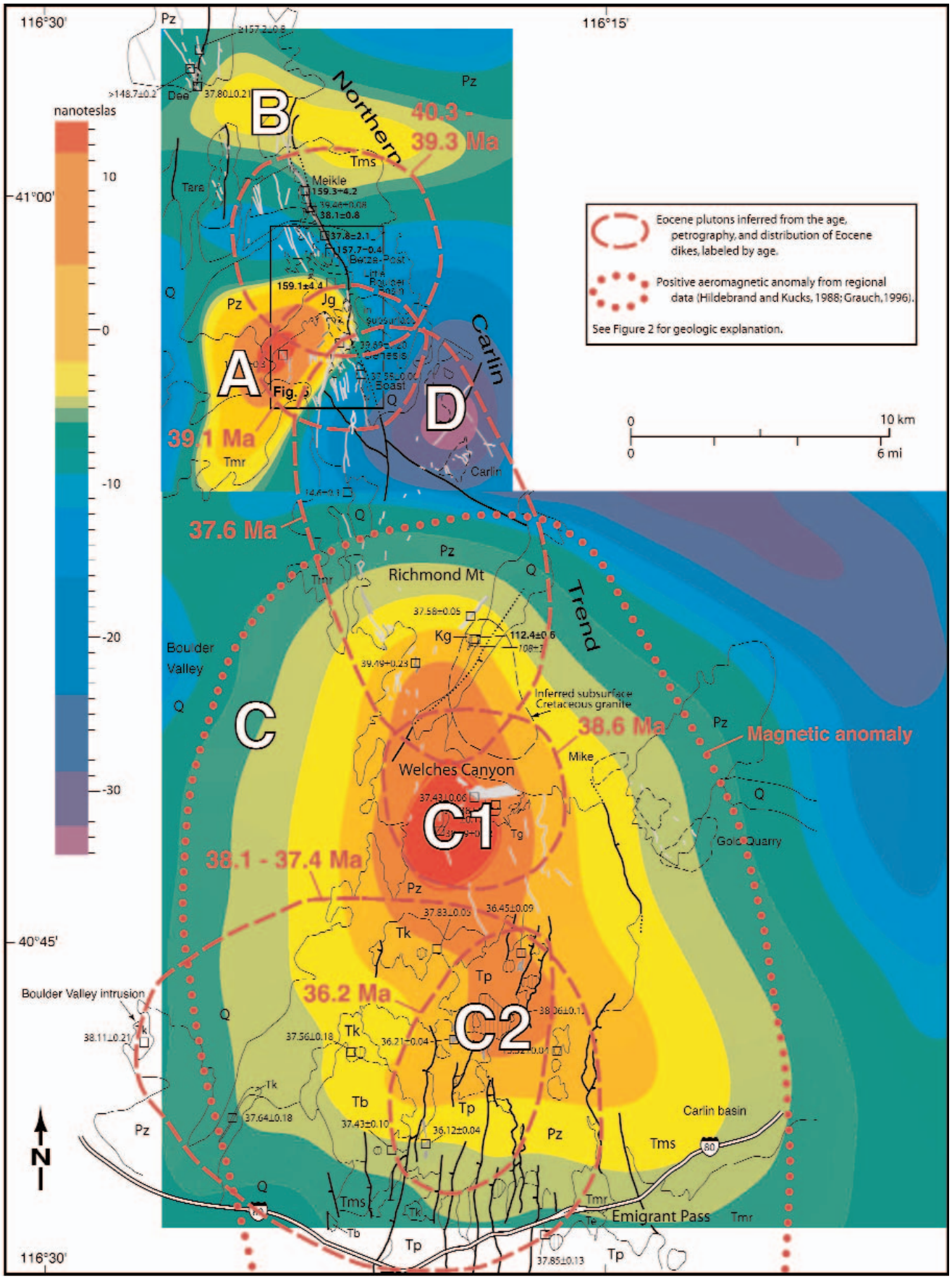
116°30'
116°15'
41°00'
40°45'
nanoteslas
10
0
-10
-20
-30
A
B
C
C1
C2
D
Northern
Carlin
Trend
40.3 - 39.3 Ma
39.1 Ma
37.6 Ma
38.6 Ma
38.1 - 37.4 Ma
36.2 Ma
Magnetic anomaly
Inferred subsurface Cretaceous granite
Eocene plutons inferred from the age, petrography, and distribution of Eocene dikes, labeled by age.
Positive aeromagnetic anomaly from regional data (Hildebrand and Kucks, 1988; Grauch, 1996).
See Figure 2 for geologic explanation.
0 10 km
0 6 mi
Fig. 5
Meikle
Beast
Beast-Post
Richmond Mt
Welches Canyon
Mike
Gold Quarry
Boulder Valley
Boulder Valley intrusion
Carlin basin
Emigrant Pass
Tara
Dee
Pz
Q
Tms
Tmr
Jg
Kg
Tg
Tk
Tb
Tp
Te
80
N

distribution of petrographically similar dikes around several Eocene igneous centers where a central stock is exposed (e.g., Tuscarora or Swales Mountain: Evans and Ketner, 1971; Henry and Ressel, 2000b; Ressel et al., 2001a; Castor et al., 2003). However, the central stock in these examples is interpreted to be a small ($\leq$3 km^2), shallow apophysis above a deeper, main chamber. The 37.6 Ma pluton in the northern Carlin trend conceivably underlies and is represented by the northern part of the large, positive aeromagnetic anomaly C, which is about in the middle of the dike distribution. Alternatively, a deep and/or relatively nonmagnetic pluton could be disguised beneath the associated negative anomaly D north of anomaly C.

Multiple plutons also presumably underlie the 38.6 Ma Welches Canyon intrusions, the 38.1 to 37.4 Ma Emigrant Pass volcanic field, and the 36.2 Ma plagioclase-biotite-hornblende-quartz ± sanidine rhyolite dikes of the Emigrant Pass field (Figs. 10, 13). The spatial separation and different ages of the Welches Canyon intrusions and the Emigrant Pass volcanic field require separate bodies. The inferred plutonic system underlying the Emigrant Pass volcanic field, which was active from ~38.1 to 37.4 Ma, could be either long-lived or composite. The distribution of subvolcanic intrusions and lava vents and the association with much of positive magnetic anomaly C (Fig. 10) suggest that the underlying plutonic system is at least 20 km across, east to west. The 36.2 Ma rhyolite dikes in the Emigrant Pass field are thought to be related to the youngest pluton of the Carlin trend. Their separation by ~1 m.y. from the rest of the field with no intervening activity indicates that they did not arise from a single, long-lived chamber that fed both systems. Their similarity to the 37.6 Ma dikes demonstrates the need for precise dating to distinguish events in areas of complex magmatism.

The Welches Canyon and Emigrant Pass rocks fall within the areas of the positive aeromagnetic anomaly of Hildenbrand and Kucks (1988) and the similar, upward continued anomaly C of Figure 10. The amplitude of anomaly C, the steep gradients at its margins, and the separate highs C1 and C2 within the anomaly indicate a shallow composite pluton (Grauch, 1996). Anomaly C1 is centered on the Welches Canyon intrusions, which are often referred to as "the Eocene pluton" of the northern Carlin trend (Chakurian et al., 2003; Emsbo et al., 2003; Hofstra et al., 2003). However, as shown here, the exposed Welches Canyon intrusions are shallow, porphyritic rocks, most likely minor apophyses of a larger and only moderately deeper body shown by the aeromagnetic data. Moreover, the Welches Canyon intrusions are distinctly younger than the dikes of the Betze-Post area and cannot have been their source. Anomaly C2 coincides with several vents of the Emigrant Pass field and with the 36.2 Ma dikes.

The relatively large, subvolcanic intrusions in Welches Canyon, Boulder Valley, and throughout the Emigrant Pass volcanic field, the presence and abundance of lavas in the Emigrant Pass field, and the amplitude and sharp boundary of the associated aeromagnetic anomaly are consistent with shallow magma chambers. In contrast, the pluton(s) beneath the northern Carlin trend were probably emplaced at greater depth (Figs. 10, 13). The fact that only dikes are present in the north and that anomaly B has a lower amplitude support a deeper body.

The Rain deposits of the southern Carlin trend lie ~8 km north of a ~10-km-diam, positive aeromagnetic anomaly 1 to 2 km southwest of the 37.4 Ma Bullion stock (Fig. 11). Hildenbrand and Kucks (1988) and Grauch (1996) interpreted this anomaly to reflect another major, underlying pluton. Aeromagnetic data that are not upward continued show a V-shaped pattern, with highs coinciding with the stock and the northwest-trending rhyolite dike swarm west of the stock. We interpret the 37.5 Ma porphyritic rhyolite dike at the Emigrant deposit, which also lies ~8 km north of the anomaly, to be related to the pluton represented by this anomaly. This interpreted pluton could have provided heat to generate the Carlin-type deposits at Rain.

The significance of the 37.8 Ma basaltic andesite at Dee and the 38.2 Ma basaltic andesite at Rain is less certain, because mafic magmas do not require crustal magma chambers. Mafic rocks of Eocene age are found elsewhere only in the Jerritt Canyon Carlin-type district (Fig. 2; Phinisey et al., 1996). This scarcity may reflect the difficulty that mafic magmas have in propagating through low-density, silicic magma chambers (Hildreth, 1981). Mafic magmas can appear after silicic magmatism has ended in an area or on the flanks of silicic centers, such as in the modern Cascade Range.

The distribution of dikes and aeromagnetic anomalies in the northern and central Carlin trend suggests that an

FIG. 10. Geologic map of the northern and central Carlin trend from Figure 2, showing aeromagnetic data upward continued to 2,000 m (Newmont Mining Corp.) and Eocene plutons (dashed lines labeled by age) inferred from the age, petrography, and distribution of Eocene dikes (see text for detailed discussion). We interpret the positive magnetic anomalies in the northern Carlin trend to indicate composite plutons at depth. Anomaly A coincides with the postulated feeder zone for the Jurassic Goldstrike laccolith sill. The barbell-shaped anomaly B is interpreted to indicate a deep-seated pluton or plutons, the map location of which partly overlaps with the position of a deep pluton inferred from dike data. Although it is impossible to determine the age of the pluton represented by anomaly B, the close proximity of the anomaly to the dike-interpreted body suggests that the anomaly marks an Eocene pluton or plutons that fed the dikes. The low magnitude of the anomaly suggests that the pluton or plutons are relatively deep. The large age range of the dike-interpreted pluton (40.3–39.0 Ma) indicates that it was composite or long-lived. The large, positive aeromagnetic anomaly C extending from Richmond Mountain to Emigrant Pass coincides closely with the aeromagnetic anomaly indicated by regional data (dotted outline: Hildenbrand and Kucks, 1988; Grauch, 1996). The large magnitude of this anomaly and the separate highs within it (C1 and C2) support the interpretation of relatively shallow, composite plutons that fed the Welches Canyon intrusions, the Emigrant Pass volcanic field, and the 36.2 Ma dike swarm. The associated, negative aeromagnetic anomaly D north of this positive anomaly could conceal a deep-seated pluton beneath the magnetic low. Airborne magnetic data were acquired in 18 surveys flown between 1983 and 1999 for Newmont Mining Corporation using inhouse and commercial helicopter-based cesium vapor magnetometers. See "Aeromagnetic Data" for further explanation.

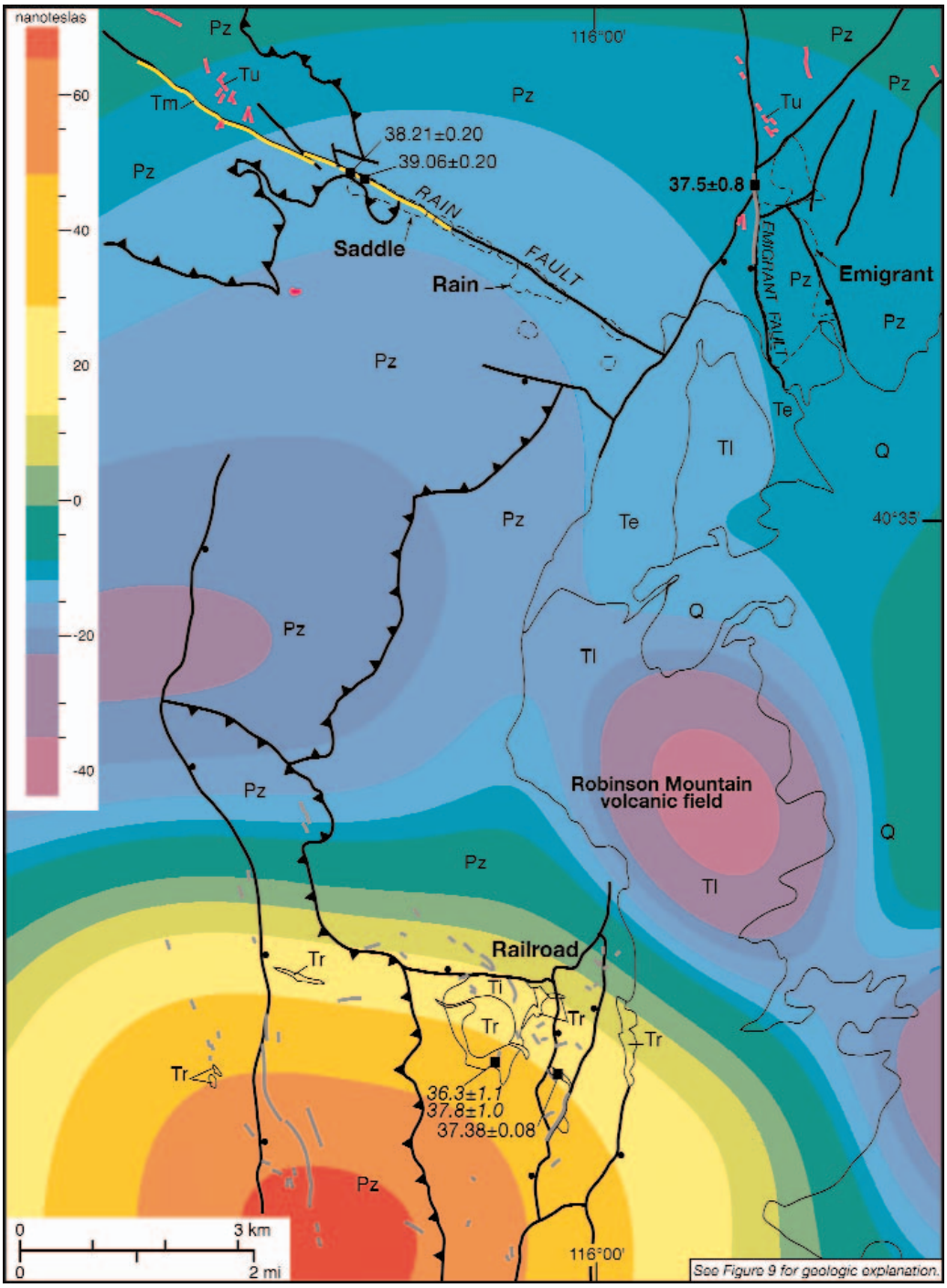

FIG. 11. Geologic map of the Rain mine area of the southern Carlin trend from Figure 9, with aeromagnetic data upward continued to 2,000 m (Newmont Mining Corporation). The distribution of dikes and aeromagnetic data indicate a large (~10 km diam) intrusion centered southwest of the Railroad district. The Bullion stock and porphyritic rhyolite dikes are interpreted to be apophyses from this larger intrusion. Airborne magnetic data from Newmont Mining Corporation; see section "Aeromagnetic Data."

Eocene plutonic complex underlies an area about 50 km north-south and between 12 and 23 km across (i.e., possibly 1,000 km^2; Figs. 10, 13). The thickness of the complex or of individual plutons is unknown, but magnetotelluric data suggest thicknesses of 10 km or more (Rodriguez, 1998). Thus, possibly 10,000 km^3 or more of Eocene magma were emplaced beneath the northern and central Carlin trend between about 40 and 36 Ma.

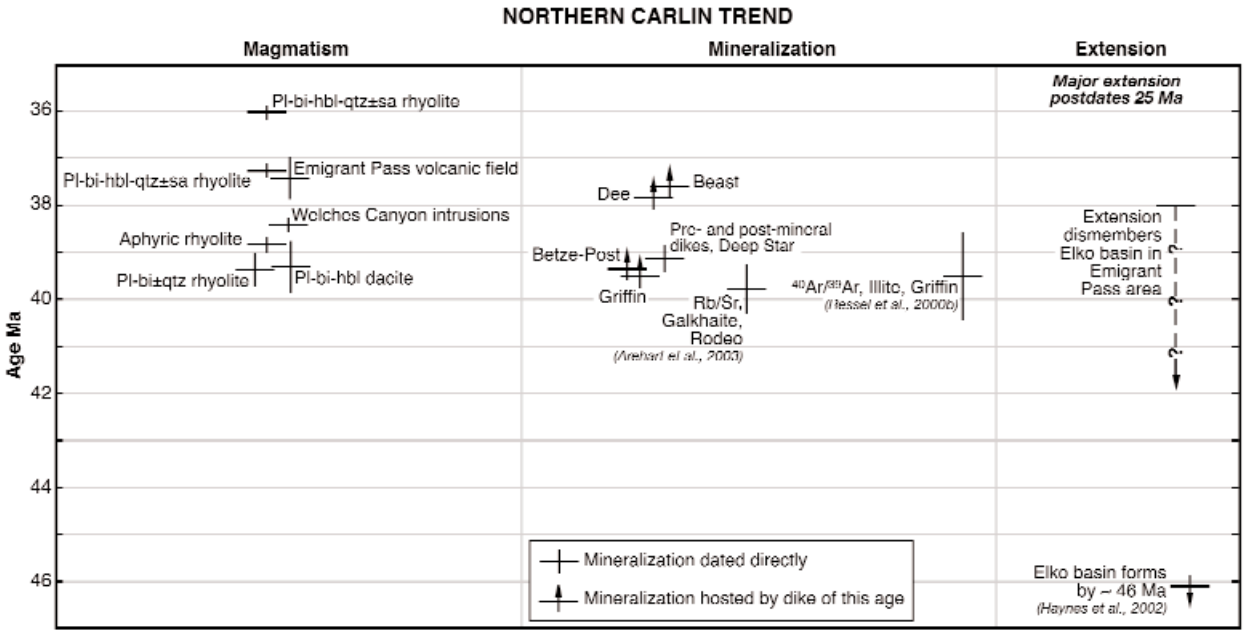

FIG. 12. Timing of Carlin-type mineralization relative to magmatism and extension in the northern Carlin trend. Vertical lines on the bars show the duration of magmatism for the various igneous suites or 1σ values for dates on mineralization. Mineralization and magmatism were coeval and may have been broadly coeval with extension, which has been dated only in adjacent areas. The Elko basin near Elko formed by ~46 Ma (Haynes et al., 2002), and Elko basin rocks in the Emigrant Pass volcanic field were tilted ~10° before 38 Ma (Henry and Faulds, 1999; Henry et al., 2001). Bi = biotite, Hbl = hornblende, Pl = plagioclase, Qtz = quartz, Sa = sanidine.

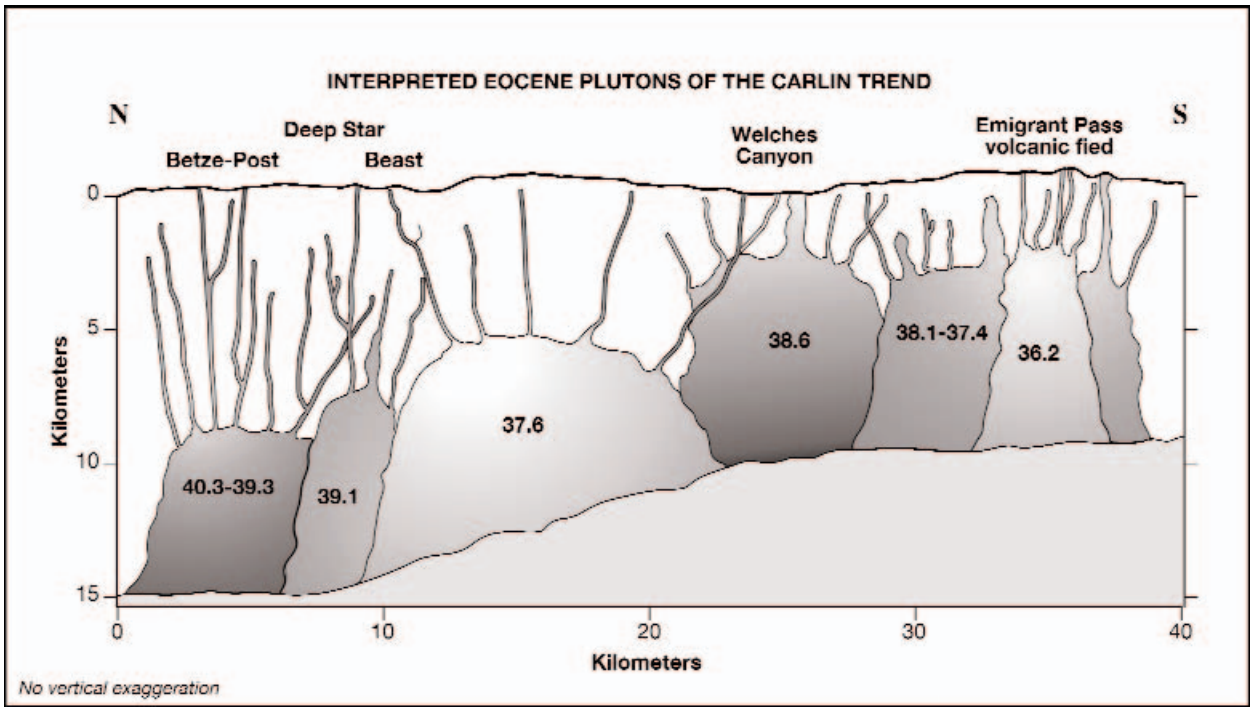

FIG. 13. Schematic but not vertically exaggerated cross section of interpreted Eocene plutons beneath the northern and central Carlin trend. The cross section runs approximately north to south through Figures 2 and 10. Geologic and aeromagnetic data suggest that plutons in the north lie at greater depths than plutons in the south. Dikes of the Carlin trend are apophyses from these plutons. See text for full discussion.

Implications of fission-track data for plutons

Chakurian et al. (2003) and Tosdal et al. (2003b) determined apatite fission-track ages of samples in and around the Carlin trend. Three samples from within the area of the large, aeromagnetic anomaly C were reset at 37 to 38 Ma (for example, a sample from the Cretaceous Richmond stock gave a fission-track age of 37.8 Ma), and one was reset at 28 Ma (Chakurian et al., 2003). Only one of these samples is close to a known Carlin-type deposit. In contrast, only two of 19 apatite samples from the northern Carlin trend outside the anomaly were similarly reset. One of three samples from the Carlin deposit gave a fisson-track age of 40.9 Ma (one was 18.6 Ma), and one of two samples from the Betze-Post deposit gave an age of 35.5 Ma. All other samples, most of which were from Carlin-type deposits, gave ages ranging from 56.1 to 129 Ma.

Although Chakurian et al. (2003) interpreted the fission-track data to indicate the time of gold mineralization, the data indicate only the time of heating to 110° to 135°C long enough to anneal fission tracks (Green et al., 1989). The distribution of ages implies that conductive, convective, or combined heating around the shallow, Eocene plutons of the Welches Canyon-Emigrant Pass area reset the fission-track ages to the time of intrusion. In contrast, heating by the Carlin-type hydrothermal systems alone was insufficient to reset ages. Although maximum hydrothermal temperatures in the northern Carlin trend are estimated to have been ~240°C (Hofstra and Cline, 2000), hydrothermal heating apparently was of insufficient duration to reset the apatite fission-track ages, even within major deposits, to the Eocene age of mineralization. The deep Eocene plutons indicated by our work also were apparently too deep to heat country rock around the northern deposits sufficiently to reset the fission-track ages.

Depth of pluton emplacement

Although the southern plutons beneath Welches Canyon and the Emigrant Pass volcanic field appear to have been emplaced at shallower depths than the northern plutons, their absolute depths are less certain (Fig. 13). Based on the steep gradients at the margins of aeromagnetic anomaly C (Grauch, 1996), resetting of apatite fission-track ages (Chakurian et al., 2003), and the high-temperature, skarn-type alteration around the Welches Canyon stocks, we infer that the southern plutons are no more than about 3 km below the present surface.

In the northern Carlin trend, the presence of abundant rhyolite dikes above the inferred plutons probably precludes a source much deeper than about 8 to 10 km, which is the maximum lateral distance that similar rhyolite dikes extend from related plutons in northeastern Nevada (Ressel et al., 2000a). The association of aeromagnetic anomalies with all inferred plutons also suggests that they cannot be extremely deep. Quantitative modeling of the fission-track data of Chakurian et al. (2003) to estimate a combined maximum size, depth, and temperature of the plutons is probably possible but beyond the scope of this report.

The 36 Ma Harrison Pass pluton in the Ruby Mountains has a very low magnetite content (Barnes et al., 2001) and no associated aeromagnetic anomaly (Hildenbrand and Kucks, 1988). This composite intrusion is estimated to have been emplaced at ~12 km (Barnes et al., 2001) and is otherwise a good analog to our postulated deep plutons.

Jurassic and Cretaceous plutons

The clustering of Jurassic dikes around the Goldstrike laccolith may also indicate the presence of a deeper pluton beneath the laccolith. This interpretation is supported by positive aeromagnetic anomaly A, which suggests a feeder beneath the southwestern end of the Goldstrike laccolith (Fig. 10). The Jurassic rocks exhibit two significant differences from the Eocene rocks. Jurassic magmatism was more mafic, dominated by the Goldstrike diorite and lamprophyre dikes, although rhyolite dikes are also present. Jurassic magmatism also may have been temporally restricted, both in the Carlin trend and more regionally (Mortensen et al., 2000; this study). All Jurassic intrusions in the Carlin trend could have emanated from a single magma body that was centered beneath the Goldstrike laccolith.

From aeromagnetic and other data (see Cretaceous Richmond Granite, above) we infer that a Cretaceous pluton underlies an area in the northeastern part of anomaly C (Fig. 10). Distinguishing the magnetic contribution of Eocene and Cretaceous rocks in this area is difficult.

Depth of formation of Carlin-type deposits

Henry and Ressel (2000a) argued on structural grounds that the tops of deposits of the northern Carlin trend probably formed at paleodepths no greater than about 1 km. The present-day elevation of the Eocene-Paleozoic unconformity in the Emigrant Pass volcanic field marks the Eocene paleosurface. Extrapolating the paleosurface northward into the northern Carlin trend must allow for relative displacements on intervening structures. The only major post-Eocene structure along this northward projection is the northeast-striking normal fault between Welches Canyon and the Cretaceous granite outcrop (Fig. 2). This fault has a maximum displacement of ~2 km at its northeast end (Evans, 1974a, b), but displacement diminishes to the southwest on a line between the northern Carlin trend and Emigrant Pass. This extrapolation suggests that the Eocene paleosurface was not much higher than the present-day surface in the northern Carlin trend. Allowing for uncertainty in this structural reconstruction, the tops of most major orebodies (not the deepest recognized mineralization) probably formed no deeper than about 1 km. Apatite fission-track and U-Th/He data confirm this interpretation (Haynes et al., 2003; Hickey et al., 2003). These data indicate that the present-day surface in the northern Carlin trend lies 500 to 1,500 m below the ~42 Ma paleosurface. Given the vertical range of mineralization, Hickey et al. (2003) and Haynes et al. (2003) concluded that Carlin-type deposits formed at depths between 500 and 2,200 m. These depths are in the shallower range of estimates of 1 to 6.5 km based on fluid inclusion data (Hofstra and Cline, 2000).

Relevance of Eocene plutons for models of the origin of Carlin-type deposits

In the most recent review of Carlin-type deposits, Cline et al. (2005, p. 451) suggested that "deep, primitive fluids" were

generated through lower crustal melting and metamorphism and that "Such fluids were likely incorporated in deep crustal melts that rose buoyantly and ultimately exsolved hydrothermal fluids, possibly containing gold" (p. 451-452).Our data demonstrate that large volumes of magma were most likely present and were a probable heat source for Carlin-type deposits of the Carlin trend, although we do not address the source of gold. Although Cline et al. (2005) suggested only a regional-scale association of Carlin-type deposits and Eocene magmatism in northern Nevada, we suggest a very close spatial and temporal association between inferred plutons of the Carlin trend and the gold deposits.

Thorough study of the igneous rocks of the three other major Carlin-type districts in Nevada, Cortez-Pipeline, Jerritt Canyon, and Getchell-Twin Creeks, is needed to evaluate these models. Eocene volcanic or intrusive rocks coeval with the time of mineralization are known in two of the three districts. At Cortez, 35 Ma, hydrothermally altered, porphyritic rhyolite dikes are variably interpreted as pre- or postmineral (Wells et al., 1969; McCormack and Hays, 1996; Mortensen et al., 2000). Eocene lavas and dikes are present at Jerritt Canyon, and some dikes are mineralized (Hofstra et al., 1999; C.D. Henry, unpub. data). Eocene intrusions have not been found in the Getchell trend, but ~41 Ma rhyolite and dacite lavas and tuffs crop out within 6 km of the trend, and the intervening area is covered by Quaternary deposits (Wallace, 1993; Henry and Ressel, 2000; Laravie, 2005).

Acknowledgments

Work contributing to this report was supported by the Center for Research in Economic Geology (Mackay School of Mines, University of Nevada, Reno) and by the U.S. Geological Survey through STATEMAP Agreement 98-HQ-AG-2036. Barrick Goldstrike Mines and Newmont Mining Corporation provided additional funds for $^{40}Ar/^{39}Ar$ dating. $^{40}Ar/^{39}Ar$ dating was done at the New Mexico Geochronology Research Laboratory and the Nevada Isotope Geochronology Laboratory. We thank Bill McIntosh, Matt Heizler, Lisa Peters, and Rich Esser at New Mexico Tech and Terry Spell and Kathy Zanetti at the University of Nevada Las Vegas for guidance. Newmont Mining Company generously allowed the use of their proprietary aeromagnetic data, and discussions with Mark Goldie greatly helped to explain the significance of these data. We thank Steve Garwin for data and discussion about the U-Pb SHRIMP date at the Emigrant deposit. David John and Richard Tosdal generously contributed samples from the Robinson volcanic field and Railroad mine area. Reviews of an early draft by Stephen Castor, Jonathan Price, and Tommy Thompson and of the submitted manuscript by Jean Cline, Charles Cunningham, and Ross Sherlock greatly improved the content and clarity of this report.

February 3, 2005; March 16, 2006

REFERENCES

Anders, E., and Grevesse, N., 1989, Abundances of the elements: Meteoritic and solar: Geochimica et Cosmochimica Acta, v. 53, p. 197–214.

Arehart, G.B., 1996, Characteristics and origin of sediment-hosted gold deposits: A review: Ore Geology Reviews, v. 11, p. 383–403.

Arehart, G.B., Foland, K.A., Naeser, C.W., and Kesler, S.E., 1993, $^{40}Ar/^{39}Ar$, K-Ar, and fission-track geochronology of sediment-hosted disseminated gold deposits at Post/Betze, Carlin trend, northeastern Nevada: Economic Geology, v. 88, p. 622–646.

Arehart, G.B., Chakurian, A.M., Tretbar, D.R., Christensen, J.N., McInnes, B.A., and Donelick, R.A., 2003, Evaluation of radioisotope dating of Carlin-type deposits in the Great Basin, western North America, and implications for deposit genesis: Economic Geology, v. 98, p. 225–248.

Armstrong, R.L., 1970, Geochronology of Tertiary igneous rocks, eastern Basin and Range province, western Utah, eastern Nevada, and vicinity, U.S.A.: Geochimica et Cosmochimica Acta, v. 34, p. 203–232.

Bakken, B.M., 1990, Gold mineralization, wall-rock alteration, and the geochemical evolution of the hydrothermal system in the main orebody, Carlin mine, Nevada: Unpublished Ph.D. thesis, California, Stanford University, 283 p.

Barker, F., 1981, Introduction to special issue on granites and rhyolites: A commentary for the nonspecialist: Journal of Geophysical Research, v. 86, p. 10131–10135.

Barnes, C.G., Burton, B.R., Burling, T.C., Wright, J.E., and Karlsson, H.R., 2001, Petrology and geochemistry of the late Eocene Harrison Pass pluton, Ruby Mountains core complex, Northeastern Nevada: Journal of Petrology, v. 42, p. 901–929.

Barton, M.D., 1996, Granitic magmatism and metallogeny of southwestern North America: Geological Society of America Special Paper 315, p. 261–280.

Bettles, K., 2002, Exploration and geology, 1962–2002, at the Goldstrike property: Nevada Bureau of Mines and Geology Bulletin 111, p. 54–75.

Branham, A., and Arkell, B., 1995, The Mike gold-copper deposit, Carlin trend, Nevada, *in* Hagni, R.D., ed., Process Mineralogy XIII: Applications to beneficiation problems, pyrometallurical products, advanced mineralogical techniques, precious metals, environmental concerns, ceramic material, hydrometallurgy and minerals exploration: Warrendale, PA, Minerals, Metals, and Materials Society, p. 204–211.

Brooks, W.E., Thorman, W.E., and Snee, L.W., 1995a, The $^{40}Ar/^{39}Ar$ ages and tectonic setting of the middle Eocene northeast Nevada volcanic field: Journal of Geophysical Research, v. 100, p. 10,403–10,416.

Brooks, W.E., Thorman, W.E., Snee, L.W., Nutt, C.W., Potter, C.J., and Dubiel, R.F., 1995b, Summary of chemical analyses and $^{40}Ar/^{39}Ar$-spectra data for Eocene volcanic rocks from the central part of the northeast Nevada volcanic field: U.S. Geological Survey Bulletin 1988–K, p. K1–K33.

Castor, S.B., Boden, D.R., Henry, C.D., Cline, J.S., Hofstra, A.H., McIntosh, W.C., Tosdal, R.M., Wooden, J.P., 2003, Geology of the Eocene Tuscarora volcanic-hosted, epithermal precious metal district, Elko County, Nevada: Economic Geology, v. 98, p. 339–366.

Cathles, L.M., Erendi, A.H.J., and Barrie, T., 1997, How long can a hydrothermal system be sustained by a single intrusive event?: Economic Geology, v. 92, p. 766–771.

Cebula, G.T., Kunk, M.J., Mehnert, H.H., Naeser, C.W., Obradovich, J.D., and Sutter, J.F., 1986, The Fish Canyon Tuff, a potential standard for the $^{40}Ar/^{39}Ar$ and fission-track dating methods: Terra Cognita, v. 6, p. 139–140.

Chakurian, A.M., Arehart, G.B., Donelick, R.A., Zhang, X., and Reiners, P.W., 2003, Timing constraints of gold mineralization along the Carlin trend utilizing apatite fission-track, $^{40}Ar/^{39}Ar$, and apatite (U-Th)/He methods: Economic Geology, v. 98, p. 1159–1171.

Christiansen, R.L., and Yeats, R.S., 1992, Post-Laramide geology of the U. S. Cordilleran region: Geological Society of America Decade in North American Geology Series, v. G-3, p. 261–406.

Cline, J.S., Shields, D., Riciputi, L., Fayek, M., Copp, T.L., Muntean, J., and Hofstra, A.H., 2003, Trace element and isotope microanalyses support a deep ore fluid source at the Getchell Carlin-type gold deposit, northern Nevada [abs.]: Geological Society of America Abstracts with Programs, v. 35, no. 6, p. 358.

Cline, J.S., Hofstra, A.H., Muntean, J.L., Tosdal, R.M., and Hickey, K.A., 2005, Carlin-type gold deposits in Nevada: Critical geologic characteristics and viable models: Economic Geology 100th Anniversary Volume, p. 451–484.

DePaolo, D.J., and Farmer, G.L., 1984, Isotopic data bearing on the origin of Mesozoic and Tertiary granitic rocks in the Western United States: Philosophical Transactions of the Royal Society of London, Series A, v. 310, p. 743–753.

DiVincenzo, G., Viti, C., and Rocchi, S.,2003, The effect of chlorite interlayering on ^{40}Ar-^{39}Ar biotite dating: an ^{40}Ar-^{39}Ar laser-probe and TEM investigations of variably chloritised biotites: Contributions to Mineralogy and Petrology, v. 145, p. 643–658.

Dobak, P.J., Arbonies, D., Hipsely, R., and Visher, M., 2002, Geology of the Storm gold deposits: Nevada Bureau of Mines and Geology Bulletin 111, p. 46–53.

Dobrin, M.B., and Savit, C.H., 1988, Introduction to geophysical prospecting, 4th ed.: New York, McGraw Hill Book Company, 867 p.

Drews-Armitage, S.P., Romberger, S.B., and Whitney, C.G., 1996, Clay alteration and gold deposition in the Genesis and Blue Start deposits, Eureka County, Nevada: Economic Geology, v. 91, p. 1383–1393.

Dunbar, W., 2001, A structural model of mineralization at Deep Star, Carlin trend, Nevada: Geological Society of Nevada Special Publication 33, p. 243–261.

Emmons, D.L., and Eng, T.L., 1995, Geologic map of the McCoy mining district, Lander county, Nevada: Nevada Bureau of Mines and Geology Map 103, scale 1:12,000, p. 1–12.

Emsbo, P., Hofstra, A., Park, D., Zimmerman, J.M., and Snee, L., 1996, A mid-Tertiary age constraint on alteration and mineralization in igneous dikes on the Goldstrike property, Carlin trend, Nevada [abs.]: Geological Society of America Abstracts with Programs, v. 28, no. 7, p. A-476.

Emsbo, P., Hutchinson, R.W., Hofstra, A.H., Volk, J.A., Bettles, K.H., Baschuk, G.J., and Johnson, C.A., 1999, Syngenetic Au on the Carlin trend: Implications for Carlin-type deposits: Geology, v. 27, p. 59–62. 2000, Proceedings, p. 46.

Emsbo, P., Hofstra, A.H., Lauha, E.A., Griffin, G.L., and Hutchinson, R.W., 2003, Origin of high-grade gold ore, source of ore fluid components, and genesis of the Meikle and neighboring Carlin-type deposits, northern Carlin trend, Nevada: Economic Geology, v. 98, p. 1069–1105.

Erickson, R.L., Silberman, M.L., and Marsh, S.P., 1978, Age and composition of igneous rocks, Edna Mountain Quadrangle, Humboldt County, Nevada: U.S. Geological Survey Journal of Research, v. 6, p. 727–743.

Evans, J.G., 1974a, Geologic map of the Welches Canyon quadrangle, Eureka County, Nevada: U.S. Geological Survey Geologic Quadrangle Map GQ-1117, scale 1:24,000.

——1974b, Geologic map of the Rodeo Creek Northeast quadrangle, Eureka County, Nevada: U.S. Geological Survey Geological Quadrangle Map GQ-1116, scale 1:24,000.

——1980, Geology of the Rodeo Creek NE and Welches Canyon quadrangles, Eureka County, Nevada: U.S. Geological Survey Bulletin 1473, 81 p.

Evans, J.G., and Ketner, K.B., 1971, Geologic map of the Swales Mountain Quadrangle and part of the Adobe Summit Quadrangle, Elko County, Nevada: U.S. Geological Survey Miscellaneous Investigations Map I-667, 1:24,000.

Evans, J.G., and Mullens, T.E., 1976, Bootstrap Window, Elko and Eureka Counties, Nevada: U.S. Geological Survey Journal of Research, v .4, p. 119–125.

Fleck, R.J., Sutter, J.F., and Elliott, D.H., 1977, Interpretation of discordant $^{40}Ar/^{39}Ar$ age-spectra of Mesozoic tholeiites from Antarctica: Geochimica et Cosmochimica Acta, v. 41, p. 15–32.

Fleck, R.J., Theodore, T.G., Sarna-Wojcicki, A., and Meyer, C.E., 1998, Age and possible source of air-fall tuffs of the Miocene Carlin Formation, northern Carlin trend: U.S. Geological Survey Open-File Report 98–338, p. 176–192.

Gillerman, V. S., 1982, Tungsten and copper skarns of the Railroad mining district, Nevada: Unpublished Ph.D. dissertation, California, University of California, Berkeley, 195 p.

Grauch, V.J.S., 1996, Magnetically interpreted, granitoid plutonic bodies in Nevada: Nevada Bureau of Mines and Geology Open-File Report 96–2, p. 7-1–7-16.

Green, P.F., Duddy, I.R., Laslett, G.M., Hegarty, K.A., Gleadow, A.J.W., and Lovering, J.F., 1989, Thermal annealing of fission tracks in apatite: 4. Quantitative modeling techniques and extension to geological time scales: Chemical Geology, v. 79, p. 155–182.

Groff, J.A., Heizler, M.T., McIntosh, W.C., and Norman, D.I., 1997, $^{40}Ar/^{39}Ar$ dating and mineral paragenesis for Carlin-type gold deposits along the Getchell trend, Nevada: Evidence for Cretaceous and Tertiary gold mineralization: Economic Geology, v. 92, p. 601–622.

Hall, C.M., Simon, G., and Kesler, S.E., 1997, Age of mineralization at the Twin Creeks SHMG Deposit, Nevada: Society of Economic Geologists Guidebook Series, v. 28, p. 151–154.

Hall, C.M., Kesler, S.E., Simon, G., and Fortuna, J., 2000, Overlapping Cretaceous and Eocene alteration, Twin Creeks Carlin-type deposit: Economic Geology, v. 95, p. 1739–1752.

Hausen, D.M., and Kerr, P.E., 1968, Fine gold occurrence at Carlin, Nevada, *in* Ridge, J.D., ed., Ore deposits of the United States, 1933–1967 (Graton-Sales volume): New York, American Institute of Mining and Metallurgial Engineers, v. 1, p. 908–940.

Hausen, D.M., Ekburg, C., and Kula, F., 1983, Geochemical and XRD-computer logging method for lithologic ore type classification of Carlin-type gold ores, in Hagni, R.D., ed., Process Mineralogy II. Applications in Metallurgy, Ceramics, and Geology: American Institute of Mining Engineers, p. 421–450.

Haynes, S.R., Hickey, K.A., Mortensen, J.K., and Tosdal, R.M., 2002, Onset of extension in the Basin and Range: Basin analysis of the Eocene Elko Formation, NE Nevada [abs.]: Geological Society of American Abstracts with Programs, v. 34, no. 6, p. 83.

Haynes, S.R., Hickey, K.A., and Tosdal, R.M., 2003, Golden highs and soggy bottoms: The link between Eocene paleogeography and gold deposition, northern Carlin trend, Nevada [abs.]: Geological Society of American Abstracts with Programs, v. 35, no. 6, p. 235–236.

Heitt, D.G., Dunbar, W.G., Thompson, T.B., and Jackson, R.G., 2003, Geology and geochemistry of the Deep Star gold deposit, Carlin trend, Nevada: Economic Geology, v. 98, p. 1107–1135.

Henry, C.D., and Boden, D.R., 1998a, Geologic map of the Mount Blitzen quadrangle, Elko County, northeastern Nevada: Nevada Bureau of Mines and Geology Map 110, scale 1:24,000.

——1998b, Eocene magmatism: The heat source for Carlin-type gold deposits of northern Nevada: Geology, v. 26, p. 1067–1070.

Henry, C.D., and Faulds, J.E., 1999, Geologic map of the Emigrant Pass Quadrangle, Nevada: Nevada Bureau of Mines and Geology Open-File Report 99-9, scale: 1:24,000.

Henry, C.D., and Ressel, M.W., 2000a, Eocene magmatism of northeastern Nevada: The smoking gun for Carlin-type gold deposits: Geological Society of Nevada, Geology and Ore Deposits 2000: The Great Basin and Beyond Symposium, Reno/Sparks, Nevada, May 15-18, 2000, Proceedings, p. 365–388.

——2000b, Eocene magmatism and its role in generating sediment-hosted gold deposits of the Carlin trend: Geological Society of Nevada, Geology and Ore Deposits 2000: The Great Basin and Beyond Symposium, Reno/Sparks, Nevada, May 15-18, 2000, Field Trip Guidebook 4, 223 p.

Henry, C.D., Faulds, J.E., Boden, D.R., and Ressel, M.W., 2001, Timing and styles of Cenozoic extension near the Carlin trend, northeastern Nevada: Implications for the formation of Carlin-type gold deposits: Geological Society of Nevada Special Publication 33, p. 115–128.

Hickey, K.A., Donelick, R.A., Tosdal, R.M., and McInnes, B.I.A., 2003, Restoration of the Eocene landscape in the Carlin-Jerritt Canyon mining district: Constraining depth of mineralization for Carlin-type Au-deposits using low-temperature apatite thermochronology [abs.]: Geological Society of American Abstracts with Programs, v. 35, no. 6, p. 358.

Hildenbrand, T.G., and Kucks, R.P., 1988, Total intensity magnetic anomaly map of Nevada: Nevada Bureau of Mines and Geology Map 93A, scale: 1:750,000.

Hildreth, W., 1981, Gradients in silicic magma chambers: Implications for lithospheric magmatism: Journal of Geophysical Research, v. 86, p. 10153–10192.

Hofstra, A.H., and Cline, J.S., 2000, Characteristics and models for Carlin-type gold deposits: Reviews in Economic Geology, v. 13, p. 163–220.

Hofstra, A.H., Snee, L.W., Rye, R.O., Folger, H.W., Phinisey, J.D., Loranger, R.J., Dahl, A.R., Naeser, C.W., Stein, H.J., and Lewchuk, M., 1999, Age constraints on Jerritt Canyon and other Carlin-type gold deposits in the western United States—relationship to mid-Tertiary extension and magmatism: Economic Geology, v. 94, p. 769–802.

Hofstra, A.H., John, D.A., and Theodore, T.G., 2003, A special issue devoted to gold deposits in northern Nevada: Part 2. Carlin-type deposits, Preface: Economic Geology, v. 98, p. 1063–1067.

Howard, K.A., 2000, Geologic map of the Lamoille Quadrangle, Elko County, Nevada: Nevada Bureau of Mines and Geology Geologic Map 125, 1:24,000.

Howard, K.A., Kistler, R.W., Snoke, A.W., and Willden, R., 1979, Geologic map of the Ruby Mountains, Nevada: U.S. Geological Survey Map I-1136, scale 1:125,000.

Humphreys, E.D., 1995, Post-Laramide removal of the Farallon slab, western United States: Geology, v. 23, p. 987–990.

Ilchik, R.P., and Barton, M.D., 1997, An amagmatic origin of Carlin-type gold deposits: Economic Geology, v. 92, p. 269–288.

John, D.A., 2001, Miocene and early Pliocene epithermal gold-silver deposits in the northern Great Basin, western United States: Characteristics, distribution, and relationship to magmatism: Economic Geology, v. 96, p. 1827–1853.

John, D.A., and Wallace, A.R., 2000, Epithermal gold-silver deposits related to the northern Nevada rift: Geological Society of Nevada, Geology and Ore Deposits 2000: The Great Basin and Beyond Symposium, Reno/Sparks, Nevada, May 15-18, 2000, Proceedings, p. 155–175.

John, D.A., Wallace, A.R., Ponce, D.A., Fleck, R.B., and Conrad, J.E., 2000, New perspectives on the geology and origin of the northern Nevada rift: Geological Society of Nevada, Geology and Ore Deposits 2000: The Great Basin and Beyond Symposium, Reno/Sparks, Nevada, May 15-18, 2000, Proceedings, p. 127–154.

John, D.A., Hofstra, A.H., Fleck, R.J., Brummer, J.E., and Saderholm, E.C., 2003,

Geologic setting and genesis of the Mule Canyon low-sulfidation epithermal gold-silver deposit, north-central Nevada: Economic Geology, v. 98, p. 425–463.

Johnston, M.K., 2000, Hypogene alteration and ore characteristics at the Cove gold-silver deposit, Lander County, Nevada: Geological Society of Nevada, Geology and Ore Deposits 2000: The Great Basin and Beyond Symposium, Reno/Sparks, Nevada, May 15-18, 2000, Proceedings, p. 621–641.

——2003, Geology of the Cove Mine, Lander County, Nevada, and a genetic model for the McCoy-Cove magmatic-hydrothermal system: Unpublished Ph.D. dissertation, University of Nevada, Reno, 353 p.

Johnston, M.K., and Ressel, M.W., 2004, Carlin-type and distal-disseminated Au-Ag deposits: Related distal expressions of Eocene intrusive centers in north-central Nevada: Society of Economic Geologists Newsletter 59, p. 12–14.

Justet, L., and Spell, T.L., 2001, Effusive eruptions from a large shallow magma chamber: The Bearhead Rhyolite, Jemez volcanic field, New Mexico: Journal of Volcanology and Geothermal Research, v. 107, p. 241–264.

Kesler, S.E., Fortuna, J., Ye, Z., Alt, J.C., Core, D.P., Zohar, P., Borhauer, J., and Chryssoulis, S.L., 2003, Evaluation of the role of sulfidation in deposition of gold, Screamer section of the Betze-Post Carlin-type deposit, Nevada: Economic Geology, v. 98, p. 1137–1157.

Ketner, K.B., 1998, Geologic map of the southern Independence Mountains, Elko County, Nevada: U.S. Geological Survey Geologic Investigations I-2629, scale 1:24,000.

Ketner, K.B., and Smith, J.F., Jr., 1963, Geology of the Railroad mining district, Elko County, Nevada: U.S. Geological Survey Bulletin 1162–B, p. B1–B27.

Kistler, R.W., Ghent, E.D., and O'Neil, J.R., 1981, Petrogenesis of two-mica granites in the Ruby Mountains, Nevada: Journal of Geophysical Research, v. 86, p. 10591–10606.

Kuehn, C.A., and Rose, A.W., 1992, Geology and geochemistry of wall-rock alteration at the Carlin gold deposit, Nevada: Economic Geology, v. 87, p. 1697–1721.

Laravie, J.A., 2005, Geologic map of the Kelly Creek area, Humboldt, Elko, and Lander Counties, Nevada: Nevada Bureau of Mines and Geology Open-File Report 05-1, scale 1:24,000.

Leavitt, E.D., Spell, T.L., Goldstrand, P.M., and Arehart, G.B., 2004, Geochronology of the Midas low-sulfidation epithermal gold-silver deposit, Elko County, Nevada: Economic Geology, v. 99, p. 1665–1686.

Le Bas, M.J., Le Maitre, R.W., Streckeisen, A., and Zanettin, B., 1986, A chemical classification of volcanic rocks based on the total alkali-silica diagram: Journal of Petrology, v. 27, p. 745–750.

Leonardson, R.W., and Rahn, J.E., 1996, Geology of the Betze-Post gold deposits, Eureka County, Nevada: Geological Society of Nevada, Geology and Ore Deposits of the American Cordillera Symposium, Reno/Sparks, Nevada, April, 1995, Proceedings, p. 61–94.

Longo, A.A., Thompson, T.B., and Harlan, J.B., 2002, Geologic overview of the Rain subdistrict: Nevada Bureau of Mines and Geology Bulletin 111, p. 168–189.

Mathewson, D., 2001, Tectono-stratigraphic setting for the Rain district gold deposits, Carlin trend, Nevada: Geological Society of Nevada Special Publication 33, p. 90–109.

McCormack, J.K., and Hays, R.C., Jr., 1996, Crescent Valley: A model for reconstruction of district mineralization in the Basin and Range: Geological Society of Nevada, Geology and Ore Deposits of the American Cordillera Symposium, Reno/Sparks, Nevada, April, 1995, Proceedings, p. 635–646.

McDougall, I., and Harrison, T.M., 1988, Geochronology and thermochronology by the $^{40}Ar/^{39}Ar$ method: Oxford Monographs on Geology and Geophysics 9, 212 p.

McGrew, A.J., and Snee, L.W., 1994, $^{40}Ar/^{39}Ar$ thermochronologic constraints on the tectonothermal evolution of the northern East Humboldt Range metamorphic core complex, Nevada: Tectonophysics, v. 238, p. 425–450.

McIntosh, W.C., Sutter, J.F., Chapin, C.E., and Kedzie, L.L., 1990, High-precision $^{40}Ar/^{39}Ar$ sanidine geochronology of ignimbrites in the Mogollon-Datil volcanic field, southwestern New Mexico: Bulletin of Volcanology, v. 52, p. 584–601.

McIntosh, W.C., Heizler, M., Peters, L., and Esser, R., 2003, $^{40}Ar/^{39}Ar$ geochronology at the New Mexico Bureau of Geology and Mineral Resources: New Mexico Bureau of Geology and Mineral Resources Open File Report OF-AR-1, 10 p.

McKee, E.H., Moring, B.C., and Huber, D.R., 1995, Cenozoic volcanic rocks and Cenozoic mineral deposits of Nevada: U.S. Geological Survey Open-file Report 95–248.

Mohling, J., 2002, Geology and gold mineralization of the Turf deposit: Nevada Bureau of Mines and Geology Bulletin 111, p. 91–105.

Moore, S., 2002, Geology of the northern Carlin trend: Nevada Bureau of Mines and Geology Bulletin 111, scale 1:24,000.

Mortensen, J.K., Thompson, J.F.H., and Tosdal, R.M., 2000, U-Pb age constraints on magmatism and mineralization in the northern Great Basin, Nevada: Geological Society of Nevada, Geology and Ore Deposits 2000: The Great Basin and Beyond Symposium, Reno/Sparks, Nevada, May 15-18, 2000, Proceedings, p. 419–438.

Morton, J.L., Silberman, M.L., Bonham, H.F., Jr., Garside, L.J., and Noble, D.C., 1977, K-Ar ages of volcanic rocks, plutonic rocks, and ore deposits in Nevada and eastern California—determinations run under the USGS-Nevada Bureau of Mines and Geology Cooperative Program: Isochron/West, no. 20, p. 19–29.

Norby, J.W., 2002, Geology of the Maggie Creek district, Carlin trend, Eureka County, Nevada: Nevada Bureau of Mines and Geology Bulletin 111, scale 1:18,000.

Norby, J.W., and Orobona, M.J.T., 2002, Geology and mineral systems of the Mike deposit: Nevada Bureau of Mines and Geology Bulletin 111, p. 143–167.

Orobona, M.J.T., 1996, Structural setting of the Bluestar subdistrict: Implications for the origin of the Carlin trend, Eureka County, Nevada: Unpublished M.S. thesis, Kingston, Ontario, Queens University, 207 p.

Peccerillo, A., and Taylor, S.R., 1976, Geochemistry of Eocene calc-alkaline volcanic rocks from the Kastamonu area, northern Turkey: Contributions to Mineralogy and Petrology, v. 58, p. 63–81.

Peters, S.G., 2003, Geologic map of the Bobs Flat Quadrangle, Eureka County, Nevada: Nevada Bureau of Mines and Geology Map 138, scale 1:24,000.

Phinisey, J. D., Hofstra, A. H., Snee, L. W., Roberts, T. T., Dahl, A. R., and Loranger, R. J., 1996, Evidence for multiple episodes of igneous and hydrothermal activity and constraints on the timing of gold mineralization, Jerritt Canyon district, Elko County, Nevada: Geological Society of Nevada, Geology and Ore Deposits of the American Cordillera Symposium, Reno/Sparks, Nevada, April, 1995, Proceedings, p. 15–39.

Radtke, A.S., 1985, Geology of the Carlin gold deposit, Nevada: U. S. Geological Survey Professional Paper 1267, 124 p.

Radtke, A.S., Rye, R.O., and Dickson, F.W., 1980, Geology and stable isotopes of the Carlin gold deposit, Nevada: Economic Geology, v. 75, p. 641–672.

Rayias, A.C., 1999, Stratigraphy, structural geology, alteration, and geochemistry of the northeastern Railroad district, Elko County, Nevada: Unpublished M.S. thesis, University of Nevada, Reno, 180 p.

Renne, P.R., Swisher, C.C., Deino, A.L., Karner, D.B., Owens, T.L., and DePaolo, D.J., 1998, Intercalibration of standards, absolute ages and uncertainties in $^{40}Ar/^{39}Ar$ dating: Chemical Geology, v. 145, p. 117–152.

Ressel, M.W., Noble, D.C., Henry, C.D., and Trudel, W.S., 2000a, Dike-hosted ores of the Beast deposit and the importance of Eocene magmatism in gold mineralization of the Carlin trend, Nevada: Economic Geology, v. 95, p. 1417–1444.

——2001, Dike-hosted ores of the Beast deposit and the importance of Eocene magmatism in gold mineralization of the Carlin trend, Nevada—a reply: Economic Geology, v. 96, p. 666–668.

Ressel, M.W., Noble, D.C., Volk, J.A., Lamb, J.B., Park, D.E., Conrad, J.E., Heizler, M.T., and Mortensen, J.K., 2000b, Precious-metal mineralization in Eocene dikes at Griffin and Meikle: Bearing on the age and origin of gold deposits of the Carlin trend, Nevada: Geological Society of Nevada, Geology and Ore Deposits 2000: The Great Basin and Beyond Symposium, Reno/Sparks, Nevada, May 15-18, 2000, Proceedings, p. 79–101.

Roberts, R.J., 1964, Stratigraphy and structure of the Antler Peak quadrangle, Humboldt and Lander Counties, Nevada: U.S. Geological Survey Professional Paper 459–A, 93 p.

Rodriguez, B.D., 1998, Regional crustal structure beneath the Carlin trend, Nevada based on deep electrical geophysical measurements: U.S. Geological Survey Open-File Report 98-338, p. 15–19.

Seedorff, E., 1991, Magmatism, extension, and ore deposits of Eocene to Holocene age in the Great Basin—mutual effects and preliminary proposed genetic relationships, *in* Raines, S, G.L., Lisle, R.E., Schafer, R.W., and Wilkinson, W.H., eds., Geology and ore deposits of the Great Basin: Symposium proceedings: Reno, Geological Society of Nevada, p. 133–178.

Seedorff, E., and Barton, M.D., 2004, Enigmatic origin of Carlin-type deposits: an amagmatic solution?: Society of Economic Geologists Newsletter 59, p. 14–18.

Shallow, L.J., 1999, Refractory ores at the Rain mine, Nevada: Structural controls, wallrock alteration, petrography, and geochemistry: Unpublished M.S. thesis, University of Nevada, Reno, 150 p.

Sillitoe, R.H., and Bonham, H.F., Jr., 1990, Sediment-hosted gold deposits: Distal products of magmatic-hydrothermal systems: Geology, v. 18, p. 157–161.

Sloan, J., Henry, C.D., Hopkins, M., and Ludington, S., 2003, Revision of National Geochronological Database: U.S. Geological Survey Open-File Report 03–236, http://wrgis.wr.usgs.gov/open-file/of03–236/.

Smith, J.F., Jr., and Ketner, K.B., 1976, Stratigraphy of post-Paleozoic rocks and summary of resources in the Carlin-Piñon Range area, Nevada: U.S. Geological Survey Professional Paper 867–B, 48 p.

——1978, Geologic map of the Carlin-Piñon Range area, Elko and Eureka Counties, Nevada: U.S. Geological Survey Miscellaneous Investigations Map I-1028.

Snoke, A.W., Howard, K.A., McGrew, A.J., Burton, B.R., Barnes, C.G., Peters, M.T., and Wright, J.E., 1997, The grand tour of the Ruby-East Humboldt metamorphic core complex, northeastern Nevada: Brigham Young University Geological Studies, v. 42, p. 1, p. 225–269.

Steiger, R.H., and Jäger, E., 1977, Subcommission on geochronology: Convention on the use of decay constants in geo- and cosmochronology: Earth and Planetary Science Letters, v. 36, p. 359–362.

Stewart, J.H., and Carlson, J. E., 1976, Geologic map of north-central Nevada: Nevada Bureau of Mines and Geology Map 50, scale 1:250,000.

——1978, Geologic map of Nevada: U.S. Geological Survey in collaboration with Nevada Bureau of Mines and Geology, scale: 1:500,000.

Teal, L., and Jackson, M., 1997, Geologic overview of the Carlin trend gold deposits and descriptions of recent deep discoveries: Society of Economic Geologists Newsletter 31, p. 1, 13–25.

Theodore, T.G., 2000, Geology of pluton-related gold mineralization at Battle Mountain, Nevada: Tucson, Arizona, Center for Mineral Resources Monographs in Mineral Resource Science 2, 271 p.

Theodore, T.G., Silberman, M.L., and Blake, D.W., 1973, Geochemistry and potassium-argon ages of plutonic rocks in the Battle Mountain mining district, Lander County, Nevada: U.S. Geological Survey Professional Paper 798–A, 24 p.

Theodore, T.G., Armstrong, A.K., Harris, A.G., Stevens, C.H., and Tosdal, R.M., 1998, Geology of the northern terminus of the Carlin trend, Nevada: Links between crustal shortening during the Late Paleozoic Humboldt orogeny and northeast-striking faults, *in* Tosdal, R.M., ed., Contributions to the Au metallogeny of northern Nevada: U.S. Geological Survey Open-file Report 98-338, p. 69–105.

Thorman, C.H., Brooks, W.E., Snee, L.W., Hofstra, A.H., Christensen, O.D., and Wilton, D.T., 1995, Eocene-Oligocene model for Carlin-type deposits in northern Nevada [abs.], Geological Society of Nevada, Geology and Ore Deposits of the American Cordillera Symposium, Reno/Sparks, Nevada, April, 1995, Proceedings, p. 75.

Tosdal, R.M., Wooden, J.L., and Kistler, R.W., 2000, Geometry of the Neoproterozoic continental breakup, and implications for location of Nevadan mineral belts: Geological Society of Nevada, Geology and Ore Deposits 2000: The Great Basin and Beyond Symposium, Reno/Sparks, Nevada, May 15-18, 2000, Proceedings, p. 451–466.

Tosdal, R.M., Cline, J.S., Fanning, C.M., and Wooden, J.L., 2003a, Lead in the Getchell-Turquoise Ridge Carlin-type gold deposits from the perspective of potential igneous and sedimentary rock sources in northern Nevada: Implications for fluid and metal sources: Economic Geology, v. 98, p. 1189–1211.

Tosdal, R.M., Hickey, K.A., Donelick, R.A., Arehart, G.A., and Chakurian, A.M., 2003b, Distinguishing hydrothermal events using apatite fission-track thermochronology; implications for Au-mineralisation in the Carlin-Jerritt Canyon region, northern Nevada [abs.]: Geological Society of America Abstracts with Programs, v. 35, no. 6 p. 402.

Tretbar, D.R., Arehart, G.B., and Christensen, J.N., 2000, Dating gold deposition in a Carlin-type gold deposit using Rb/Sr methods on the mineral galkhaite: Geology, v. 28, p. 947–950.

Wallace, A.R., 1993, Geologic map of the Snowstorm Mountains and vicinity, Elko and Humboldt Counties, Nevada: U.S. Geological Survey Miscellaneous Investigation Series Map I-2394, scale 1:50,000.

——2003a, Geologic map of the Willow Creek Reservoir SE Quadrangle, Elko, Eureka, and Lander Counties, Nevada: Nevada Bureau of Mines and Geology Map 136, 1:24,000, 15 p.

——2003b, Geology of the Ivanhoe Hg-Au district, northern Nevada: Influence of Miocene volcanism, lakes, and active faulting on epithermal mineralization: Economic Geology, v. 98 p. 409–424.

Wells, J.D., Stoiser, L.R., and Elliot, J.E., 1969, Geology and geochemistry of the Cortez gold deposit: Economic Geology, v. 64, p. 526–537.

Williams, C.L., Thompson, T.B., Powell, J.L., and Dunbar, W., 2000, Gold-bearing breccias of the Rain mine, Carlin trend, Nevada: Economic Geology, v. 95, p. 391–404.

Wooden, J.L., Kistler, R.W., and Tosdal, R.M., 1998, Pb isotopic mapping of crustal structure in the northern Great Basin and relationships to Au deposit trends: U.S. Geological Survey Open-File Report 98-338, p. 20–33.

Zoback, M.L., McKee, E.H., Blakely, R.J., and Thompson, G.A., 1994, The northern Nevada rift: Regional tectonomagmatic relations and middle Miocene stress direction: Geological Society of America Bulletin, v. 106, p. 371–382.

APPENDIX

$^{40}Ar/^{39}Ar$ Methodology

Samples for $^{40}Ar/^{39}Ar$ analysis were crushed in a cone crusher, then sieved to appropriate mesh size (20–40 for sanidine in all separates and for plagioclase in samples H98-78 and H98-102; 60–80 for hornblende, biotite, sericite, and all other plagioclase separates). Minerals were concentrated with a magnetic separator followed by heavy liquids. Sanidine and plagioclase were leached with 5 percent HF for 1 h. Final samples were handpicked for maximum purity, which was greater than 99 percent for all samples.

The Nevada Isotope Geochronology Laboratory and the New Mexico Geochronological Research Laboratory use mostly similar methods. Samples were irradiated at the Nuclear Science Center reactor at Texas A&M University for 7 to 14 h (Justet and Spell, 2001; McIntosh et al., 2003; Leavitt et al., 2004). Sanidine from Fish Canyon Tuff was the monitor of neutron fluence at both labs. Nevada uses an assigned age of 27.9 Ma (Cebula et al., 1986), whereas New Mexico uses 28.02 Ma (Renne et al., 1998). All ages reported here, including those from other laboratories, were recalculated to 28.02 Ma to allow direct comparison. However, see the footnote of Table 1. Single sanidine or plagioclase grains were fused with a CO_2 laser. Other samples were heated in a molybdenum resistance furnace. Extracted gases were purified with SAES GP-50 getters. Argon was analyzed with a Mass Analyzer Products (MAP) model 215-50 mass spectrometer operated in static mode.

Calculation and General Interpretation of $^{40}Ar/^{39}Ar$ Ages

$^{40}Ar/^{39}Ar$ ages were calculated several ways. Single crystal ages are the weighted mean of nine to 15 grains (sanidine) to as many as 34 grains (plagioclase) and are displayed as age probability diagrams (Fig. 4L). Individual analyses were discarded if they were obvious xenocrysts or had low ^{39}Ar contents or radiogenic yields. Ages for step-heated samples were determined by the age spectrum (plateau), inverse isochron, or total gas methods. A plateau age is defined as three contiguous steps that agree within analytical uncertainty and contain at least 50 percent of the released ^{39}Ar (Fleck et al., 1977). This method assumes that any trapped Ar has an atmospheric $^{40}Ar/^{36}Ar$ value of 295.5. Inverse isochron analysis (Fig. 4F, P) tests for the presence of excess Ar (i.e., trapped Ar with a nonatmospheric $^{40}Ar/^{36}Ar$ value: McDougall and Harrison, 1988). Agreement between plateau and isochron ages, which is the case for almost all our samples, is strong evidence that the age of the sample is correct. Because the dated rocks cooled rapidly following eruption or shallow intrusion as dikes, the ages are interpreted to be those of eruption or intrusion.

All ages from this study agree with stratigraphic relationships in the Emigrant Pass volcanic field and with the few crosscutting relationships of dikes. Among phenocrysts in rapidly cooled igneous rocks, single crystal analysis of sanidine provides the most precise ages (McIntosh et al., 1990, 2003). Single crystal or step-heating ages of inclusion-free plagioclase phenocrysts are less precise, in large part because of their much lower K content, but generally agree within uncertainties with sanidine ages from the same or related rocks (Table 1). Hornblende also provides consistent but less precise ages than does sanidine (see also Castor et al., 2003).

Many of the modern $^{40}Ar/^{39}Ar$ dates in the Carlin trend are on biotite (Fig. 4), in part because it commonly survived alteration in rocks where feldspar and hornblende phenocrysts were destroyed. However, many biotite spectra are disturbed, which suggests that minor alteration, not always observable in hand specimen or thin section, has affected Ar retention and release. This interpretation is consistent with experimental studies that show that biotite with submicroscopic chlorite layers gives hump-shaped spectra with meaningless old and young ages (DiVincenzo et al., 2003). In some cases, total gas ages of these disturbed biotites approximate emplacement age. We consider flat spectra of biotite to reliably indicate age, but the emplacement age of samples that give hump-shaped or otherwise disturbed spectra cannot be determined as precisely.